

POLYMER BRUSHES: FROM BIOSENSORS TO MEMBRANES

A Dissertation

Presented to the Faculty of the Graduate School

of Cornell University

In Partial Fulfillment of the Requirements for the Degree of

Doctor of Philosophy

by

Mary Elizabeth Welch

January 2014

UMI Number: 3579172

All rights reserved

INFORMATION TO ALL USERS

The quality of this reproduction is dependent upon the quality of the copy submitted.

In the unlikely event that the author did not send a complete manuscript and there are missing pages, these will be noted. Also, if material had to be removed, a note will indicate the deletion.



UMI 3579172

Published by ProQuest LLC (2014). Copyright in the Dissertation held by the Author.

Microform Edition © ProQuest LLC.

All rights reserved. This work is protected against unauthorized copying under Title 17, United States Code



ProQuest LLC.
789 East Eisenhower Parkway
P.O. Box 1346
Ann Arbor, MI 48106 - 1346

© 2014 Mary Elizabeth Welch

POLYMER BRUSHES: FROM BIOSENSORS TO MEMBRANES

Mary Elizabeth Welch, Ph. D.

Cornell University 2014

The first synthetic polymer was Bakelite, phenol-formaldehyde resin, developed from 1905-1909 by chemist Leo Baekeland. Since then, polymer chemistry and technology has enhanced our way of life from transportation to food storage to communication and electronics. These advances have breached the barrier of pure polymer science and transcended into the fields of material science, physics, and biology. Currently, innovative research in polymers is enabling the nanotechnology revolution with a focus on the design and production of polymer thin films that have tunable properties. One such thin film is polymer brushes, and it is the focus of this dissertation.

Polymer brushes, broadly defined, are an assembly of polymer chains anchored to a surface from some point in the chain, typically the end. They have desirable characteristics such as the ability to tether molecules to a substrate, or change the properties of a surface. Over the years, polymer brushes have found use in a number of applications such as in the development of new adhesive materials, biosurfaces and nonfouling biosurfaces. This work will illustrate several types of biosensors that have been enhanced through the incorporation of polymer brushes as well as investigate brushes as detached membranes.

The first biosensor is an electrochemical detector is based on the intrinsic catalytic activity of antibodies. As a means of amplifying the signal, polymer brushes have been integrated to bind the antibodies to the surface as well as to prevent non-specific

adsorption of other antibodies or contaminants that may be present in the test fluid. A second device includes a PEDOT:PSS based microelectrode which measures neuronal activities *in vivo*. This requires the tethering of glucose oxidase by brushes for specific charge exchange reactions to occur between the biological media and the conducting polymer. The third sensor uses functionalized polymer brushes to act as a scaffold for monitoring cellular motility.

Lastly, we have developed a method of detaching polymer brushes for further exploration. This method provides the opportunity to test initiator quality, immobilization conditions, optimization parameters, and has provided insight to the nature of polymer brushes in a stretched state.

BIOGRAPHICAL SKETCH

Mary Elizabeth Welch is the daughter of Dr. John B. Welch and Mary W. Welch. She was born in Racine, WI and later moved to Sturgeon Bay, WI. In May 2008 she graduated *summa cum laude* from Saint Olaf College in Northfield, MN with her B.A. degree in chemistry (ACS major). She received distinction in chemistry and was inducted into the Phi Beta Kappa Honor Society.

Since the fall of 2008, Liz has pursued her Ph.D. in the Department of Chemistry and Chemical Biology at Cornell University under the supervision of Professor Christopher K. Ober in the Department of Material Science and Engineering. The topic of her thesis includes the synthesis and characterization of polymer brushes relevant to patterning and biosensing device geometries as well as the fabrication and characterization of detached polymer brush membranes.

Dedicated to my family
for their love, support and encouragement

ACKNOWLEDGMENTS

The old saying, “There is no “I” in team” applies just as much in graduate school as it does in sports. Although individual candidates do a large portion of their work independently, it is through the help, assistance, and support of others that brings the goal into sight. I’d like to take this opportunity to acknowledge and thank those who’ve helped me throughout my studies at Cornell.

First, and above all, I’d like to express my deepest gratitude to my advisor, Christopher K. Ober. I am so very fortunate to have had the opportunity be a part of his group. His enthusiasm for my topic and tremendous expertise was very much appreciated. Even more, I’m so thankful for all of the support and encouragement he showed me over the years. I have never met a more patient, understanding person who is willing to sacrifice his time to mentor and assist his students. Thank you for your tutelage, advice, and guidance during my years at Cornell. Your friendship, although at first unexpected, has been the driving force of my success and for that I am forever grateful.

I would also like to thank my exceptional committee members, Professor Barbara A. Baird and Professor Héctor D. Abruña for their significant research discussions and suggestions. Their expertise and patience to explain topics outside of my field of research has been invaluable. Without their collaboration and contributions, this thesis would be incomplete.

I am grateful for having the opportunity to work with numerous research groups and gain a greater understanding and appreciate for their field of work. Prof. George Malliaras and has been very kind to invite me several times to his lab in Centre Microélectronique de Provence, France for collaboration on a sensor project. His discussions on transistors have been very beneficial. Additionally, Thomas Doublet

was very helpful teaching me about glucose sensing and PEDOT:PSS electrodes and it was a pleasure to work with him.

Although our project is relatively new, I have enjoyed working with Dr. Katherine Hajjar to explore the world of interfacing biological media and polymer brushes. Our research discussions provided direction with great potential in the future. Thanks to Dena Almeida and Arun Deora for their work testing our brush samples and for providing enzyme/cell related guidance and suggestions.

For the biosensor work, my longest ongoing project, I would like to thank all of the past and present people who made contributions. Thank you to Norah Smith, Michele Tague, Youyong Xu, Hongjun Chen, Nicole L. Ritzert, Marcus Wilkes, and Devin Wakefield. Collaboratively we have made so much progress and it has been exciting working with each of you and seeing the development and advancement over time.

Over the years group members have always been a source of help and support. Special thanks to Dr. Youyong Xu who taught me lab technique and who was an excellent role model and source of information during my first few years. I am so grateful for the help and support from all the Ober group members past and present. I appreciate your friendships and collaborations.

I gratefully acknowledge the funding support from the National Science Foundation (NSF) in which much of this work was made possible. Also I would like to thank the technical support from the staff in the Cornell Nanobiotechnology Center (NBTC), the Cornell Nanofabrication Facility (CNF), Cornell Center for Materials Research (CCMR), and Cornell High Energy Synchrotron Source (CHESS). Special thanks to Rob Ilic who was instrumental in teaching me everything about lithography and device fabrication and John Grazul for his help with the TEM.

Finally, I am so grateful to all of my friends and family. I have made friendships

here at Cornell that I will cherish for a life time. Our fun times together got me through some very frustrating periods in the lab and I will treasure those memories the rest of my life. My family's love and faith in me also provided the support I needed to succeed. I am so thankful for everything my parents provided for me and everything they did to get me to where I am today. Thank you for your love, assurance and encouragement. A heartfelt thanks to everyone, I have now joined the Ph.D. community.

TABLE OF CONTENTS

BIOGRAPHICAL SKETCH.....	v
DEDICATION.....	vi
ACKNOWLEDGEMENTS.....	vii
TABLE OF CONTENTS	x
LIST OF FIGURES.....	xvi
LIST OF TABLES.....	xx
ABBREVIATIONS.....	xxi
CHAPTER 1: POLYMER BRUSHES AS RESPONSIVE, PATTERNED, SENSING MATERIALS	
Abstract	1
Introduction	2
Types of Brushes	3
<i>Homopolymer Brushes</i>	
<i>Mixed Brushes</i>	
<i>Block Copolymer Brushes</i>	
<i>Responsive Brushes</i>	
Lithography of Brushes	16
<i>UV Lithography</i>	
<i>Electron Beam Lithography</i>	
<i>Soft Lithography</i>	
<i>AFM Lithography</i>	

Detached Polymer Films	30
<i>Crosslinked Sublayer</i>	
<i>Free Membranes</i>	
<i>Characterization of Detached Films</i>	
Electrochemical Biosensors	41
<i>Advantages of Polymer Brushes for Biosensors</i>	
<i>Polymer Brushes in Electrochemical Sensors</i>	
Summary	53
References	59

CHAPTER 2: A GENERALIZED PLATFORM FOR ANTIBODY DETECTION USING THE ANTIBODY CATALYZED WATER OXIDATION PATHWAY

Abstract	73
Introduction	73
Experimental	77
<i>Materials</i>	
<i>Synthesis and Immobilization of Surface Initiators</i>	
<i>Polymerization and Functionalization of POEGMA Brushes:</i>	
<i>Quantification of DNP Surface Coverage</i>	
<i>Antibody adsorption measurements using Quartz Crystal Microbalance</i>	
<i>Immobilization of Photosensitizer</i>	
<i>Hydrogen Peroxide Generation and Detection using SWV</i>	
<i>Device Fabrication</i>	
<i>Equipment</i>	
Results and Discussion	83
<i>Polymer Brush Synthesis and Functionalization</i>	

<i>Polymer Brush Characterization and Non-specific Adsorption Measurement</i>	
<i>DNP and Antibody Quantification</i>	
<i>Electrochemical Polymerization of Photosensitizer</i>	
<i>Square-wave Voltammetry of Generated H₂O₂</i>	
Conclusions	94
Acknowledgements	95
References	96
CHAPTER 3: OECT GLUCOSE SENSOR WITH POLYMER BRUSHES	
Abstract	98
Introduction	98
Experimental	101
<i>Materials</i>	
<i>Pattern and deposition of PEDOT:PSS and PEDOT:TOS</i>	
<i>Plasma and Immobilization</i>	
<i>Brush Growth</i>	
<i>OECT Functionalization by Glucose oxidase</i>	
<i>Electrochemical</i>	
<i>Tools</i>	
Results and Discussion	106
<i>Polymer Brush Initiator Immobilization</i>	
<i>Characterization of Polymer Brushes</i>	
<i>Optimization of Plasma Oxidation Surface Activation</i>	
<i>Device Conductivity Testing</i>	
<i>Device Response to Glucose</i>	
<i>Stabilization of Electrode</i>	

Conclusions	116
Acknowledgements	117
References	118

CHAPTER 4: CHARACTERIZATION OF POLYMER BRUSH MEMBRANES VIA HF LIFTOFF TECHNIQUE

Abstract	121
Introduction	121
Experimental	124
<i>Materials</i>	
<i>Synthesis of Silane Initiator and Immobilization</i>	
<i>PGMA Brush Polymerization</i>	
<i>PS Brush Polymerization</i>	
<i>Polymer Brush Patterning</i>	
<i>Brush Crosslinking</i>	
<i>Membrane LiftOff</i>	
<i>Characterization</i>	
Results and Discussion	128
<i>Membrane Fabrication</i>	
<i>Image Analysis</i>	
<i>Crosslinking Methods</i>	
Conclusions	145
Acknowledgements	146
References	147

CHAPTER 5: EXPANSION AND STRETCHING OF DETACHED POLYMER BRUSH MEMBRANES

Abstract	150
Introduction	150
Experimental	154
<i>Materials</i>	
<i>Synthesis of Silane Initiator and Immobilization</i>	
<i>Brush Polymerization</i>	
<i>Polymer Brush Patterning</i>	
<i>Membrane Liftoff</i>	
<i>Ellipsometry</i>	
<i>Characterization</i>	
Results and Discussion	157
<i>Etching Process</i>	
<i>Membrane Expansion Observations</i>	
<i>Isovolumetric Argument</i>	
<i>Glass Transition Temperature</i>	
Conclusions	167
Acknowledgements	169
References	170

CHAPTER 6: SUMMARY AND FUTURE DIRECTIONS.....172

<i>Electrochemical Biosensor</i>
<i>OECT Glucose Sensor</i>
<i>Polymer Brushes for Cellular Motility</i>
<i>Polymer Brush Membrane Detachment</i>

APPENDIX: POLYMER BRUSHES AS SURFACE SCAFFOLDS FOR
CELLULAR MOTILITY

Abstract	182
Introduction	182
Experimental	184
<i>Materials</i>	
<i>Synthesis of Silane Initiator and Immobilization</i>	
<i>Brush Growth</i>	
<i>Brush Functionalization</i>	
<i>Cell Culture</i>	
<i>Cell Staining</i>	
<i>Characterization</i>	
Results and Discussion	189
<i>Polymer Brush Polymerization and Functionalization</i>	
<i>Characterization of Functionalized Polymer Brushes</i>	
<i>Cell Culture on Polymer Brushes</i>	
<i>Cell Mobility on Polymer Brushes</i>	
Conclusions	200
Acknowledgements	201
References	202

LIST OF FIGURES

CHAPTER 1

Figure 1: Illustration of different polymer brush systems	5
Figure 2: Preparation of V-shaped PS- <i>b</i> -PEO brush on the planar gold surface and AFM images with polymer treated with THF	7
Figure 3: Mechanism of motion of nanoparticles by phase separation of polymer brushes	11
Figure 4: Loading and release schematic of reservoir equipped with thermally responsive brushes	15
Figure 5: Illustration of patterned nanochannel fabrication process	20
Figure 6: Illustrations of steps in μ CP of initiator patterns and their subsequent amplification into patterned polymer-brush microstructures	25
Figure 7: Parallel fabrication of 3D polymer brushes by p-DNL	29
Figure 8: Scheme of the preparation of polymer carpets	33
Figure 9: Illustrations and AFM images of buckling patterns on patterned gold electrodes	37
Figure 10: Degree of dissociation and swelling behavior of weak PAA brushes in solution at different pH values	46
Figure 11: Scheme of brushes that electrochemically induce reversible conversion of an electrode interface between an active and inactive state	48
Figure 12: Representation of the quantification of antibodies on DNP functionalized PAA brush modified gold electrode	50
Figure 13: Schematic representation of the preparation of polymer brush modified graphite electrode	52

Figure 14: Representation of induced-fit binding of DAD with fiber-sol-gel-MIP in aqueous media	54
--	----

CHAPTER 2

Figure 1: Schematic of biosensor platform based on the ACWOP process	76
Figure 2: Synthesis and DNP functionalization of polymer brushes	85
Figure 3: DNP quantification	86
Figure 4: QCM measurements of surface coverage of the antibodies and non-specific adsorption control experiments	87
Figure 5: Patterned QCM and Silicon device	89
Figure 6: Cyclic voltammograms of photosensitizer	91
Figure 7: Square-wave voltammetry of generated H ₂ O ₂	93

CHAPTER 3

Figure 1: Mixed polymer brush and glucose oxidase (GOx) fabrication on electrode device	102
Figure 2: NEXAFS data characterizing polymer brush on PEDOT:PSS and AFM determining brush thickness	108
Figure 3: Reaction cycles for detection of glucose	112
Figure 4: Normalized response to glucose of PEDOT:PSS/Brush/GOx electrode	114
Figure 5: Stability versus time of PEDOT:PSS/Brush/GOx electrode	115

CHAPTER 4

Figure 1: Detachment scheme producing membranes that can be transferred to TEM grids	125
---	-----

Figure 2: Illustration of initiator SAM formation via island mechanism	130
Figure 3: TEM images of crosslinked PS brush membranes and uncrosslinked PGMA brush membranes	132
Figure 4: AFM of uncrosslinked PGMA film	133
Figure 5: Brush layer showing uniform layer and folded region and optical density calculation areas	135
Figure 6: Patchy film of PS brushes	139
Figure 7: Schematic of chemical and lithographic methods of crosslinking polymer brushes	141
Figure 8: Shows IR spectra of a detached PGMA film	143
CHAPTER 5	
Figure 1: TEM images of PMMA and PGMA brush membranes	158
Figure 2: Illustration of isovolumetric film expansion	161
Figure 3: Glass transition temperature of PMMA membranes measured thickness as a function of temperature	165
CHAPTER 6	
Figure 1: Construction of an interdigitated system for detection amplification of electrochemical biosensor	173
Figure 2: Illustration of an electrode that can record both neurological and metabolic activity	176
Figure 3: Chemical structure of the original coumarin dye and possible new dye that incorporates CF_3 moiety	178

APPENDIX

Figure 1: Illustration of a cell moving across functionalized brush surface	185
Figure 2: Functionalization of PGMA brushes with peptide-dye	190
Figure 3: XPS of PGMA brushes functionalized with diethylamine	191
Figure 4: Shows IR spectra of PGMA-PHEMA brush systems	192
Figure 5: Fluorescent images of polymer brushes functionalized with coumarin dye	194
Figure 6: HUVEC cells were plated on PGMA-NH ₂ brushes	196
Figure 7: HUVEC cells were stained with Phalloidin, Autofluorescence, and DAPI	197
Figure 8: Cells were plated on fibronectin coated brushes. HUVEC cells were stained with Phalloidin, and DAPI after 4 days in culture	199

LIST OF TABLES

CHAPTER 4

Table 1: The optical density of the holes in patchy films	137
Table 2: Expansion of hole diameter in membranes after liftoff measured by TEM	144

CHAPTER 5

Table 1: PMMA and PGMA film thicknesses measured before and after membrane detachment by AFM	160
---	-----

ABBREVIATIONS

- 2,4-dinitrophenyl (DNP)
Antibody-catalyzed water oxidation pathway (ACWOP)
Atom transfer radical polymerization (ATRP)
Atomic force microscopy (AFM)
Bovine serum albumin (BSA)
Cyclic voltammetry (CV)
Dichloromethane (DCM)
Dimethyl formamide (DMF)
Enzyme-linked immunosorbent assay (ELISA)
Fourier transform infrared spectroscopy (FTIR)
Glass transition temperature (T_g)
Glucose oxidase (GOx)
Horseradish peroxidase (HRP)
Human umbilical vein endothelial cells (HUVECs)
Hydrofluoric (HF)
Hydrogen peroxide (H_2O_2)
Lift-off resist (LOR)
Near Edge X-Ray Absorption Fine Structure (NEXAFS)
N-hydroxysuccinimide (NHS)
Organic electrochemical transistors (OECTs)
PEDOT:PSS/PGMA/PHEMA/GOx (PPPG)
Phosphate-buffered saline solution (PBS)
Poly(2-hydroxyethyl methacrylate) (PHEMA)
Poly(3,4-ethylenedioxythiophene) (PEDOT)
Polyelectrolyte brushes (PE)

Poly(glycidyl methacrylate) (PGMA)
Poly(propylene glycol) methacrylate (POEGMA)
Polystyrene (PS)
Poly(styrene sulfonate) (PSS)
Post exposure bake (PEB)
Quartz crystal microbalance (QCM)
Self-consistent field (SCF)
Silicon oxide (SiO_2)
Square wave voltammetry (SWV)
Transmission electron microscopy (TEM)

CHAPTER 1

POLYMER BRUSHES AS RESPONSIVE, PATTERNED, SENSING MATERIALS

Abstract While polymer brush systems continue to grow in popularity, so does their complexity and sophistication. Advances in polymerization and specific functionalization methods have led to novel applications in diverse research fields. The marriage of top-down lithography with bottom-up brush processing is becoming increasingly important in the development and progress of nanotechnology. In addition, a major obstacle in the development of highly sensitive electrochemical biosensors is the issue of electrode fouling due to non-specific adsorption of biomolecules on the electrode/sensor surface. The efficacy of such systems is also limited by the need for high densities of immobilized bioactive molecules on the sensor surface. Polymer brushes have recently attracted considerable interest for generating molecularly defined surfaces for applications in nanotechnology, molecular biology, and biomedical sciences. Two main advantages of using polymer brush

*Portions are excerpted from M. E. Welch and C. K. Ober. Responsive and patterned polymer brushes. *J. Polym. Sci. Pol. Phys.* 2013, DOI: 10.1002/polb.23356. Copyright 2013 John Wiley and Sons. M. E. Welch, A. Rastogi, C. K. Ober. Polymer brushes for electrochemical biosensors. *Soft Matter.* 2011, 7, 297-302. Copyright Royal Society of Chemistry

systems are their ability to mitigate non-specific adsorption and the creation of tailor-made surfaces to control the immobilization of bioanalytes through specific receptor recognition interactions. The use of polymer brushes allows the formation of uniform surfaces with controlled chemical architectures that exhibit good chemical and thermal stability. The aim of this chapter is to examine different approaches taken to generate tailored polymer brush systems through surface-initiated polymerizations, patterning techniques, as well as detached, free-standing membranes. Lastly, the role of polymer brushes in the development of sensitive electrochemical biosensors with low detection limits is highlighted.

1.1. Introduction

In recent years, polymer brushes have been widely explored for their versatility as surface coatings. Common applications include but are not limited to biosurfaces (biosensors, implants)¹⁻³, chromatographic separation⁴, lithium batteries⁵, and nonfouling surfaces^{6,7}. They can also be fabricated on the macro and nanoscale for electronics and microfluidic devices.^{8,9} A thickness of just a few nanometers is enough to convert an inorganic surface to an organic, biologically friendly one that provides additional entities for attachment or functionalization. Use of polymer brushes have been realized in fields ranging from mechanical engineering to food science technology; an exceptional degree of advancement considering their first applications as colloidal particle stabilizers in the 1950s.^{10,11}

Broadly defined, a polymer brush system comprises a forest of polymer chains tethered at some point in the chain to a surface or substrate. The distance between

neighboring chains influences the natural architecture of the brush. At low grafting density, polymer chains prefer to interact with themselves, adapting a mushroom like structure. As the density increases, the brushes begin stretching away from the surface to reduce unfavorable interactions with neighboring chains, thus leading to a loss of entropy. The method of attachment significantly impacts the type of brush that can be produced. In general, two techniques are used, described as “grafting from” and “grafting to”.¹² The “grafting to” method involves first synthesizing a polymer chain in solution with an active end-group that can bind to a substrate.¹³⁻¹⁶ This method of preparation leads to low grafting densities due to slow diffusion and steric repulsion between incoming units and already grafted chains. After a certain threshold is reached, bulky tethered chains prevent the access of new chains to the surface. On the other hand, the “grafting from” method produces high-density brushes by first immobilizing a self-assembled-monolayer (SAM) of initiator molecules and subsequently polymerizing the brush chains directly from the surface. Numerous types of surface initiated polymerization are available including ring-opening,^{17,18} ring-opening metathesis polymerization (ROMP),^{19,20} reversible addition fragmentation transfer (RAFT),^{21,22} radical polymerization,²³ nitroxide-mediated polymerization (NMP),^{24,25} and atom transfer radical polymerization (ATRP).²⁶⁻³⁰ All of these methods provide control over grafting density and brush thickness; however, the radical polymerization systems also have a wide variety of monomers available.

Homopolymer brushes are very common, but a wide range of different types are being investigated. Ayres *et al.* has explored blood compatible surfaces by generating polymer brushes that mimic heparin, an anticoagulant, via synthesizing brushes of

sulfonated sugar repeat residues.³¹ Henry and coworkers prepared acrylamide-DNA polymer brushes by surface initiated ATRP in an electrochemical sensor for the detection of a breast cancer related marker.³² A broad range of homopolymer brushes are available and can be further classified into neutral and charged polymer brushes.

For this review, more complex polymer brush systems will be highlighted. The preparation and application of polymer brushes such as mixed, block copolymer and responsive systems will be presented. Another focus will include current lithographic techniques for the fabrication of patterned brush surfaces. Lastly we will spotlight a new and emerging field of polymer brushes in which the films are detached from the surface creating ultra thin membranes. The schematic in figure 1 illustrates the feature points in this article.

1.1.1. Mixed brushes

Mixed brush systems, on the other hand, are more complex but offer tunable surface properties. The most straightforward preparation consists of mixing two monomers and generating chains with random mixed units.³³ However, both monomers must be soluble in the same polymerization environment and individual chain segregation is not possible. In order to construct a switchable surface, two chemically distinct homopolymers must be tethered to a surface such that there is selective solvation of one of the chain types and the grafting density must be controlled and low. These systems can be produced by either the “grafting to” method³⁴ or preparing a surface with two different initiator sites which can be used to polymerize separate monomers.³⁵ Mixed brushes are often responsive to environmental stimuli and have switchable surface properties such as wettability,

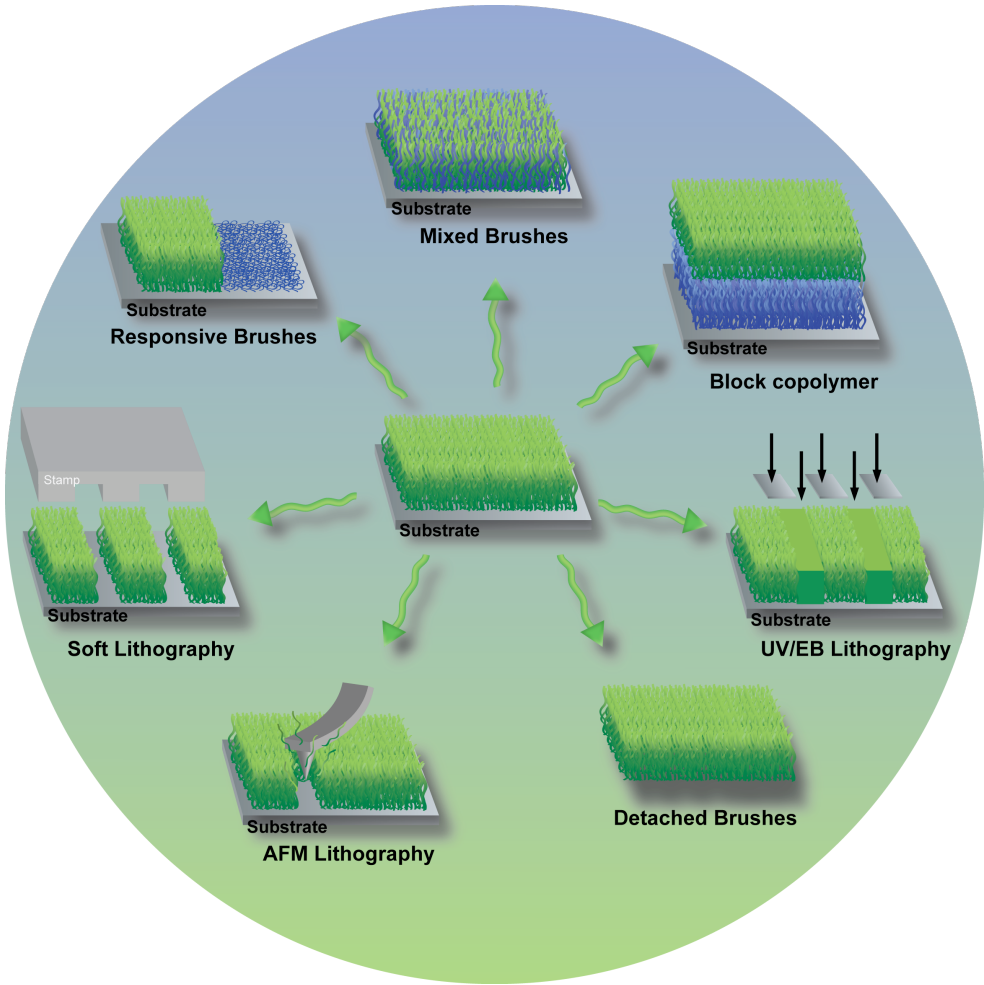


Figure 1. Illustration of different polymer brush systems that can be generated by polymerization methods or various lithography techniques.

architecture, and surface charge and composition. Triggers commonly include changes in pH, temperature, and salt concentration. Motornov *et al.* grafted poly(dimethylsiloxane) (PDMS-NH₂) and carboxy-terminated poly(2-vinylpyridine) (P2VP-COOH) onto an epoxy functionalized electrode surface to create mixed brushes with morphological transitions that could be regulated via changes in pH.³⁶ The switchable brushes allowed for control of ion transport through nanoscopic channels to create a gating mechanism. Others have produced temperature sensitive mixed systems by incorporating a high percentage of poly(*N*-isopropyl acrylamide) (PNIPAAM) units.^{37,38} These mixed brush compositions have shown promise for biological purposes such as protein-resistant surfaces. Additionally, microphase separation of mixed brush systems has been investigated through solvent annealing treatments.³⁹ Wang *et al.* synthesized a V-shaped brush in which a trithiocarbonate group, located between PS and PEO chains, can be anchored to a gold surface creating an amphiphilic mixed brush system (Figure 2).¹⁴ Different lateral and vertical microphase morphologies were observed depending on solvent treatment and chain structure. The advantage of this system is the incorporation of two different chains tethered at the same point, thus providing an equal contribution from both polymers.

1.1.2. Block copolymer brushes

Similar to mixed brushes, block copolymer brushes can be generated to fabricate nanostructured surfaces. The grafting to method is most commonly used for mixed systems, but block copolymer brushes can be easily produced by both grafting to and grafting from. Living anionic polymerization,⁴⁰ ATRP⁴¹ and RAFT⁴² are possible forms of surface initiated polymerization used to produce high grafting density block

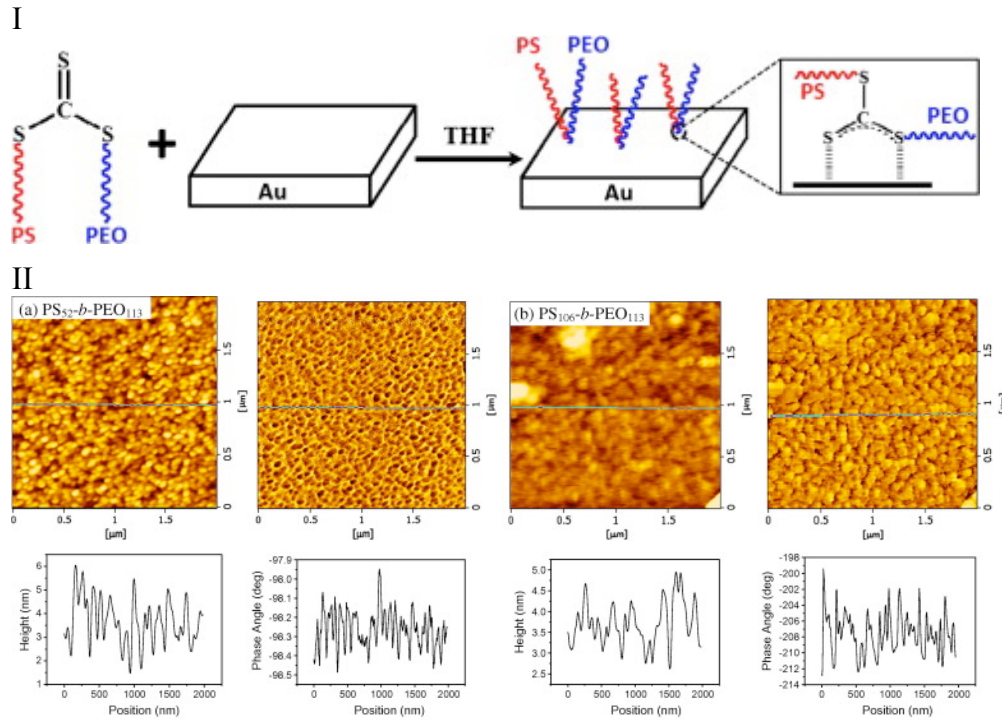


Figure 2. (I) Preparation of V-shaped PS-*b*-PEO brush on the planar gold surface. (II) AFM height (left side) and phase (right side) images of the V-shaped PS-*b*-PEO brushes on gold surface after treatment with THF. (a) PS₅₂-*b*-PEO₁₁₃ brush, (b) PS₁₀₆-*b*-PEO₁₁₃ brush. The figures below the height and phase images show the height or phase fluctuation profiles corresponding to the lines in the AFM images. Reproduced from ref. 14, with permission from Elsevier.

copolymer brushes. As a result, increased control over block thicknesses helps to tune the responsive properties of these systems. Xu and coworkers took a systematic approach to study the effect of block length on solvent responsive behaviors by creating a gradient of the top brush.⁴³ A bottom block of poly(*n*-butyl methacrylate) (PBMA) was held constant while a molecular mass gradient of poly(2-(*N,N*-dimethylamino)ethyl methacrylate) (PDMAEMA) was polymerized on top via ATRP. Water contact angle measurements were used to characterize the response and rearrangement of the PDMAEMA block when exposed to water or hexane. Results indicated shorter blocks of PDMAEMA were able to rearrange while a thick layer suppressed any response from the PBMA. Additionally, increasing thickness of the bottom PBMA block enhanced the responsiveness of the system.

Switching the top and bottom block can also lead to different behavior responses. Yu *et al.* examined poly(acrylic acid)-*b*-poly(2-vinylpyridine) (PAA-*b*-P2VP) brushes and P2VP-*b*-PAA brushes (inverted) at different block lengths and at different pH regions.⁴⁴ In neutral pH ranges, both sets of block brushes exhibited similar behaviors due to electrostatic interaction between oppositely charged blocks. Decreasing the pH and lengthening the PAA in the PAA-*b*-P2VP system resulted in increased hydrogen-bonding between the blocks which allowed P2VP segments to loop back towards the PAA block. Basic pH conditions, on the other hand, showed the smallest degree of surface rearrangement.

Triblock copolymers have also been generated. Poly(2-hydroxyethyl methacrylate) (PHEMA) -*b*-poly(*n*-butyl methacrylate) (PBMA) -*b*-PHEMA was

synthesized via surface-initiated ATRP from a gold substrate.⁴⁵ The amphiphilic triblock brushes were characterized by Fourier transform infrared spectroscopy, polarization modulation infrared reflection absorption spectroscopy (PM-IRRAS), ellipsometry, contact angle, and AFM and their response to selective solvents was studied for potential use as membranes for biosensing applications.

The rearrangement capability of these systems has been taken one step further and used as an approach to move nano-objects. Rühe *et al.* investigated the movement of silica particles on a diblock copolymer surface of poly(methyl methacrylate-*b*-glycidyl methacrylate) (p(MMA-*b*-GMA)).⁴⁶ By increasing the degree of polymerization of the bottom block, different topographical patterns (ripple-like, worm-like, and spherical, respectively) are generated when exposed to selective solvents. Results showed the motion of the particles is due to the switching chemical conformations of the block copolymer brushes as well as the changes in the interfacial energy during the phase transition. Particles tended to aggregate into islands during morphology rearrangement regardless of vapor versus solvent annealing conditions and topographical patterns. This gripping and releasing mechanism has not proven directional motion; however, by potentially pre-shaping the polymer surface into channels it may be possible to better control and tune nano-object movement.

In a similar study, Yu *et al.* demonstrated the perpendicular movement of CdS nanoparticles based on the phase separation of a block copolymer brush.⁴⁷ Polystyrene-*b*-(poly(methyl methacrylate)-*co*-poly(methacrylic acid)(CdS)) (PS-*b*-(PMMA-*co*-PMAA(CdS))) brushes were synthesized via ATRP and a H₂S gas exposure process followed by attachment of CdS nanoparticles to the carboxylic

groups of the PMAA segment. Yu and coworkers were able to reversibly lift and lower the CdS nanoparticles by exposure to selective solvents which induced perpendicular phase separation (Figure 3). However, when the thickness of the top block (PMMA-co-PMAA(CdS)) was increased, surface rearrangement decreased and thus movement of the nanoparticles was limited.

1.1.3. Responsive brushes

Whether a homo, mixed, or block copolymer architecture, the responsive nature of polymer brushes has been frequently investigated. Stimuli-responsive polymers are appealing due to the conformational changes in chain morphology with exposure to external triggers such as temperature, solvent, pH, ionic strength, light, and electrical and magnetic fields. For example, polyelectrolyte brushes are susceptible to influences that can affect their charge and thus their chain conformation (brush to mushroom regime). Responsive polymer brushes are well suited for applications such as drug release, surface wettability, microfluidics, and biosensors.

When considering charged brushes, there is a noteworthy difference between “strong” and “weak” polyelectrolytes (PEL). Strong polyelectrolyte brushes refer to chains in which the number and position of the charge is permanent, the charge is chemically fixed in the monomer. Weak polyelectrolytes, on the other hand, have variable, dynamic charges which are pH dependent. Common examples of weak PEL brushes include poly(2-vinyl pyridine) (P2VP), poly(2-(trimethylamino)ethyl methacrylate) (PTMAEMA), and poly(acrylic acid) (PAA).

For weak PEL at low salt concentrations, small amounts of added salt results in an increase in brush thickness.⁴⁸⁻⁵³ The reason is because there is higher proton

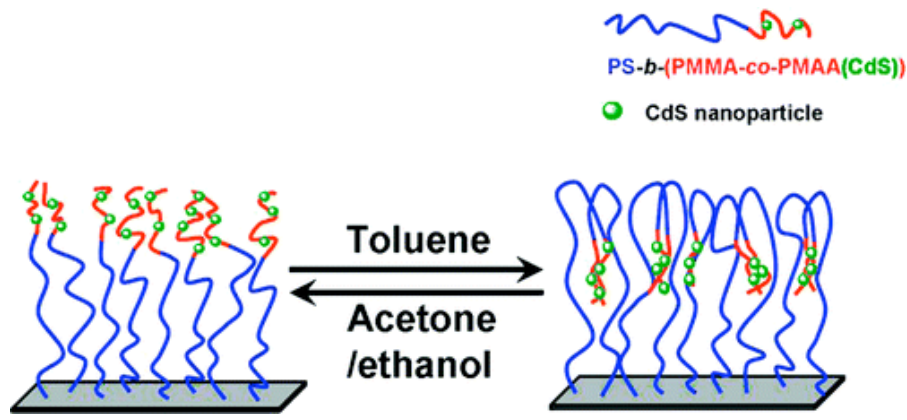


Figure 3. Proposed mechanism of motion of integrated CdS nanoparticles by perpendicular phase separation of polymer brushes when exposed to select solvents. Reproduced from ref. 47, with permission from American Chemical Society.

concentration inside the brush then in the bulk phase. Addition of salt can lead to substitution of the protons with salt counterions which changes the degree of dissociation of the acid/base moieties on the polymer chains. The net increase of charge results in an increase in osmotic pressure and thus the swelling of the brushes (called the “osmotic brush” regime). At high salt concentrations, studies have shown that strong and weak PEL behave similarly, whereas with increasing salt concentration brush thickness decreases. When the ionic strength of solution is equivalent to that of the free counter-ions inside the brush, the screening associated with the external salt reduces the osmotic pressure of the mobile ions inside the brush. Increased screening of charged groups reduces the electrostatic repulsion between the individual chains therefore reducing brush thickness (known as the “salted brush” regime). Theoretical and experimental studies have been used to explore the behavior of mixed PEL brushes, and results are similar to that of the homo PEL.^{54,55} A system composed of two oppositely charged weak polyelectrolytes shows a switching behavior mechanism depending on pH. At low pH, the acidic brush becomes protonated and the charge density increases, swelling the chains, while the other brush is in a collapsed complex. This behavior switches at high pH values; the basic chains swell and preferentially occupy the top of the brush system while the acidic chains become compact on the bottom. Moreover, the system was shown to be reversible for at least 10 cycles.

Liu *et al.* grafted PAA and P2VP onto the inner wall of a silica capillary to create mixed brushes with morphological transitions that could be regulated via changes in pH.⁵⁶ The switchable brushes were allowed for control of the electroosmotic flow and were able to separate a series of basic and acidic protein standards with minimal

adsorption.

Others have investigated using PEL brushes for lubrication applications. One of the first examples was demonstrated by Raviv *et al.* who attached the diblock copolymer PMMA-b-poly(sodium sulphonate glycidyl methacrylate) (PSGMA) to a hydrophobized mica surface.⁵⁷ The PMMA moieties attach to the surface allowing the charged PSGMA segments to be exposed to the environment. They achieved excellent lubrication ability in water that can be attributed to low interpenetration of opposing brushes, high fluidity of the hydration layers surrounding the charged brushes, and mobile counterions in and outside of the brush that contribute to osmotic pressure. However, because the block copolymer was not covalently attached, the brush layer was damaged at high pressures. It has been shown that the surface density of block copolymers non-covalently attached to mica substrates are affected and can vary by changes in salt concentration.⁵⁸ To overcome this concern, Liberelle *et al.* used the Langmuir-Schaeffer technique to irreversibly attach the diblock copolymer PS-b-PAA to a mica surface with an end-grafted PS monolayer, in which the PS block of the copolymer is permanently entangled with PS surface chains.⁵⁹ Results were consistent with theoretical predictions mentioned above, an increase in salt concentration increased brush thickness and the degree of ionization of the PAA segment (osmotic regime). Furthermore, additional increase in salt concentration (salted regime) reduced brush thickness due to screening effects. Although relatively high friction coefficients were observed, surface and polymer damage was not an issue.

Not all responsive systems are composed of charged brushes that undergo a

transition based on change in pH or ionic strength. Thermoresponsive brushes in particular, poly(*N*-isopropylacrylamide) (PNIPAM). Below its lower critical solution temperature (LCST) of 32°C, the hydrophilic chains exhibit a swollen or extended conformation.^{60,61} Raising the temperature above the LCST induces a phase transition into a hydrophobic collapsed state. Such responsive materials are often combined with biological systems and implemented in sensors,⁶² drug delivery,⁶³ protein attachment,⁶⁴⁻⁶⁶ and as biocompatible materials.^{67,68} Additionally PNIPAM has applications for surfaces with controlled antimicrobial properties. Pangilinan *et al.* polymerized PNIPAM brushes from carbon nanotube (CNT) surfaces and studied the antibacterial properties against *Exiguobacterium sibiricum* 255-15 and *Exiguobacterium* sp. AT1b.⁶⁹ The results showed that CNT without brushes are antimicrobial at all temperatures; however, if functionalized with PNIPAM the system was only antibacterial below the LCST. Above the LCST allowed biofilm formation, offering the ability to tune the toxicity of CNT at specific temperature ranges. Deviating from biological applications, Szuwarzyński *et al.* utilized PNIPAM thermal properties to create a gating platform of nanocontainers to entrap and release particles. The brushes were grown on surfaces with different pore sizes and shown to successfully seal small particles in the valves at temperatures below LCST. Above the LCST, the brush reversed into a collapsed state allowing the pore channels to open and release molecules (Figure 4).⁷⁰

UV light can also be used to trigger a conformational change in brushes. Samanta *et al.* polymerized brushes containing spiropyran moieties via ROMP.¹⁹ Spiropyrans contain a photocleavable C-O bond that can be reversibly switched between a ring

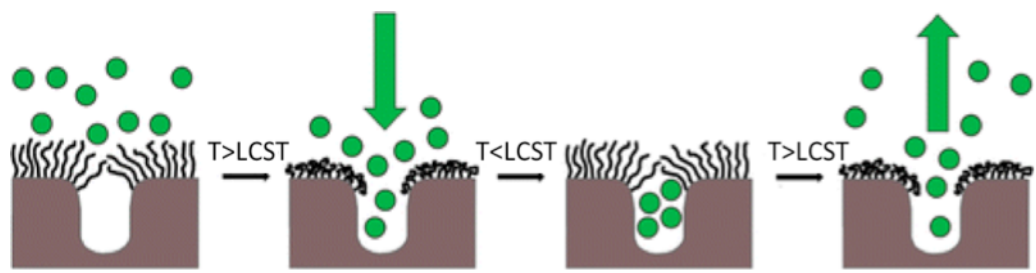


Figure 4. Schematic drawing of loading and release processes using a nanoporous smart reservoir equipped with thermally responsive nanovalves built of PNIPAM brushes. Reproduced from ref. 70, with permission from American Chemical Society.

closed spiropyran (SP) and the ring-opened merocyanine (MC) form. The light-induced conformational change gave rise to switchable color, wettability, and morphology. These properties could be tuned based on alkyl spacer length of the spiropyran tether, complexing with metal ions, and solvent conditions.

1.2. *Lithography*

Lithographic techniques ranging from microcontact printing, electron beam (e-beam), nanoimprint, and conventional photolithography have been used for fabricating patterned surfaces in polymer brushes. Patterning of polymer films has been an area of great interest due to the broad range of applications in the production of integrated circuits, information storage devices, light-emitting displays (LEDs), microfluidic devices, biochips, and in bio-related and medical research including the study of cell-surface interactions and tissue engineering.

1.2.1. *UV lithography*

A bottom-up lithographic approach can be employed by first patterning a surface and growing brushes from the fabricated regions. It has been demonstrated that upon exposure to UV light (244 nm wavelength), surface initiators containing a halogen group for radical polymerization can be deactivated.⁷¹ Ahmad *et al.* dehalogenating selective areas and polymerized poly[oligo(ethylene glycol) methyl ether methacrylate] (POEGMA) brushes via ATRP from the unexposed regions.⁷² Patterns in the micrometer range were generated by employing a standard mask in conjunction with the incident laser beam. Polymer brushes with features in the nanometer regime

were achieved by interferometric lithography (IL) utilizing a Loyd's mirror arrangement. Both UV and interferometric lithography techniques produced micro and nanostructured POEGMA brushes and showed resistance to protein adsorption.

Optical lithography was also used by Dong *et al.* to study protein immobilization on patterned polymer brushes.⁷³ A silicon wafer with a self-assembled monolayer of poly(ethylene glycol) (PEG) was patterned using a conventional photoresist in which the exposed regions were etched by oxygen plasma and back-filled with an ATRP initiator. Poly(acrylic acid) (PAA) brushes were polymerized from the fabricated regions and could then be used to covalently attach amino functionalities on biomolecules. These multi-component systems provide the ability to pattern biological molecules with greatly reduced nonspecific adsorption.

Interference lithography (IL) can be used to produce repeating arrays of fine features without use of a photomask and complex, high numerical aperture optical systems. Padeste *et al.* first established the use of this technique by irradiating a polymer substrate to create patterned regions of free radicals.⁷⁴ Radicals in the exposed regions can then be used to initiate the polymerization of methacrylates to produce grafted polymer brushes. Instead of using IL as a bottom up patterning method, Schuh *et al.* have demonstrated that it can be used as a top-down technique as well.⁷⁵ Polymer brushes with azo-benzene moieties have been synthesized and changed conformation upon irradiation with UV light. Results suggest that the motion of the exposed azo dyes creates stresses large enough to rupture the backbone of polymer brush chains leading to the formation of surface relief gratings.

1.2.2. Electron beam lithography

Although optical lithography is a common patterning method, there are disadvantages. If a mask is used, defects in the mask can easily be transferred to the substrate. Additionally, resolution is limited by the wavelength of light used. Decreasing wavelength leads to smaller feature sizes, but advanced tools are required. One option is electron beam lithography (EBL), in which the wavelength is less than a tenth of a nanometer. Despite slow process times and high instrumentation costs, this is the only technique capable of producing sub 20-nm features.

One of the first examples to employ EBL to pattern polymer brushes was demonstrated by Tsujii *et al.*⁷⁶ Using a bottom-up approach, they patterned a monolayer of initiator, 2-(4-chlorosulfonylphenyl)ethyltrichlorosilane, at doses large enough to decompose and thus deactivated exposed regions. Polymer brushes were then grown via ATRP from the unexposed regions to produce fine features. Alternatively, instead of directly exposing the initiator layer, a standard EB photoresist can be used. Chen *et al.* spin coated a HMDS treated silicon wafer with a photoresist and etched the EB patterned regions with oxygen plasma to chemically activate the surface for ATRP initiator immobilization.⁷⁷ After polymerizing PMMA brushes in the patterned areas, the photoresist was removed and the line resolution was analyzed by immersion in tetrahydrofuran (THF) and water. Kaholek *et al.* used a combination of lift-off EBL and UV techniques to create nano- and microfabricated arrays of weak polyelectrolyte brushes.⁷⁸ A PMMA resist was patterned via EBL and a layer of chromium and gold was thermally evaporated on top. The resist was lifted-off leaving behind 31 nm thick Au lines which were then functionalized with a self assembled

monlayer of azo-initiator. Weak polyelectrolyte brushes were then polymerized from the gold surfaces by conventional, UV-light-induced free radical polymerization. Results showed changes in both pH and salt concentration triggered conformational changes. Furthermore the height was also dependent on feature size, which increased with increasing pattern dimensions.

Directly patterning polymer brushes has also been demonstrated. It has been well established that the commonly used EB resist, PMMA, undergoes a backbone chain scission mechanism upon exposure.⁷⁹ This degradation mechanism can be used to pattern other types of positive tone EB methacrylate polymer brushes. Rastogi *et al.* investigated the EB sensitivity of polymer brushes including PMMA, PHEMA, poly(isobutyl methacrylate) (PIBMA), poly(neopentyl methacrylate) (PNPMA), and poly(2,2,2-trifluoroethyl methacrylate) (PTFEMA).⁸⁰ Polymer brushes were grown from a substrate via ATRP and directly patterned using EBL to generate features as small as 50 nm. Results showed that methacrylates able to form a more stable main chain and R' radical, based on chemical moieties at the β-position to the carbonyl group, were more inclined to be electron beam sensitive. Taking this simple patterning approach one step further, Ober and coworkers created subsurface nanochannels using a diblock copolymer brush system (Figure 5).⁸¹ The bottom layer was composed of an EB positive tone PMMA or PHEMA brush, while the top layer was negative tone polystyrene. When the block copolymer system was exposed to EB, the bottom layer underwent a chain scissioning reaction and dissolved away whereas the top layer crosslinked, creating a bridge over the voided regions. The

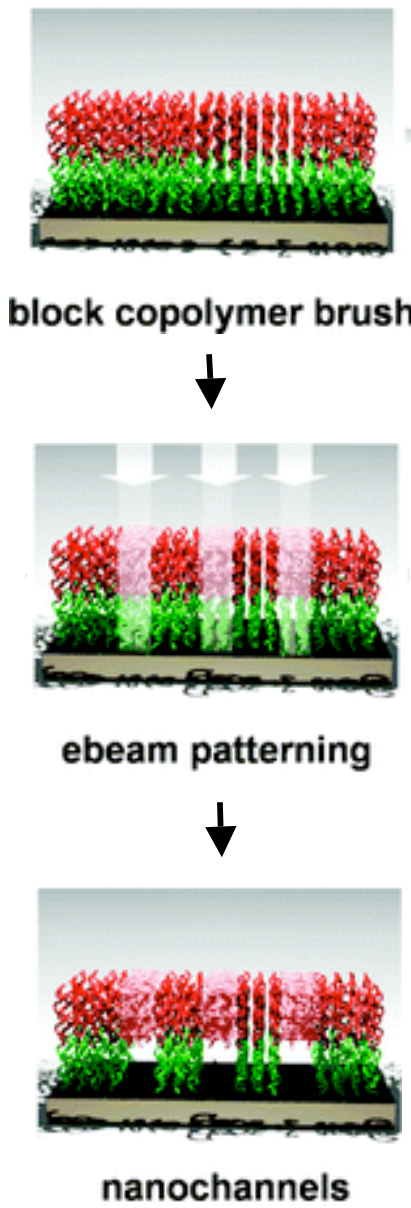


Figure 5. An illustration representing the nanochannel fabrication process. The diblock brush undergoes electron beam exposure and development to generate polymer brush nanochannels. Reproduced from ref. 81, with permission from American Chemical Society.

structural integrity of these nanochannels was found to be associated with select developers. A poor solvent will develop the chain fragments of the sublayer and concurrently keep neighboring chains rigid, hence retaining the bridged structures. A good solvent, on the other hand, will still wash away the small fragments but it will also soften the neighboring chains and lead to structure collapse. Another form of EBL is electron-beam chemical lithography (EBCL) in which a self assembled monolayer of EB sensitive material is directly exposed. The SAM is chemically modified in the irradiated regions such that it can be functionalized with another moiety or it can be used directly as an initiator. Schmelmer *et al.* patterned an initiator layer of 4'-nitro-1,1'-biphenyl-4-thiol (NBT) via EBCL.⁸² Previous reports have shown that electron irradiation of the monolayer NBT reduces the nitro functionalities to amino groups and at the same time cross-links the aromatic biphenyl layer.⁸³ The generated amino groups were then diazotized and coupled with malonodinitrile to produce an asymmetric azo initiator (cAMBT) capable of radical polymerization of vinyl compounds. Steenackers *et al.* showed that instead of functionalizing the amino groups to form cAMBT, self-initiated photografting and photopolymerization (SIPGP) can be performed directly on the irradiated cABT surface.⁸⁴ The selective patterning of this system has two major contributing factors.

First, patterned areas are crosslinked and adhere to the surface, while the unexposed non-crosslinked SAM molecules can be desorbed from the gold substrate by UV irradiation due to the low photostability of thiols on gold. Second, the applied EB dose effects the degree of crosslinking and head group conversion. In general, larger doses produced thicker brush layers.

Other SAMs can be used as primary templates as well. Schilp *et al.* immobilized 11-aminoundecanethiol (AUDT) hydrochloride on gold.⁸⁵ After EB exposure, a surface initiator, bromoisobutyryl bromide (BIBB), was attached to the tail groups and PNIPAM brushes were grown from the surface to thicknesses up to 110 nm. It should be noted, however, that although the majority of unexposed amino groups were deactivated, PNIPAM polymerization of up to 4 nm was observed. The source of the amino deactivator is unknown, but they have shown it can be removed by electron irradiation. Moreover, they also report that the extent of head group conversion/activation can be controlled by the electron dose.

1.2.3. Soft lithography

Not every system requires the precise energy dose control and nanometer resolution as EBL provides. Soft lithographic techniques can also produce micro- and nanoscale patterns, but through a simplified process. Fundamentally, it is a nanomolding process wherein the topography of a stamp or template (typically poly(dimethylsiloxane) (PDMS)) is transferred to a substrate to create patterns with features ranging from 30 nm to 100 μm . Advantages of this process include low costs, high throughput, and simplicity. However there are some challenges, mainly defects in the stamp itself and the transfer of defects to the pattern. PDMS stamp are elastomeric and thus subject to pattern distortion due to their high coefficient of thermal expansion. Regardless, soft lithography, especially microcontact printing (μCP) is one of the most common and often employed methods to fabricate arrays of SAMs on a surface through contact template transfer.⁸⁶⁻⁸⁹

One of the first examples of μCP of SAMs for polymer brush polymerization was

reported by Husemann *et al.* A PDMS stamp was used to microcontact print an inert SAM of $\text{CH}_3(\text{CH}_2)_{15}\text{SH}$ on a gold surface.⁹⁰ The bare regions were then backfilled with $\text{HO}(\text{CH}_2\text{CH}_2\text{O})_2(\text{CH}_2)_{11}\text{SH}$, an initiator that could then be used for surface initiated ring-opening polymerization (ROP) of ϵ -caprolactone. Others have demonstrated the same method can be used to deposit ATRP initiators on gold.²⁸ This allows for a wider variety of monomers and greater control of brush thickness and chemical functionality.

More complex printing systems have been realized by Huck and coworkers.⁹¹ They were able to grow multiple types of brushes to create an intricate array of brush patterns. They first attached a thiol terminated ATRP initiator to a gold surface by microcontact printing and grew squares of PMAA. Chain ends still “living” after polymerization were deactivated via a nucleophilic substitution reaction with NaN_3 . New initiator was then stamped ($5 \times 10 \mu\text{m}$ lines) in bare regions and another brush was grown. This process can be repeated for numerous printing steps and finished by backfilling the remaining unmodified gold surface with initiator to polymerize the final monomer. Not surprisingly, the topography of the stamps requires additional consideration. In order to have bare space after grafting cycles, templates must have small patterns and large spacings.

Instead of a hard stamp, unconventional templates can be fabricated from sources such as microspheres.⁹² Zauscher *et al.* self assembled PS microspheres in highly ordered, hexagonally packed monolayers on a substrate to create a stamp template for direct patterning. The nanospheres are coated with a thiol initiator and brought into contact with a gold substrate in which the initiator is then transferred in a spotted

pattern. Deposited initiator forms a radially symmetric gradient with greater density at the center than at the periphery due to diffusion. Cone-shaped brush microstructures were produced and the morphology could be fine tuned by altering the microspheres diameter, printing contact time and printing contact load. The stamping process itself can also affect the structures of polymer brushes. The same group also explored “dynamic μ CP”, a strategy in which the stamp is moved or jumped during the printing process (figure 6).⁹³ They found that by sliding a stamp coated in an initiator ink across a surface, gradient brushes can be produced. This result is due to a difference in contact-time from the moving start region to the moving end region during stamp propagation, where the ending areas have a greater initiator density. Additionally, by lifting the stamp and moving to a new location while keeping contact time constant for each jump, polymer brushes of comparable heights were observed. This suggests that multiple reprints are still able to transfer the same amount of initiator to form similar SAM densities.

Li *et al.* used PS microspheres to pattern surfaces for polymer brush growth, but instead of coating the microspheres with initiator they were used as a mask.⁹⁴ PS colloidal crystals were packed over a surface of ATRP initiator and etched by O₂ plasma to slowly decrease the diameter of the microspheres until ATRP molecules below them are also etched. Removal of the etched PS colloidal crystals reveals patterns of the initiator in highly ordered arrays with feature sizes down to 100 nm. By adjusting the etching time and thus the spacing between patterned regions polymer brushes of different morphologies can be produced, namely joint, isolated and transition state.

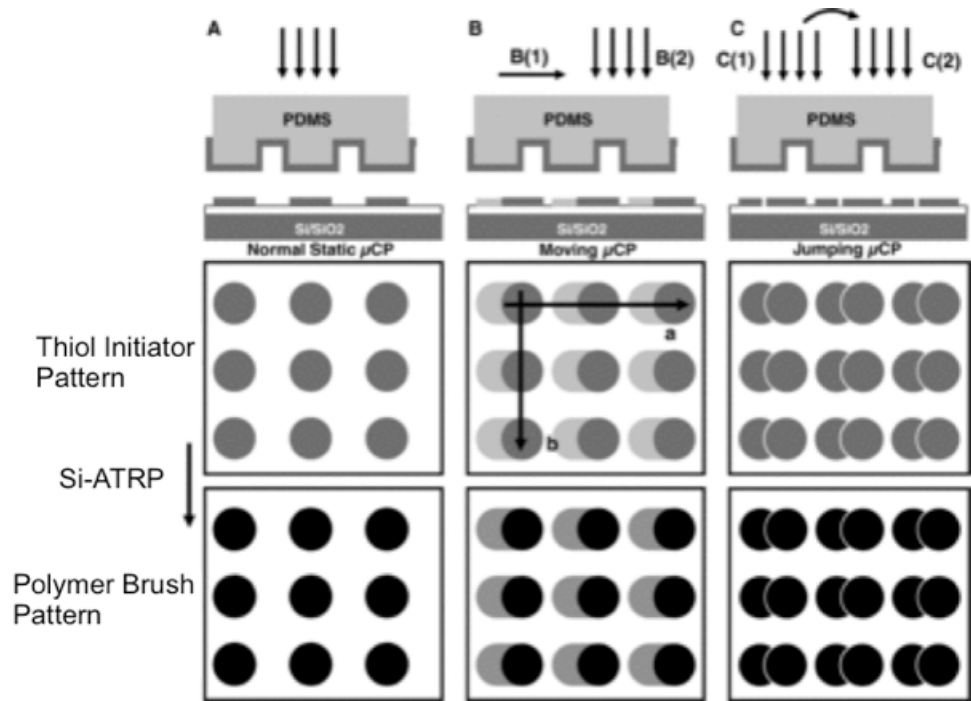


Figure 6. Schematic illustrations showing the main steps involved in various μ CP of initiator patterns and their subsequent amplification into patterned polymer-brush microstructures by SI-ATRP. A) Normal μ CP: printing an inked stamp with a gentle force. B) Moving μ CP: placing an inked stamp on gold surface with subsequent moving (B-1) and printing under normal μ CP conditions (B-2). C) Jumping μ CP: normal printing (C-2) following a normal printing (C-1) after a raised and replaced stamp on the surface. Reproduced from ref. 93, with permission from John Wiley and Sons.

1.2.4. AFM lithography

Although atomic force microscopy (AFM) is a common method of polymer brush characterization, it has also been employed in different approaches for patterning purposes. Conventionally AFM is used in tapping mode to analyze brush surfaces; however, by switching to contact mode the tip can be scanned under strong loading forces to remove SAMs of initiator. Referred to as nanoshaving, elevated local pressure results in a high shear force which causes the displacement of thiol resist on a gold surface to create patterns. This technique can be carried out in air or in solvent.

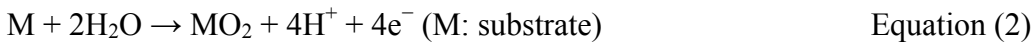
Nanografting is essentially the same, except it is performed a solution containing a reactive molecule that will self assemble on the newly scratched areas.⁹⁵ Nanoshaving has been employed by applying large normal forces (~50 nN) and high scan speeds (~20 $\mu\text{m}/\text{s}$) to remove resist and backfilling with an ATRP thiol initiator to form patterned parallel lines which can polymerize vinyl monomers.⁹⁶ By increasing loading forces it has been demonstrated that polymer brushes themselves can be removed by AFM lithography. Studer *et al.* investigated the difference between nanoscratching polymer brushes versus spin coated polymer films. Results indicated better resolution was possible with the brushes because chains in the vicinity of the scratched areas are covalently attached and could not be dragged along with the moving tip, unlike the spin-coated films.⁹⁷ They also applied this technique PS and poly(n-butyl acrylate) (PNBA) brushes of thicknesses greater than 40nm to test their protein repellent properties.⁹⁸ Loading forces of about 22 μN reproducibly produced patterned features down to 200 nm.

Another form of AFM lithography is dip-pen nanolithography (DPN). In this case, the AFM tip is considered the “pen”, molecules or initiator as “ink” and a surface is the “paper”. Patterns are generated by capillary transport of the molecules on the tip to the surface.⁹⁹ This initiator deposition technique has been demonstrated on various surfaces and shown to then polymerize brushes via methods such as ROMP¹⁰⁰ and ATRP.¹⁰¹ Instead of directly grafting initiator molecules, others have taken a different approach and deposited gold nanowires and subsequently grow brushes from the fabricated platforms. Zapotoczny *et al.* used DPN to transfer AuCl^{4-} to a hydrogenated silicon surface which could then be reduced to metallic gold to produce sub-20nm wide lines.¹⁰² Disulfide iniferters were immobilized on the fabricated templates and used to initiate PMAA growth via photopolymerization.

DPN has proven to be a fast, simplistic technique that has the ability to produce patterned features on the subnanometer scale. However there are some drawbacks that are sometimes associated with this method. First, the diffusion rate of the transferred molecules on the surface is difficult to control and can vary between types of initiator. Second, some initiator molecules are quite volatile and can be distributed to other regions of the surface through the air. One way to resolve these issues is through a combination of nanografting and DPN, termed dip-pen nanodisplacement lithography (DNL). Just like nanografting, an inert SAM is used which will act as a protective layer against stray initiator contamination. AFM tips are inked with activated initiator molecules and dragged along the surface of inert SAMs, cleaving them away. While the SAM molecules are being removed, the initiator molecules can then fill into the cleared areas and attain “nanodisplacement”. Zheng *et al.* used this approach to

patterned brushes down to feature sizes of 25 nm.¹⁰³ They reported this method showed limited diffusion and could be used for patterning volatile molecules in the air. Additionally, results showed the grafting density of the patterned molecule is force-depending, suggesting surface control that can be tuned at a molecular level. In order to increase throughput, they took the concept of DPL one step further and developed parallel dip-pen nanodisplacement lithography (p-DNL).¹⁰⁴ p-DNL is the same as DNL but with multiple cantilevers that simultaneously remove inert SAMs while depositing initiator molecules (Figure 7). Using an 18-tip array, they report reproducible structures between tips with deviations less than 10 nm laterally and 5 nm vertically.

Patterned polymer brush structures have also been generated from AFM anodization lithography. AFM anodization is a scanning probe lithography (SPL) technique in which a biased voltage is applied to the tip which causes an oxidation reaction process on the surface.^{105,106} Water from the atmosphere is absorbed on the surface between creating an “electrochemical cell”. The electrochemical reactions taking place on the surface are shown in Eqs. (1) and (2)



Depending on the intensity and length of time of the applied voltage, a monolayer of acid groups or growth of silicon oxide on the surface is possible. Other factors

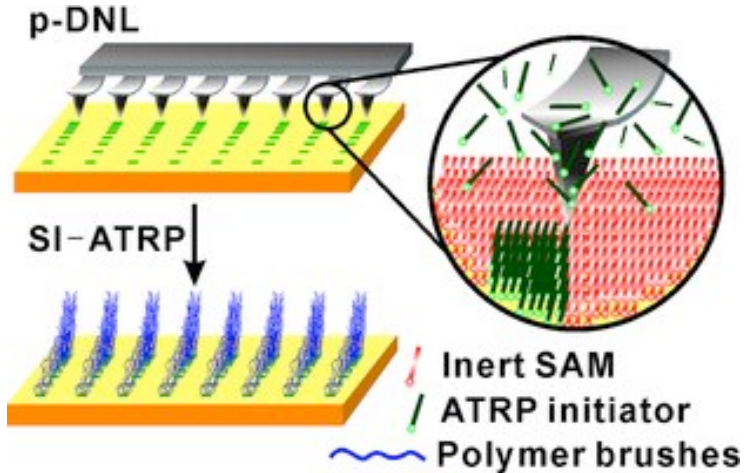


Figure 7. Schematic illustration of the large-area, parallel fabrication of 3D polymer brushes by p-DNL and SI-ATRP. Reproduced from ref. 104, with permission from John Wiley and Sons.

affecting influencing the process include geometry of the AFM tip, applied voltage amplitude, relative humidity, patterning speed, and electronic state of tip and surface material. Lee *et al.* attached a Grubbs catalyst to anodic oxide patterns generated by this process on silane resist coated silicon substrates.¹⁰⁷ From the metathesis initiator, ROMP was carried out on two olefin monomers, cyclooctatetraene (COT) or 5-ethylidene-2-norbornene (ENB). Polymerization in both the liquid and vapor phase produced brush feature sizes around 200 nm and up to 5 nm thick; however some contamination was observed which may be attributed to catalyst attachment to defects in the resist layer.

1.3. Detached polymer films

The majority of polymer brush applications utilize the feature of covalent attachment of the chains to the surface. This aspect provides a robust, stable surface ideal for patterning, functionalization and harsh characterization procedures, but there can also be eminent value in detaching these coatings. Ultrathin polymer films have been a prevalent field of study for practical interests concerning microfluidics, ultrafine filtration, and microelectronics.¹⁰⁸⁻¹¹⁰ Common preparation techniques include layer-by-layer (LbL),^{111,112} Langmuir-Blodgett,¹¹³ self assembly,¹¹⁴ and cast films¹¹⁵ however recent studies have shown detaching polymer brushes to be a means that can offer control and tunability. One novelty of this approach is the potential to gain fundamental knowledge of the structure and properties of polymer brushes experimentally. Theoretical studies have modeled and calculated the strain and stretching associated with the polymer brush chains in their extended form. In high grafting density systems, polymer chains develop a balance between the interaction

energy of the statistical segments (F_{int}) and the elastic free energy (F_{el}). By stretching away from the surface, chains can lower their neighboring interaction energy, but at the price of a high elastic free energy. The thickness of a polymer brush is therefore dependent on the equilibrium of these two factors. A simplified equation using the Alexander model¹¹⁶ for the free energy of per chain is given as

$$F = F_{\text{int}} + F_{\text{el}}$$

A more in depth analysis for free energy can be derived using the “Flory approximation” which estimates the reduction in entropy from results for an ideal random walk chain constrained to travel L from the surface to the outer edge of the polymer brush.^{12,117} For this model the free energy per chain is expressed in the following equation:

$$\frac{F}{kT} \approx \frac{v\varphi^2 d^2 L}{a^3} + \frac{L^2}{R_0^2}$$

where v is a dimensionless volume parameter, d is the average distance between two anchored points, a is the diameter of the polymer segment, and R_0 is the radius of an ideal coil. A key aspect of these theoretical expressions is that the equilibrium thickness of the polymer brush varies linearly with the degree of polymerization, which signifies a deformed chain configuration. Regardless of solvent conditions (good, theta, or bad solvent) and unlike free polymers in solution, this significant characteristic of tethered chains establishes the foundation of polymer brush behavior.

Thus far, there are two different approaches to creating detached polymer brush films. First, a crosslinked sublayer can be fabricated from which brushes are grown

directly and after removal the free energy per chain remains unchanged. Alternatively, brushes can be directly detached from the surface in which case chain relaxation does affect the free energy per chain.

1.3.1. Crosslinked sublayer

Sublayers of just a few nm thick can be crosslinked and functionalized with an initiator that will polymerize polymer brushes directly from the surface producing what is often termed “polymer carpets”. By fabricating a crosslinked sublayer, the polymer brushes themselves do not have to be crosslinked in order to maintain mechanical stability of the film. Depending on the system and application, this could be very beneficial due to greater sensitivity and reactivity of uncrosslinked brushes towards external stimuli. One of the first examples of polymer carpets was reported by Amin *et al.* who irradiated a SAM of biphenyl via electron-beam to generate a crosslinked support film with available amino group moieties on the surface (Figure 8). PS, poly (4-vinyl pyridine) (P4VP), and PMMA were then subsequently grown from the surface through self-initiated surface photopolymerization and photografting (SIPGP).¹¹⁸ Increasing brush thickness, regulated by longer polymerization times or higher electron-beam doses¹¹⁹, produced films with greater buckling amplitude. Results showed the brush morphologies were reversibly responsive to external triggers (solvent and pH) and demonstrated buckling and changes in film properties (optical, wetting). Additionally, both positive and negative resist properties of the aromatic framework can be used to fabricate patterned polymer carpets.¹²⁰

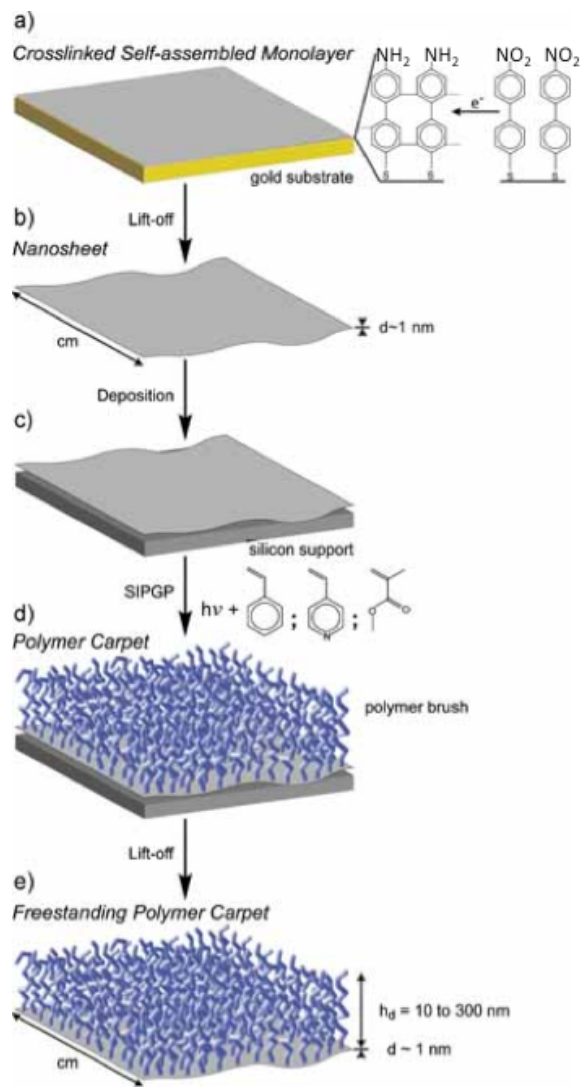


Figure 8. Scheme of the preparation of polymer carpets. a) A crosslinked cABT SAM is prepared by electron irradiation of NBT and b) detached by dissolving the gold substrate with a KI/I_2 solution. c) The nanosheet is deposited on a silicon substrate with thin silicon oxide or silicon nitride layer. d) Supported polymer carpets are obtained by SIPGP of a vinyl monomer (styrene, 4VP, or MMA). e) Freestanding polymer carpets are obtained by dissolving the underlying layer (Si_3N_4) with HF. Reproduced from ref. 118, with permission from John Wiley and Sons.

Graphene has also been investigated as a possible polymer brush support film due to its excellent mechanical, optical, structural, thermal and electrical properties. This two-dimensional (2D) material has been extensively investigated and used for a broad range of applications including biosensors. However care must be taken when covalently functionalizing the surface because conversion of the sp^2 to sp^3 -carbon hybridization often leads to a decrease in electrical transport. Attachment of chemical moieties must be balanced with a certain level of carrier mobility. It has been demonstrated that SIPGP can be carried out on basal plane graphene defects where hydrogen atoms are available for abstraction to generate radical initiation sites.^{121,122} Raman spectroscopy showed brushes were polymerized from defect sites while other measurements verified the electronic properties of the graphene were retained after photopolymerization thus establishing its potential as a support layer. In addition, remote hydrogen plasma treatment can be applied to enhance defect density and regulate the concentration of surface-bound hydrogen and thus brush grafting density. Single layer graphene was vapor deposited on Cu foil and PS was grown from the surface via SIPGP. The Cu foil was etched to produce free-standing polymer brush graphene carpets which are stable enough to transfer. Although the grafting of PS was reproducible and controllable, no polymerization of methacrylates was observed. The reason(s) for this selectivity is unknown; however, by copolymerizing styrene with acrylic monomers this limitation can be circumvented to a certain extent.

Support layers don't have to be comprised of a crosslinked network in order to maintain integrity and stability of a detached brush film. Layer-by-layer (LbL) is a thin film deposition technique based on electrostatic interactions in which a surface is

primed with an initial charge and alternating layers of oppositely charged materials are assembled. Polyelectrolytes with ATRP moieties have been synthesized and used as macroinitiators for surface-initiated polymerization of polymer brushes from the charged surfaces.^{123,124} Advincula and coworkers have explored these systems to generate free-standing polymer brush films and have demonstrated two possible means of detachment.^{125,126} First, they used cellulose acetate (CA) as a sacrificial layer because it carries a negative charge and thus polyelectrolyte ATRP macroinitiators can be assembled. The LbL brush film fabricated on top of the CA can be detached by immersion in an acetone solvent for a period of time. Although the CA is dissolved enough to detach the films, results indicate some is still leftover and perhaps longer incubation times may be required for complete dissolution. A second lift off approach incorporated drop-casting a solution of poly(vinyl alcohol) (PVA) on the LbL brush film and pealing the entire coating off the surface after drying. The LbL brush film could then be recovered by dissolving the PVA in water. In both cases brush morphology and opacity was investigated in response to select solvent conditions as well as structural rigidity.

Ohm *et al.* have also investigated using PVA to lift off brush membranes, but as the sacrificial layer instead of a peelable coating.¹²⁷ PVA was spin coated and functionalized with an ATRP unit, bromo isobutyrylbromide, and PS brushes were grown from the ATRP initiator. The brushes were patterned in order to expose edges of the PVA layer to the surroundings for film release in water. Similar to CA, a layer of PVA was observed on the film after lift-off that was associated with its chain length, specifically the higher the molecular weight of the PVA the thicker the

remaining layer. This can be explained from a couple viewpoints. First, the PVA is acting as a macroinitiator in which they brushes are covalently bound and second there is likely a strong entanglement effect where the PS chains act as nails, holding the PVA chains together and preventing them from detangling. In effect, the PVA is acting as a crosslinked nanolayer much like the irradiated biphenyl support layer mentioned earlier.

1.4.2. Free membranes

Fabricating a detachable sublayer to generate polymer brush carpet films allows for the brushes to be preserved in their natural, stretched state. The responsive features of brushes can be investigated and tuned in response to external stimuli for specific applications. However, there are also advantages of detaching brushes such that they are free-standing films with no nanofilm sublayer. In this case, information regarding the nature of the brush chains can be analyzed. Many theoretical studies have investigated and calculated the strain polymer brushes experience, but we are now just starting to experimental data that can shed some light on the subject.

One of the first examples of brush detachment was reported by Huck *et al.*¹²⁸ ATRP thiol initiators were immobilized on patterned gold surfaces and PGMA brushes were grown and chemically crosslinked. Electrolysis was performed in which the gold was the cathode and a short pulse was applied to weaken the gold-thiol bond thus generating buckling patterns (Figure 9). Buckling patterns were found to be dependent on the shape of the patterned gold electrode and it was theorized these observations were due to relief of internal stresses introduced to the chains during brush growth. Once the anchor point is disconnected, a chain will assume a more

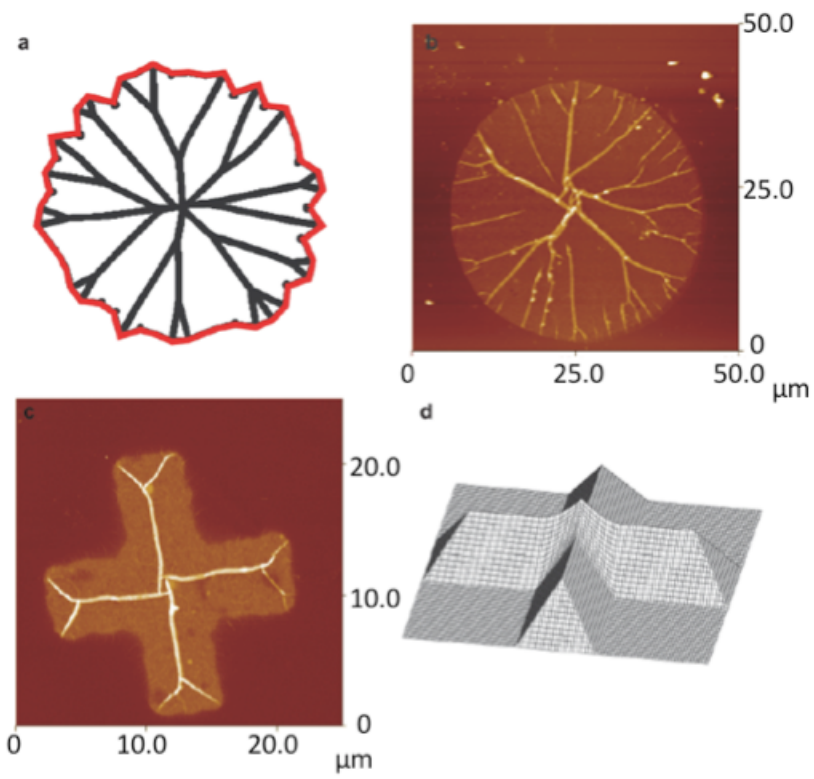


Figure 9. a) Ridging pattern for a circular object with a slightly irregular outline, predicted using the algorithm detailed in the text. b) AFM image of a 40 μm wide, 15 nm thick polymer circle after electrolysis (z -scale: 200 nm). c) AFM image of a 20 lm wide, 24 nm thick polymer cross after electrolysis (z -scale: 200 nm). d) 3D representation of the predicted blister shape for the object in (c) before blister collapse. Upon collapse, ridges will form at discontinuities in the height profile. Data was obtained from the algorithm detailed in the text. Reproduced from ref. 128, with permission from John Wiley and Sons.

entropically favorable coil conformation thus relaxing in the z-direction and leading to lateral expansion, known as buckle-driven delamination.¹²⁹ They note that delamination is independent of starting location but proceeds until reaching an edge at which point it remains pinned to the surface. The buckled film creates a “dome” where the eigen strain is taken into account such that the chains arrange to minimize the elastic energy in the overall film. Once detached, the film begins to collapse back to the surface where the final buckling dimensions are determined by the balance between the interface energy of the film/gold contact and the strain energy. This technique is not limited to PGMA, but can be utilized in studying buckling properties and dimensional analysis of other organic films.

Welch *et al.* have also developed an approach to detaching free standing polymer brush membranes both crosslinked and uncrosslinked.¹³⁰ Polymer brushes were grown from a silicon oxide layer via ATRP and subsequently etched off using hydrofluoric acid (HF). The oxide layer provides a surface identical to a conventional silicon wafer used in polymer brush growth, and thus unlike the PVA system we are not limited to the type of brushes that can be grown. Applying an HF solution etches away the oxide layer allowing the polymer brush film to lift off undamaged. Similar to the buckling system mentioned above, chain relaxation was also observed as the membranes expanded in the lateral direction. Going one step further, this approach was then implemented for membrane crosslinking analysis. Lithographic (UV crosslinked) and chemical crosslinking (KOH and triflic acid) methods were investigated and compared to the uncrosslinked films. Results indicated that application of a crosslinking process produced films that retained shapes closer to that

of the original pattern dimensions. Thus by detaching polymer brush films from the surface and analyzing the expansion or retention of the patterned regions, the efficiency of various crosslinking techniques can be explored.

1.4.3. Characterization of detached brush films

Common characterization techniques for polymer brushes include water contact angle, ellipsometry, fourier transform infrared spectroscopy (*FTIR*), and AFM. However contact angle, ellipsometry, and FTIR are all methods that average over a large area and provide little detailed information. AFM does give more detail, but it is limited to surface analysis. Therefore, by detaching polymer brushes from the surface additional forms of characterization can be carried out. Of the detachment procedures detailed above numerous analysis methods were employed. The micromechanical and robust behavior of the polymer carpets grown from the crosslinked monolayer were examined using a bulging test. Gölzhäuser's group constructed a pressure cell consisting of a rectangular window where samples were mounted and pressure from both sides could be applied. The pressure deflection response was then measured by AFM and the collected data was fitted to give the Young's modulus and the film's residual stress at zero pressure. Taking into account the added effect of the crosslinked biphenyl sublayer, values of the elastic modulus for PS carpets with various thicknesses were in agreement with previous reports on tethered PS brushes. This approach to analyze mechanical properties of polymer brushes may lead to greater understanding of the brush morphology and the effect of features such as thickness.

Ohm used scanning electron microscopy (SEM) to characterize the patterned PS

nanosquares once freed from the surface. The contrasts between PVA and PS in the SEM images clearly show the deformation resulting from changes in the polymer layer(s) thickness. Of the released films, a few retained their original flat square shape, but the majority folded or rolled into three-dimensional particles, mainly triangles and tubes. This may be because the PVA still contains large amounts of free alcohol groups which cause the sub-layers to swell during lift-off. After drying, the PVA layer shrinks while the PS part remains unchanged, resulting in a rolling or bending deformations.

To characterize the polymer brushes released by HF etching, we employed transition electron microscopy (TEM). By viewing these membranes via TEM, fine detail and contrast information can be generated and modeled to the first approximation by Beer's law. The superior sensitivity and contrast formation data from this technique provides novel characterization of polymer brushes such as membrane homogeneity. Our results showed some of our films were not homogeneous as expected, but instead were "patchy" with regions of lower and higher density. These brushes were produced when the initiator was immobilized at lower concentrations. When the concentration was significantly increased, the membranes became homogeneous and uniform. These results suggest the initiator immobilization process follows an island formation mechanism, in agreement with previous reports of SAM immobilization. Previous studies have reported that at room temperature, self assembled monolayers will form island domains that nucleate in the plane of the surface.¹³¹⁻¹³⁴ We observe similar results that consequently transfer to the polymer brushes being produced. The coverage density of the polymer brushes is dependent on

the initiator coverage. Therefore by examining our samples via TEM bright field mode, we can acquire information regarding our initiator deposition and brush regime (patchy or homogeneous).

1.5. Electrochemical Biosensors

Electrochemical sensing has recently emerged as a powerful method for quantitatively studying biological events and has attracted considerable interest from scientific, technological, and medical communities.¹³⁵ An electrochemical biosensor typically consists of two elements: a biochemical recognition component and a physical transducer which converts a primary biological or chemical response to an electrochemical signal. Bound biological elements such as antibodies, enzymes, microorganisms and selected cells catalyze reactions or binding events that produce a transfer of electrons (current) or can alter the ion activity (charge accumulation). Such changes in solution can be measured by various methods including potentiometry, conductometry, and amperometry. Potentiometric devices measure an electrostatic potential or charge accumulation, conductometric devices measure ionic strength and thus the conductive properties of a solution, and amperometric devices measure current. Compared to traditional analytical techniques, these electrochemical methods are relatively inexpensive, simple, require short acquisition times, and can easily be reduced to nanoscale dimensions and incorporated into various device geometries. However, amperometric systems have been shown to be the most economical and most sensitive to date.¹³⁶

Several electrochemical techniques such as voltammetry, chronoamperometry, and

electrical impedance spectroscopy (EIS) have been particularly effective tools in probing biological activity.¹³⁷ Of these, cyclic voltammetry (CV), a form of amperometry, is the most common and widely used method for studying biological redox activity and rates.^{138,139} By applying a forward and reverse bias between two designated values at a fixed rate, the electrochemical potential can be plotted *vs.* the resulting current and information can be obtained for the forward and reverse reactions.¹⁴⁰ Shan *et al.* used cyclic voltammetry to detect the quasi-reversible electron transfer between glucose oxidase and an underlying glassy carbon electrode via colloidal laponite nanoparticles.¹⁴¹ To imitate metal-mediated DNA damage *in vivo*, Wang *et al.* used CV to measure the catalytic current of Ru(NH₃)₆³⁺ as an application for a sensor that can gauge the genotoxicity of chemicals.¹⁴²

Despite the broad application of electrochemical methods, these techniques typically suffer from poor selectivity and interference from highly buffered solutions.¹⁴³⁻¹⁴⁶ Obstruction from other compounds in the sample matrix can be avoided by adjusting the potential, sample dilution, and target molecule immobilization or trapping. Immobilizing a biochemical reagent not only requires the functionalized surface to efficiently transport electrons, but the surface must also be resistant to fouling and background interferences. Wang *et al.* modified a poly(dimethylsiloxane) (PDMS) microchip with chitosan-g-mpoly(ethylene glycol) (mPEG) that was coupled with end-channel amperometric detection with a copper electrode. Their device showed resistance to nonspecific absorption and separated biomolecules quickly and effectively.¹⁴⁷

To improve detection limits, many research groups have used electrodes coated

with conducting, non-conducting, natural, and ionic polymers.^{148,149} Coatings can provide properties such as immobilization, nonspecific absorption, electron exchange, redox recyclability, and biocompatibility. For example, glucose sensors detection limits have increased from 1-20 μM ¹⁵⁰⁻¹⁵² to $2.5 \times 10^{-3} \mu\text{M}$ ¹⁵³ by using polymer interfaces such as ferrocene-containing polythiophene derivatives. Miao and Bard reported an ultrasensitive DNA hybridization detection method based on electrogenerated chemiluminescence (ECL) using polystyrene beads.¹⁵⁴ Bard's group has shown that graphite or platinum electrodes coated with specific polymer films using electrodeposition or dip-coating may be used to detect redox mediators on the surface.¹⁵⁵

1.5.1. Advantages of Polymer Brushes for Biosensors

Most biological systems have a tendency to physically adsorb onto a solid substrate without specific receptor-recognition interactions (non-specific adsorption).^{156,157} This non-specific interaction typically reduces the functionality of the biosensor. In the case of electrochemical sensors, this typically leads to electrode fouling. Non-specific adsorption of bioactive species on the sensor surface also produces undesirable features such as “false positives” and “false negatives” that render the biosensor unreliable. Therefore, much effort has been directed toward creating surfaces with enhanced specific adsorption and reduced non-specific adsorption.

It has been shown that self-assembled monolayers (SAMs) of poly(ethylene glycol) (PEG) or oligo(ethylene glycol) (OEG) prevent nonspecific absorption.

However, shorter chain lengths lead to a decrease in surface efficiency.¹⁵⁸⁻¹⁶¹ Accordingly, the increased thickness of polymer brushes containing PEG moieties provides longer protein resistance and device lifetime, even in cell culture media.^{101,162-166} The high grafting densities associated with polymer brushes also provide increased binding capacities, which allows lower detection limits to be reached.¹⁶⁷

Andruzzi *et al.* prepared OEG-containing styrene-based homopolymer and block copolymer brushes on silicon oxide surfaces and characterized these films for protein adsorption.¹⁶⁶ They showed that protein absorption and cell binding was significantly reduced on surfaces functionalized with polymer brushes containing short OEG side chains in comparison to assemblies of only short OEG chains. This result can be attributed to greater thickness and surface coverage of the polymer brushes with respect to self-assembled monolayers (SAMs). Additionally, Langmuir-Blodgett techniques have been used to deposit ultrathin films of different ionomeric polymers on glassy carbon, gold and indium-tin oxide electrodes. These coated electrodes showed ion-exchange-preconcentration capabilities useful for ion-exchange voltammetric applications.^{168,169} More recently, Rastogi *et. al.* used electrochemical methods to demonstrate that poly(acrylic) acid brushes grown from an OEG containing ATRP initiator were very effective in suppressing non-specific adsorption of antibodies on gold surfaces.¹⁷⁰ They used cyclic voltammetry and quartz crystal microbalance (QCM) experiments to demonstrate that the non-specific binding of antibodies can be reduced significantly while using gold electrodes coated with polymer brushes.

Polyelectrolyte brushes have recently become the subject of much research due to their capability of switching between a swollen and shrunken state in response to pH changes. This pH-sensitivity has broad applications in sensing, purification, tunable drug release, and stimulus-responsive surfaces.^{124,171} Dong *et al.* provided one of the first experimental demonstrations of charge fraction variation within weak poly electrolyte brushes. Namely, she synthesized weak polyelectrolyte brushes of poly(acrylic acid) (PAA) and poly(methacrylic acid) (PMMA) on gold substrates to investigate the charge fraction at different pH values.¹⁷² FTIR titration results showed a large difference between pK_a^{bulk} and pK_a^{surface} brush values for both PAA and PMMA (pK_a^{bulk} between 6.5 and 6.6 for PAA and 6.9 and 7.0 for PMMA; pK_a^{surface} is 4.4 ± 0.01 for PAA and 4.6 ± 0.1 for PMMA). Therefore, acid groups further away from the gold surface have smaller pK_a values and are more easily ionized (Figure 10). These brush qualities can play important roles in studying the charge sensitivity of biological interfaces with biomolecules, cells, enzymes, and tissues.

1.5.2. Polymer Brushes in Electrochemical Sensors

In many biological systems, electrochemical techniques are becoming a popular alternative for probing catalytic reactions, enzyme recognition and small molecule detection.¹⁷³⁻¹⁷⁵ Depending on the properties and activity of the biological molecule being studied, electrochemical probes can easily be tuned to meet the specific demands of the experimental conditions and systems.

Tam *et al.* have employed polyelectrolyte properties to prepare brushes that electrochemically induce the reversible conversion of an electrode interface between

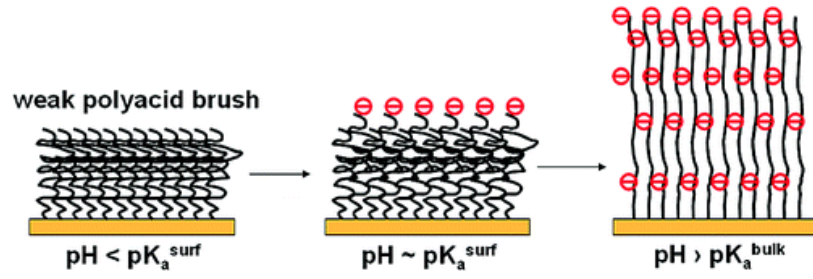


Figure 10. Degree of dissociation and swelling behavior of weak PAA brushes in solution at different pH values. Reproduced from ref. 172 with permission from the American Chemical Society.

an active and inactive state.¹⁷⁶ Poly(4-vinylpyridine) (P4VP) brushes were prepared and grafted to indium tin oxide (ITO) coated electrode surfaces. At pH values around 4.5, the pyridine functional groups became positively charged to yield a hydrophilic swollen state. When pH values increased to 9.1 the neutral pyridine groups resulted in hydrophobic polymer brushes that collapsed into monolayers of pinned micelles (Figure 11). The swollen “ON” state allows for anionic species such as $[Fe(CN)_6]^{4-}$ to permeate through the polymer brush and undergo an electrochemical redox process at the electrode surface. When the brushes are collapsed, the electrode is in the “OFF” state and anionic species are blocked from the interface. By applying a small voltage to reduce oxygen near the substrate surface, the pH can be adjusted enough to switch the polymer brush from a hydrophilic state to a hydrophobic state. The reverse is then achieved by stirring the solution or by slow diffusion exchange with the bulk solution. Tam *et al.* predict their electrochemically switchable electrode surface has future applications in enhancing selectivity and biocompatibility of biosensors and implanted drug delivery devices. Polymer brushes with pH-sensitivity have also been used in an enzyme-based biofuel cell. Amir *et al.* showed the reversibility of a poly(4-vinylpyridine) (P4VP) polymer brush modified with an Os-complex redox species on a ITO electrode.¹⁷⁷ When the pH was < 4.5 the polymer brushes were in a swollen state and the electrode was activated for oxygen reduction; however, when the pH was > 5.5 the polymer brushes were in a shrunken state, thus inhibiting the electrochemical process of the Os-complex. CV confirmed the activated or muted state of the electrode based on the reduction of O_2 . The environment was controlled by external enzymatic systems linked with Boolean logic AND/OR operations to facilitate

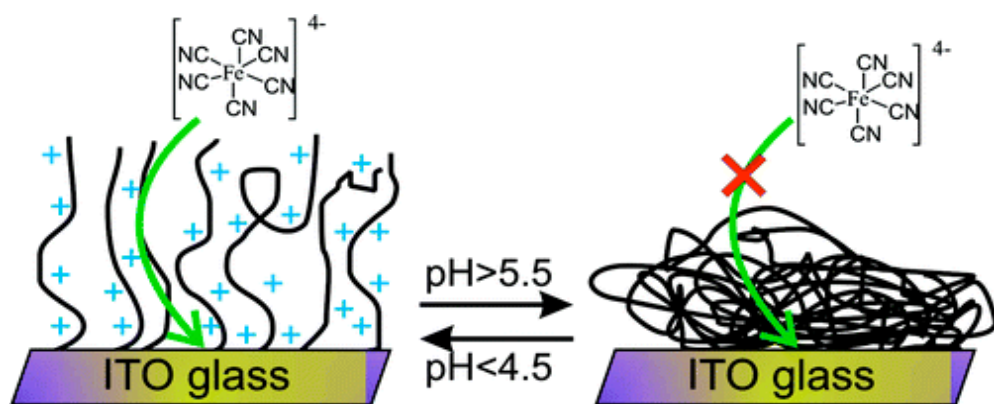


Figure 11. ON/OFF state of poly(4-vinylpyridine) brushes as result of pH change and permeability of anionic reducing species. Reproduced from ref. 176 with permission from the American Chemical Society.

biochemical signals that lead to a change in pH. Specific biochemical signals were selected to activate the biofuel cell by decreasing the pH while other signals switched the cell to the OFF state by increasing the pH to around 6.0. Amir *et al.* suggest that their enzyme logic operations may be coupled with any bioelectrocatalytic process directed by a pH-switchable electrode to create a fully functioning implantable device. Through biochemical reactions, the device can produce electrical power on-demand according to physiological needs.

The same concept of pH-sensitive brushes was employed for the study of the redox protein cytochrome c (Cyt c). Zhou *et al.* electrochemically polymerized PAA brushes on a gold and used a dip-coating technique to immobilize Cyt c.¹⁷⁸ In slightly basic conditions, Cyt c adheres to the PAA brushes due to its positive charge below pH 10. In acidic conditions, however, Cyt c does not adhere to the fully protonated PAA brushes and is hence free in solution. This behavior, as well as the film coverage of Cyt c has been measured by CV and EIS. This reversible immobilization approach may have applications in protein separation, biosensing and future possibilities in artificial models of biological redox systems.

An example of an electrochemical antibody sensor is reported by Rastogi *et al.*¹⁷⁰ Using amperometric methods, their system detects antibodies in a solution assay based on the antibody catalyzed water oxidation pathway (ACWOP)¹⁷⁹ which eliminates the need for labeled secondary antibodies (Figure 12). Gold electrode surfaces are coated with PAA brushes modified with an oligo(ethylene glycol) (OEG) ATRP initiator (to prevent non-specific absorption) and end functionalized with 2,4-dinitrophenyl(DNP)-antigen.¹⁷⁰ The DNP-antigens bind DNP-antibodies which produce hydrogen peroxide

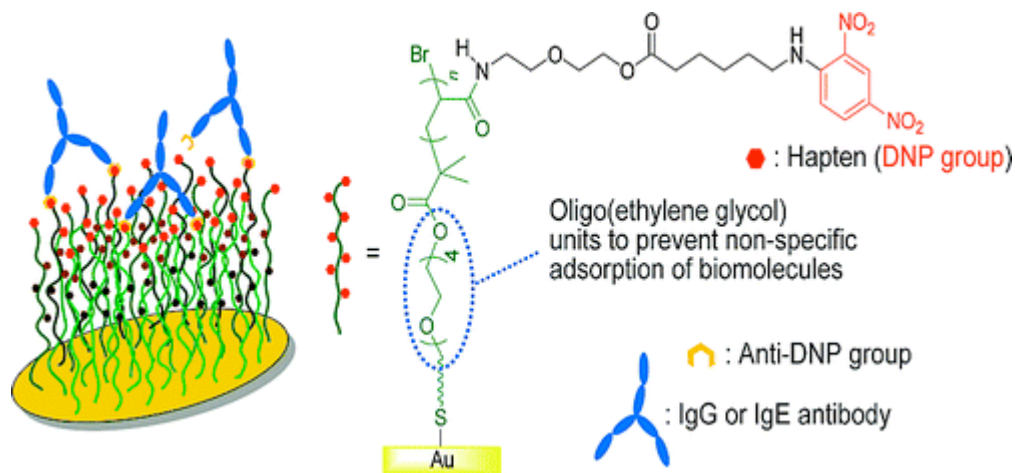


Figure 12. Representation of the quantification of antibodies on DNP functionalized PAA brush modified gold electrode. Note this illustration is not drawn to scale. Reproduced from ref. 170 with permission from the American Chemical Society

(H₂O₂) through the ACWOP process by intercepting singlet oxygen (¹O₂) generated by the photo-oxidation of riboflavin. The production of H₂O₂ irreversibly oxidizes Amplex Red (N-acetyl-3,7-dihydroxyphenoxazine) in the solution assay to resorufin (7-hydroxy-3H-phenoxazin-3-one), a stable and electroactive redox mediator.¹⁸⁰ Resorufin can then be electrochemically reversibly reduced to dihydroresorufin and the current measured by CV indicates the initial amount of H₂O₂ and thus the number of antibodies bound to the brushes. According to Rastogi *et al.*, the PAA brush system can also be functionalized with different antigens for detecting a variety of viruses such as the avian influenza or swine flu species.

A device reported by Patel *et al.* uses differential pulse cathodic stripping voltammetric analysis (DPCSV) for the detection of uric acid (UA).¹⁸¹ They grafted molecularly imprinted polymer (MIP) brushes of poly(melamine-co-chloranil) on sol-gel modified graphite electrodes to resolve non-specific binding from cross-reactivity and matrix effects. Through multiple hydrogen bonding interactions, the terminal chl moiety of MIP has been shown to bind UA (Figure 13). The quasi-reversible electrochemical oxidation of UA (dication) followed by cathodic stripping generates DPCSV signals that are able to detect UA concentrations down to 4.10 μ g \times mL⁻¹. Currently, this detection limit satisfies the requirement to diagnose hyperuricemic patients.

Similarly, Prasad *et al.* also used DPCSV along with a homemade solid-phase microextraction (SPME) fiber for dopamine (DA) detection.¹⁸² MIP brushes of poly(melamine-co-chloranil) were “grafted to” a sol-gel matrix attached to a poly(methyl methacrylate) (PMMA) optical fiber. Unlike UA, dopamine is bound

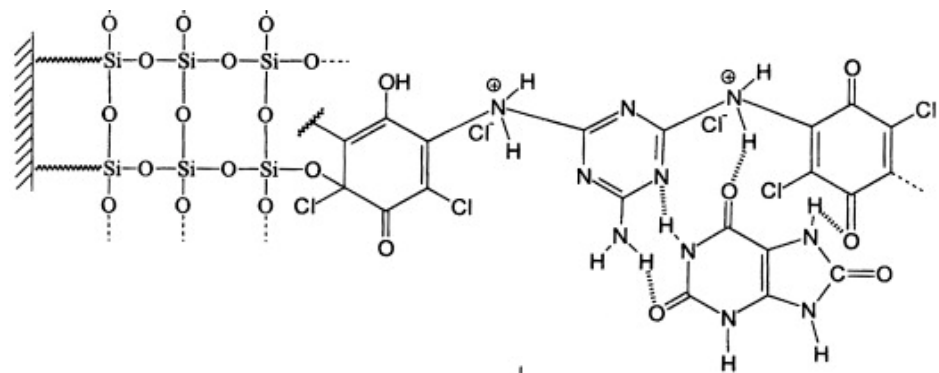


Figure 13. Schematic representation of the preparation of UV-MIP-sol-gel modified graphite electrode. Reproduced from ref. 181 with permission from Elsevier.

through “induced-fit” electrostatic attractions which alters the charge distribution and causes deformation of DA producing a stereospecific recognition (Figure 14). Due to such polarized attractions between the MIP and analyte in the respective cavities, non-specific binding can be removed by multiple washes with water, leaving nearly full recovery of DA. Using dilute samples of human blood serum and cerebrospinal fluid (CSF), dopamine detection limits of $0.018 \text{ ng} \times \text{mL}^{-1}$ were achieved without any non-specific absorption.

1.6. Summary

This chapter has explored and outlined some of the novel, stimulating work being conducted in the field of polymer brushes. For years polymer brushes have been used to alter the polarity or chemical functionality of a substrate. They can be bound to a range of surfaces and provide ample dense coverage for functionalization and selective binding, or instead they can be constructed to resist non-specific binding of molecules and/or living cells. The covalent attachment of brushes to a surface, their uniform size and structure and the topological constraints induced by the brush polymerization process, make polymer brushes suitable materials for the fabrication of extremely small scale structures or molecular objects.

While a large portion of research has investigated different types of homopolymer brushes, more complex systems are being examined as well. Mixed brushes, block copolymer brushes, and responsive brush arrangements have shown promise in the area of “bottom up” nanostructure fabrication. Desired morphologies and properties can be generated by environmental triggers such as temperature, ionic concentration,

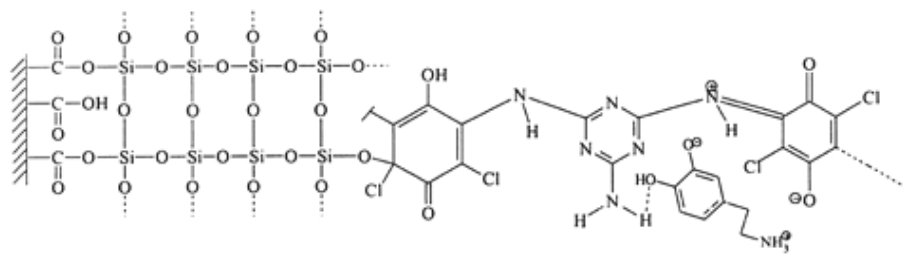


Figure 14. Schematic representation of induced-fit binding of DAD with fiber-sol-gel-MIP in aqueous media. Reproduced from ref. 182 with permission from Springer Science.

pH, solvent, light and electric fields. The combination of self-assembly with lithography is a powerful tool for the creation of small-scale structures. The patterning of polymer brushes with high fidelity and enhanced resolution has gained a lot of attention in the past decade. Some techniques such as uv photolithography, e-beam lithography, microcontact printing, and AFM lithography have emerged as attractive tools for exploratory research. However the challenge is still to develop a system with high reproducibility and control but at low cost and high throughput. One direction to consider may be the use of flexible materials as future surfaces and substrates. Flexible circuits/electronics have been one of the fastest growing markets and thus integrating polymer brushes with the latest advanced technology could be profitable on numerous accounts. If brushes could be interfaced with flexible electronics and printed on plastic films, novel applications in biological, solar cell, and electronic circuit fields would become available and potentially at lower cost.

Currently combining the use of advanced top down patterning methods with the bottom up nature of brush growth has proven successful advances in the production of supported membranes, nanochannels and nanosheets. Beyond patterning techniques, a novel field of polymer brush research that has emerged over the last few years is the concept of thin film detachment. Additional microscopy and mechanical property characterization procedures become available when brush chains are no longer tethered to a surface. Besides the methods mentioned above, other approaches can be implemented such as *gel permeation chromatography (GPC)* or mass spectrometry for determining molecular weight. Conventionally, measuring the molecular weight of polymer brushes consists of adding “free” initiator and then evaluating the free

polymer chains formed in solution, however, there is much debate whether this free polymer in solution is truly representative of the chains polymerized from the surface. By detaching the polymer brushes in a nondestructive manner, the molecular weights and polydispersity can be collected and conclusions regarding the nature of polymer brushes better understood.

In addition to patterning brushes and the properties of detached films, applications for polymer brushes in biosensors was also reviewed. Although biosensors have made much progress in the past decade, offering numerous advances in electrochemical detection and polymer interface compatibility, significant challenges to their full application remain. Not only must devices be specific to target biomolecules, but they must also prevent non-specific adsorption and maintain the ability to detect signals from the biological process. To address these limitations, electrochemistry is growing in popularity namely due to its low cost, durability, speed, and enhanced sensitivity compared to other analytical methods. Moreover, due to the biocompatibility and specific binding capability of polymer brushes, the combination of brushes and electrochemical systems have elicited much interest among researchers in many different fields. Approaches to such integrated schemes will allow for an extensive range of applications which incorporate the reduction of nonspecific interferences and controlled biomolecular binding for enhanced detection of cellular or enzymatic responses.

Overall it is an exciting time for the field of high resolution patterning of polymer thin films. There is great promise and prospects in the design of new structures and interactions for novel applications. With the growing need for patterned polymer thin

films in many areas of research including microelectronics, nanofluidic devices, biosensing, and other areas of nanotechnology, polymer brushes have picked up momentum towards realizing their full potential.

This thesis consists of multiple projects that incorporate the use of polymer brushes as patternable, functional surfaces and as detached free membranes. Chapter 2 describes the fabrication of an electrochemical biosensor in which polymer brushes are utilized as anchor points for antibody immobilization. Polymer brushes were synthesized via ATRP from gold and silicon surfaces and shown to prevent non specific adsorption. The advantages of electrochemically polymerizing a photosensitizer directly next to the brushes are discussed and very low limits of antibody detection are highlighted.

In chapter 3 a second biosensor is demonstrated however this example includes a PEDOT:PSS based microelectrode which measures neuronal activities *in vivo*. This device requires the tethering of glucose oxidase for specific charge exchange reactions to occur between the biological medium and the conducting polymer sensor. In this case, polymer brushes are used as a way of anchoring these molecules to the electrode surface without altering the conductivity of the transistor. The fabrication and characterization of polymer brush attachment to this unconventional surface is emphasized as well as the long-term stability of the electrode.

Chapter 4 describes polymer brushes used as a scaffolding platform for monitoring cellular mobility. Here the functionalization and characterization of polymer brushes for a peptide containing fluorogenic plasmin substrate are illustrated. Cell cultures have been performed on the brush surface to test compatibility and cellular mobility

has been recently investigated.

Chapters 5 and 6 describe a novel polymer brush membrane detachment method. Using an HF etching process, polymer brushes can be lifted from the surface and characterized via TEM, a form of analysis not available when attached to a surface. Features such as initiator immobilization conditions, polymer brush homogeneity, crosslinking efficiency, and membrane expansion can be investigated thanks to this technique. Additionally the nature of the stretching of polymer brushes based on theoretical calculations and studies can be experimentally explored.

REFERENCES

- (1) Akkahat, P.; Hoven, V. P. *Colloid Surf. B* **2011**, *86*, 198.
- (2) Gao, G. Z.; Lange, D.; Hilpert, K.; Kindrachuk, J.; Zou, Y. Q.; Cheng, J. T. J.; Kazemzadeh-Narbat, M.; Yu, K.; Wang, R. Z.; Straus, S. K.; Brooks, D. E.; Chew, B. H.; Hancock, R. E. W.; Kizhakkedathu, J. N. *Biomaterials* **2011**, *32*, 3899.
- (3) Welch, M.; Rastogi, A.; Ober, C. *Soft Matter* **2011**, *7*, 297.
- (4) Shen, Y.; Qi, L.; Wei, X. Y.; Zhang, R. Y.; Mao, L. Q. *Polymer* **2011**, *52*, 3725.
- (5) Li, Z. M.; Wei, J. G.; Shan, F.; Yang, J.; Wang, X. L. *J. Polym. Sci. Part B: Polym. Phys.* **2008**, *46*, 751.
- (6) Rodriguez-Emmenegger, C.; Brynda, E.; Riedel, T.; Houska, M.; Subr, V.; Alles, A. B.; Hasan, E.; Gautrot, J. E.; Huck, W. T. S. *Macromol. Rapid Comm.* **2011**, *32*, 952.
- (7) Hucknall, A.; Rangarajan, S.; Chilkoti, A. *Adv. Mater.* **2009**, *21*, 2441.
- (8) Wang, A. J.; Feng, J. J.; Fan, J. *J. Chromatogr. A* **2008**, *1192*, 173.
- (9) Paoprasert, P.; Spalenka, J. W.; Peterson, D. L.; Ruther, R. E.; Hamers, R. J.; Evans, P. G.; Gopalan, P. *J. Mater. Chem.* **2010**, *20*, 2651.
- (10) Iwanade, A.; Umeno, D.; Saito, K.; Sugo, T. *Biotechnol. Prog.* **2007**, *23*, 1425.
- (11) Bielecki, R. M.; Crobu, M.; Spencer, N. D. *Tribol. Lett.* **2013**, *49*, 263.
- (12) Zhao, B.; Brittain, W. J. *Prog. Polym. Sci.* **2000**, *25*, 677.

- (13) Han, Y.; Gao, C. *Sci. China-Chem.* **2010**, *53*, 2461.
- (14) Wang, Z. L.; Xu, J. T.; Du, B. Y.; Fan, Z. Q. *J. Colloid Interface Sci.* **2012**, *384*, 29.
- (15) Vyas, M. K.; Schneider, K.; Nandan, B.; Stamm, M. *Soft Matter* **2008**, *4*, 1024.
- (16) Kan, L. Y.; Xu, Z.; Gao, C. *Macromolecules* **2011**, *44*, 444.
- (17) Yang, Y. F.; Wu, D. X.; Li, C. X.; Liu, L.; Cheng, X. H.; Zhao, H. Y. *Polymer* **2006**, *47*, 7374.
- (18) Olivier, A.; Raquez, J. M.; Dubois, P.; Damman, P. *Eur. Polym. J.* **2011**, *47*, 31.
- (19) Samanta, S.; Locklin, J. *Langmuir* **2008**, *24*, 9558.
- (20) Kong, B.; Lee, J. K.; Choi, I. S. *Langmuir* **2007**, *23*, 6761.
- (21) Zhai, G. Q.; Yu, W. H.; Kang, E. T.; Neoh, K. G.; Huang, C. C.; Liaw, D. J. *Ind. Eng. Chem. Res.* **2004**, *43*, 1673.
- (22) Demirci, S.; Caykara, T. *Mater. Sci. Eng. C:Mater. Biol. Appl.* **2013**, *33*, 111.
- (23) Prucker, O.; Ruhe, J. *Macromolecules* **1998**, *31*, 592.
- (24) Cimen, D.; Caykara, T. *J. Mater. Chem.* **2012**, *22*, 13231.
- (25) Parvole, J.; Montfort, J. P.; Reiter, G.; Borisov, O.; Billon, L. *Polymer* **2006**, *47*, 972.
- (26) Kizhakkedathu, J. N.; Kumar, K. R.; Goodman, D.; Brooks, D. E. *Polymer* **2004**, *45*, 7471.
- (27) Rakhmatullina, E.; Braun, T.; Kaufmann, T.; Spillmann, H.; Malinova,

- V.; Meier, W. *Macromol. Chem. Phys.* **2007**, *208*, 1283.
- (28) Shah, R. R.; Merreceyes, D.; Husemann, M.; Rees, I.; Abbott, N. L.; Hawker, C. J.; Hedrick, J. L. *Macromolecules* **2000**, *33*, 597.
- (29) Savin, D. A.; Pyun, J.; Patterson, G. D.; Kowalewski, T.; Matyjaszewski, K. *J. Polym. Sci. Part B: Polym. Phys.* **2002**, *40*, 2667.
- (30) Ramakrishnan, A.; Dhamodharan, R.; Ruhe, J. *J. Polym. Sci. Part A-Polym. Chem.* **2006**, *44*, 1758.
- (31) Ayres, N.; Holt, D. J.; Jones, C. F.; Corum, L. E.; Grainger, D. W. *J. Polym. Sci. Part A-Polym. Chem.* **2008**, *46*, 7713.
- (32) Henry, O. Y. F.; Kirwan, S.; Debela, A. M.; O'Sullivan, C. K. *Electrochemistry Commun.* **2011**, *13*, 1155.
- (33) Pei, Y. W.; Travas-Sedjic, J.; Williams, D. E. *Langmuir* **2012**, *28*, 13241.
- (34) Delcroix, M. F.; Huet, G. L.; Conard, T.; Demoustier-Champagne, S.; Du Prez, F. E.; Landoulsi, J.; Dupont-Gillain, C. C. *Biomacromolecules* **2013**, *14*, 215.
- (35) Jiang, X. M.; Zhao, B.; Zhong, G. J.; Jin, N. X.; Horton, J. M.; Zhu, L.; Hafner, R. S.; Lodge, T. P. *Macromolecules* **2010**, *43*, 8209.
- (36) Motornov, M.; Sheparovych, R.; Katz, E.; Minko, S. *ACS Nano* **2008**, *2*, 41.
- (37) LeMieux, M. C.; Peleshanko, S.; Anderson, K. D.; Tsukruk, V. V. *Langmuir* **2007**, *23*, 265.
- (38) Burkert, S.; Bittrich, E.; Kuntzsch, M.; Muller, M.; Eichhorn, K. J.;

- Bellmann, C.; Uhlmann, P.; Stamm, M. *Langmuir* **2010**, *26*, 1786.
- (39) Wang, J. F.; Muller, M. *J. Phys. Chem. B* **2009**, *113*, 11384.
- (40) Sakellariou, G.; Park, M.; Advincula, R.; Mays, J. W.; Hadjichristidis, N. *J. Polym. Sci. Part A-Polym. Chem* **2006**, *44*, 769.
- (41) Iwata, R.; Satoh, R.; Iwasaki, Y.; Akiyoshi, K. *Colloid. Surf. B* **2008**, *62*, 288.
- (42) Rowe-Konopacki, M. D.; Boyes, S. G. *Macromolecules* **2007**, *40*, 879.
- (43) Xu, C.; Wu, T.; Drain, C. M.; Batteas, J. D.; Fasolka, M. J.; Beers, K. L. *Macromolecules* **2006**, *39*, 3359.
- (44) Yu, K.; Han, Y. C. *Soft Matter* **2009**, *5*, 759.
- (45) Rakhmatullina, E.; Mantion, A.; Burgi, T.; Malinova, V.; Meier, W. J. *J. Polym. Sci. Part A-Polym. Chem.* **2009**, *47*, 1.
- (46) Santer, S.; Ruhe, J. *Polymer* **2004**, *45*, 8279.
- (47) Yu, K.; Wang, H. F.; Han, Y. C. *Langmuir* **2007**, *23*, 8957.
- (48) Lyatskaya, Y. V.; Leermakers, F. A. M.; Fleer, G. J.; Zhulina, E. B.; Birshtein, T. M. *Macromolecules* **1995**, *28*, 3562.
- (49) Zhulina, E. B.; Borisov, O. V. *J. Chem. Phys.* **1997**, *107*, 5952.
- (50) Zhulina, E. B.; Wolterink, J. K.; Borisov, O. V. *Macromolecules* **2000**, *33*, 4945.
- (51) Fleer, G. J. *Ber. Bunsen-Ges. Phys. Chem.* **1996**, *100*, 936.
- (52) Zhang, H. N.; Ruhe, J. *Macromolecules* **2005**, *38*, 4855.
- (53) Naji, A.; Netz, R. R.; Seidel, C. *Eur. Phys. J. E* **2003**, *12*, 223.
- (54) Ionov, L.; Houbenov, N.; Sidorenko, A.; Stamm, M.; Luzinov, I.;

- Minko, S. *Langmuir* **2004**, *20*, 9916.
- (55) Uhlmann, P.; Houbenov, N.; Brenner, N.; Grundke, K.; Burkert, S.; Stamm, M. *Langmuir* **2007**, *23*, 57.
- (56) Liu, J. X.; Zhao, M. Z.; Deng, Y.; Tie, C.; Chen, H. X.; Zhou, Y. L.; Zhang, X. X. *Electrophoresis* **2013**, *34*, 1352.
- (57) Raviv, U.; Giasson, S.; Kampf, N.; Gohy, J. F.; Jerome, R.; Klein, J. *Nature* **2003**, *425*, 163.
- (58) Abraham, T.; Giasson, S.; Gohy, J. F.; Jerome, R. *Langmuir* **2000**, *16*, 4286.
- (59) Liberelle, B.; Giasson, S. *Langmuir* **2008**, *24*, 1550.
- (60) Heskins, M.; Guillet, J. E. *J. Macromol. Sci. Chem.* **1968**, *A2*, 1441.
- (61) Feil, H.; Bae, Y. H.; Feijen, J.; Kim, S. W. *Macromolecules* **1993**, *26*, 2496.
- (62) Zhao, X.; Liu, Y.; Lu, J.; Zhou, J. H.; Li, J. H. *Chem. Eur. J.* **2012**, *18*, 3687.
- (63) Dong, L. C.; Hoffman, A. S. *J. Controlled Release* **1991**, *15*, 141.
- (64) Ge, X.; Guan, Y. X.; Chen, J.; Yao, Z.; Cao, K.; Yao, S. J. *J. Appl. Polym. Sci.* **2009**, *114*, 1270.
- (65) Xue, C. Y.; Choi, B. C.; Choi, S.; Braun, P. V.; Leckband, D. E. *Adv. Funct. Mater.* **2012**, *22*, 2394.
- (66) Cho, E. C.; Kim, Y. D.; Cho, K. *J. Colloid Interface Sci.* **2005**, *286*, 479.
- (67) Yang, Y.; Yan, X. H.; Cui, Y.; He, Q.; Li, D. X.; Wang, A. H.; Fei, J.

- B.; Li, J. B. *J. Mater. Chem.* **2008**, *18*, 5731.
- (68) Yamato, M.; Konno, C.; Kushida, A.; Hirose, M.; Utsumi, M.; Kikuchi, A.; Okano, T. *Biomaterials* **2000**, *21*, 981.
- (69) Pangilinan, K. D.; Santos, C. M.; Estillore, N. C.; Rodrigues, D. F.; Advincula, R. C. *Macromol. Chem. Phys.* **2013**, *214*, 464.
- (70) Szuwarzynski, M.; Zaraska, L.; Sulka, G. D.; Zapotoczny, S. *Chem. Mater.* **2013**, *25*, 514.
- (71) Sun, S. Q.; Montague, M.; Critchley, K.; Chen, M. S.; Dressick, W. J.; Evans, S. D.; Leggett, G. J. *Nano Lett.* **2006**, *6*, 29.
- (72) Ahmad, S. A.; Leggett, G. J.; Hucknall, A.; Chilkoti, A. *Biointerphases* **2011**, *6*, 8.
- (73) Dong, R.; Krishnan, S.; Baird, B. A.; Lindau, M.; Ober, C. K. *Biomacromolecules* **2007**, *8*, 3082.
- (74) Padeste, C.; Farquet, P.; Potzner, C.; Solak, H. H. *J. Biomater. Sci.: Polym. E.* **2006**, *17*, 1285.
- (75) Schuh, C.; Lomadze, N.; Ruhe, J.; Kopyshev, A.; Santer, S. *J. Phys. Chem. B* **2011**, *115*, 10431.
- (76) Tsujii, Y.; Ejaz, M.; Yamamoto, S.; Fukuda, T.; Shigeto, K.; Mibu, K.; Shinjo, T. *Polymer* **2002**, *43*, 3837.
- (77) Chen, J. K.; Hsieh, C. Y.; Huang, C. F.; Li, P. M.; Kuo, S. W.; Chang, F. C. *Macromolecules* **2008**, *41*, 8729.
- (78) Kaholek, M.; Lee, W. K.; Feng, J. X.; LaMattina, B.; Dyer, D. J.; Zauscher, S. *Chem. Mater.* **2006**, *18*, 3660.

- (79) Slimani, K.; Moine, L.; Aymes-Chodur, C.; Laurent, A.; Labarre, D.; Yagoubi, N. *Polym. Degrad. Stab.* **2009**, *94*, 584.
- (80) Rastogi, A.; Paik, M. Y.; Tanaka, M.; Ober, C. K. *ACS Nano* **2010**, *4*, 771.
- (81) Paik, M. Y.; Xu, Y. Y.; Rastogi, A.; Tanaka, M.; Yi, Y.; Ober, C. K. *Nano Lett.* **2010**, *10*, 3873.
- (82) Schmelmer, U.; Jordan, R.; Geyer, W.; Eck, W.; Golzhauser, A.; Grunze, M.; Ulman, A. *Angew. Chem. Int. Ed.* **2003**, *42*, 559.
- (83) Eck, W.; Stadler, V.; Geyer, W.; Zharnikov, M.; Golzhauser, A.; Grunze, M. *Adv. Mater.* **2000**, *12*, 805.
- (84) Steenackers, M.; Kuller, A.; Stoycheva, S.; Grunze, M.; Jordan, R. *Langmuir* **2009**, *25*, 2225.
- (85) Schilp, S.; Ballav, N.; Zharnikov, M. *Angew. Chem. Int. Ed.* **2008**, *47*, 6786.
- (86) Liu, J. X.; Ye, Q.; Yu, B.; Wang, X. L.; Zhou, F. *Chem. Commun.* **2012**, *48*, 398.
- (87) Hung, M. K.; Wang, Y. H.; Lin, C. H.; Lin, H. C.; Lee, J. T. *J. Mater. Chem.* **2012**, *22*, 1570.
- (88) Hamelinck, P. J.; Huck, W. T. S. *J. Mater. Chem.* **2005**, *15*, 381.
- (89) Farhan, T.; Huck, W. T. S. *Eur. Polym. J.* **2004**, *40*, 1599.
- (90) Husemann, M.; Mecerreyes, D.; Hawker, C. J.; Hedrick, J. L.; Shah, R.; Abbott, N. L. *Angew. Chem. Int. Ed.* **1999**, *38*, 647.
- (91) Zhou, F.; Zheng, Z. J.; Yu, B.; Liu, W. M.; Huck, W. T. S. *J. Am.*

- Chem. Soc.* **2006**, *128*, 16253.
- (92) Chen, T.; Jordan, R.; Zauscher, S. *Soft Matter* **2011**, *7*, 5532.
- (93) Chen, T.; Jordan, R.; Zauscher, S. *Small* **2011**, *7*, 2148.
- (94) Li, Y. F.; Zhang, J. H.; Fang, L. P.; Jiang, L. M.; Liu, W. D.; Wang, T. Q.; Cui, L. Y.; Sun, H. C.; Yang, B. *J. Mater. Chem.* **2012**, *22*, 25116.
- (95) Xu, S.; Liu, G. Y. *Langmuir* **1997**, *13*, 127.
- (96) Kaholek, M.; Lee, W. K.; LaMattina, B.; Caster, K. C.; Zauscher, S. *Nano Letters* **2004**, *4*, 373.
- (97) Hirtz, M.; Brinks, M. K.; Miele, S.; Studer, A.; Fuchs, H.; Chi, L. F. *Small* **2009**, *5*, 919.
- (98) Wagner, H.; Li, Y.; Hirtz, M.; Chi, L. F.; Fuchs, H.; Studer, A. *Soft Matter* **2011**, *7*, 9854.
- (99) Piner, R. D.; Zhu, J.; Xu, F.; Hong, S. H.; Mirkin, C. A. *Science* **1999**, *283*, 661.
- (100) Liu, X. G.; Guo, S. W.; Mirkin, C. A. *Angew. Chem. Int. Ed.* **2003**, *42*, 4785.
- (101) Ma, H. W.; Hyun, J. H.; Stiller, P.; Chilkoti, A. *Adv. Mater.* **2004**, *16*, 338.
- (102) Zapotoczny, S.; Benetti, E. M.; Vancso, G. J. *J. Mater. Chem.* **2007**, *17*, 3293.
- (103) Liu, X. Q.; Li, Y.; Zheng, Z. *J. Nanoscale* **2010**, *2*, 2614.
- (104) Zhou, X. C.; Liu, Z. L.; Xie, Z.; Liu, X. Q.; Zheng, Z. *J. Small* **2012**, *8*, 3568.

- (105) Gordon, A. E.; Fayfield, R. T.; Litfin, D. D.; Higman, T. K. *J. Vac. Sci. Technol. B* **1995**, *13*, 2805.
- (106) Sugimura, H.; Nakagiri, N. *J. Am. Chem. Soc.* **1997**, *119*, 9226.
- (107) Lee, W. K.; Caster, K. C.; Kim, J.; Zauscher, S. *Small* **2006**, *2*, 848.
- (108) Nolte, M.; Donch, I.; Fery, A. *Chemphyschem* **2006**, *7*, 1985.
- (109) Zimnitsky, D.; Shevchenko, V. V.; Tsukruk, V. V. *Langmuir* **2008**, *24*, 5996.
- (110) Frank, C. W.; Rao, V.; Despotopoulou, M. M.; Pease, R. F. W.; Hinsberg, W. D.; Miller, R. D.; Rabolt, J. F. *Science* **1996**, *273*, 912.
- (111) Li, M.; Ishihara, S.; Akada, M.; Liao, M. Y.; Sang, L. W.; Hill, J. P.; Krishnan, V.; Ma, Y. G.; Ariga, K. *J. Am. Chem. Soc.* **2011**, *133*, 7348.
- (112) Ram, M. K.; Yavuz, O.; Aldissi, M. *Synth. Met.* **2005**, *151*, 77.
- (113) Cai, L.; Qu, H. W.; Lu, C. X.; Ducharme, S.; Dowben, P. A.; Zhang, J. *D. Phys. Rev. B* **2004**, *70*.
- (114) Ouyang, Q. Y.; Chen, Y. J.; Li, C. Y. *Mater. Chem. Phys.* **2012**, *134*, 80.
- (115) Hong, J. D.; Kim, D.; Cha, K.; Jin, J. I. *Synth. Met.* **1997**, *84*, 815.
- (116) Alexander, S. *J. Phys. (Paris)* **1977**, *38*, 977.
- (117) Flory, P. J.; Cornell University Press: Ithaca, NY, 1981.
- (118) Amin, I.; Steenackers, M.; Zhang, N.; Beyer, A.; Zhang, X. H.; Pirzer, T.; Hugel, T.; Jordan, R.; Golzhauser, A. *Small* **2010**, *6*, 1623.
- (119) Meyerbroker, N.; Zharnikov, M. *Langmuir* **2012**, *28*, 9583.
- (120) Amin, I.; Steenackers, M.; Zhang, N.; Schubel, R.; Beyer, A.;

- Golzhauser, A.; Jordan, R. *Small* **2011**, *7*, 683.
- (121) Steenackers, M.; Gigler, A. M.; Zhang, N.; Deubel, F.; Seifert, M.; Hess, L. H.; Lim, C.; Loh, K. P.; Garrido, J. A.; Jordan, R.; Stutzmann, M.; Sharp, I. D. *J. Am. Chem. Soc.* **2011**, *133*, 10490.
- (122) Seifert, M.; Koch, A. H. R.; Deubel, F.; Simmet, T.; Hess, L. H.; Stutzmann, M.; Jordan, R.; Garrido, J. A.; Sharp, I. D. *Chem. Mater.* **2013**, *25*, 466.
- (123) Fulghum, T. M.; Patton, D. L.; Advincula, R. C. *Langmuir* **2006**, *22*, 8397.
- (124) Edmondson, S.; Armes, S. P. *Polym. Int.* **2009**, *58*, 307.
- (125) Estillore, N. C.; Advincula, R. C. *Macromol. Chem. Phys.* **2011**, *212*, 1552.
- (126) Estillore, N. C.; Advincula, R. C. *Langmuir* **2011**, *27*, 5997.
- (127) Ohm, C.; Ober, C. K.; RSC Adv.: 2013, p in press.
- (128) Edmondson, S.; Frieda, K.; Comrie, J. E.; Onck, P. R.; Huck, W. T. S. *Adv. Mater.* **2006**, *18*, 724.
- (129) Hutchinson, J. W.; Suo, Z. *Adv. Appl. Mech.* **1992**, *29*, 63.
- (130) Welch, M. E.; Ober, C. K. *ACS Macro Lett.* **2013**, *2*, 241.
- (131) Bierbaum, K.; Grunze, M.; Baski, A. A.; Chi, L. F.; Schrepp, W.; Fuchs, H. *Langmuir* **1995**, *11*, 2143.
- (132) Brzoska, J. B.; Benazouz, I.; Rondelez, F. *Langmuir* **1994**, *10*, 4367.
- (133) Parikh, A. N.; Allara, D. L.; Azouz, I. B.; Rondelez, F. *J. Phys. Chem.* **1994**, *98*, 7577.

- (134) Brzoska, J. B.; Shahidzadeh, N.; Rondelez, F. *Nature* **1992**, *360*, 719.
- (135) Belluzo, M. S.; Ribone, M. E.; Lagier, C. M. *Sensors* **2008**, *8*, 1366.
- (136) Chaubey, A.; Malhotra, B. D. *Biosens. Bioelectron.* **2002**, *17*, 441.
- (137) Grieshaber, D.; MacKenzie, R.; Voros, J.; Reimhult, E. *Sensors* **2008**, *8*, 1400.
- (138) Lima, P. R.; Santos, W. D. R.; de Oliveira, A. B.; Goulart, M. O. F.; Kubota, L. T. *Biosens. Bioelectron.* **2008**, *24*, 448.
- (139) Kikkeri, R.; Kamena, F.; Gupta, T.; Hossain, L. H.; Boonyarattanakalin, S.; Gorodyska, G.; Beurer, E.; Coullerez, G.; Textor, M.; Seeberger, P. H. *Langmuir* **2010**, *26*, 1520.
- (140) Heinze, J. *Angew. Chem. Int. Ed.* **1984**, *23*, 831.
- (141) Shan, D.; Zhang, J.; Xue, H. G.; Ding, S. N.; Cosnier, S. *Biosens. Bioelectron.* **2010**, *25*, 1427.
- (142) Wang, X. L.; Yang, T.; Jiao, K. *Biosens. Bioelectron.* **2009**, *25*, 668.
- (143) Moattisirat, D.; Velho, G.; Reach, G. *Biosens. Bioelectron.* **1992**, *7*, 345.
- (144) Choi, S.; Chae, J. *Biosens. Bioelectron.* **2009**, *25*, 527.
- (145) Pedrero, M.; Campuzano, S.; Pingarron, J. M. *Sensors* **2009**, *9*, 5503.
- (146) Ram, M. K.; Bertoncello, P.; Ding, H.; Paddeu, S.; Nicolini, C. *Biosens. Bioelectron.* **2001**, *16*, 849.
- (147) Wang, A.-J.; Xu, J.-J.; Chen, H.-Y. *J. Chrom. A* **2007**, *1147*, 120.
- (148) Fei, J. J.; Wu, Y. H.; Ji, X. B.; Wang, J.; Hu, S. S.; Gao, Z. Q. *Anal. Sci.* **2003**, *19*, 1259.

- (149) Ivanov, Y.; Marinov, I.; Gabrovska, K.; Dimcheva, N.; Godjevargova, T. *J. Mol. Catal. B-Enzym.* **2010**, *63*, 141.
- (150) Yuan, J. H.; Wang, K.; Xia, X. H. *Adv. Funct. Mater.* **2005**, *15*, 803.
- (151) Ming, L.; Xi, X.; Liu, J. *Biotechnology Letters* **2006**, *28*, 1341.
- (152) Li, K.; Liu, B.; Zheng, J.; Sheng, Q.; Liu, R. *Electroanalysis* **2010**, *22*, 701.
- (153) Abasiyanik, M. F.; Senel, M. *J. Electroanal. Chem.* **2010**, *639*, 21.
- (154) Miao, W. J.; Bard, A. J. *J. Anal. Chem.* **2004**, *76*, 5379.
- (155) Rubinstein, I.; Bard, A. J. *J. Am. Chem. Soc.* **1980**, *102*, 6641.
- (156) Mrksich, M. *Cellular and Molecular Life Sciences* **1998**, *54*, 653.
- (157) Senaratne, W.; Andruzzi, L.; Ober, C. K. *Biomacromolecules* **2005**, *6*, 2427.
- (158) Prime, K. L.; Whitesides, G. M. *J. Am. Chem. Soc.* **1993**, *115*, 10714.
- (159) Herrwerth, S.; Eck, W.; Reinhardt, S.; Grunze, M. *J. Am. Chem. Soc.* **2003**, *125*, 9359.
- (160) Ostuni, E.; Chapman, R. G.; Holmlin, R. E.; Takayama, S.; Whitesides, G. M. *Langmuir* **2001**, *17*, 5605.
- (161) Flynn, N. T.; Tran, T. N. T.; Cima, M. J.; Langer, R. *Langmuir* **2003**, *19*, 10909.
- (162) Leckband, D.; Sheth, S.; Halperin, A. *J. Biomat. Sci. Polym. E.* **1999**, *10*, 1125.
- (163) Dalsin, J. L.; Lin, L. J.; Tosatti, S.; Voros, J.; Textor, M.; Messersmith, P. B. *Langmuir* **2005**, *21*, 640.

- (164) Zhang, Z.; Feng, X.; Luo, Q.; Liu, B.-F. *Electrophoresis* **2009**, *30*, 3174.
- (165) Otsuka, H.; Nagasaki, Y.; Kataoka, K. *Biomacromolecules* **2000**, *1*, 39.
- (166) Andruzzi, L.; Senaratne, W.; Hexemer, A.; Sheets, E. D.; Ilic, B.; Kramer, E. J.; Baird, B.; Ober, C. K. *Langmuir* **2005**, *21*, 2495.
- (167) Raynor, J. E.; Petrie, T. A.; Fears, K. P.; Latour, R. A.; Garcia, A. J.; Collard, D. M. *Biomacromolecules* **2009**, *10*, 748.
- (168) Ugo, P.; Bertoncello, P.; Vezza, F. *Electrochimica Acta* **2004**, *49*, 3785.
- (169) Moretto, L. M.; Kohls, T.; Chovin, A.; Sojic, N.; Ugo, P. *Langmuir* **2008**, *24*, 6367.
- (170) Rastogi, A.; Nad, S.; Tanaka, M.; Da Mota, N.; Tague, M.; Baird, B. A.; Abruna, H. D.; Ober, C. K. *Biomacromolecules* **2009**, *10*, 2750.
- (171) Bruening, M. L.; Dotzauer, D. M.; Jain, P.; Ouyang, L.; Baker, G. L. *Langmuir* **2008**, *24*, 7663.
- (172) Dong, R.; Lindau, M.; Ober, C. K. *Langmuir* **2009**, *25*, 4774.
- (173) Stuart, M. A. C.; Huck, W. T. S.; Genzer, J.; Muller, M.; Ober, C.; Stamm, M.; Sukhorukov, G. B.; Szleifer, I.; Tsukruk, V. V.; Urban, M.; Winnik, F.; Zauscher, S.; Luzinov, I.; Minko, S. *Nature Mater.* **2010**, *9*, 101.
- (174) Won, B. Y.; Yoon, H. C.; Park, H. G. *Analyst* **2008**, *133*, 100.
- (175) Jena, B. K.; Raj, C. R. *Anal. Chem.* **2006**, *78*, 6332.
- (176) Tam, T. K.; Pita, M.; Trotsenko, O.; Motornov, M.; Tokarev, I.;

- Halamek, J.; Minko, S.; Katz, E. *Langmuir* **2010**, *26*, 4506.
- (177) Amir, L.; Tam, T. K.; Pita, M.; Meijler, M. M.; Alfonta, L.; Katz, E. *J. Am. Chem. Soc.* **2009**, *131*, 826.
- (178) Zhou, J.; Lu, X.; Hu, J.; Li, J. *Chem. Eur. J.* **2007**, *13*, 2847.
- (179) Wentworth, P.; Jones, L. H.; Wentworth, A. D.; Zhu, X. Y.; Larsen, N. A.; Wilson, I. A.; Xu, X.; Goddard, W. A.; Janda, K. D.; Eschenmoser, A.; Lerner, R. A. *Science* **2001**, *293*, 1806.
- (180) Gajovic-Eichelmann, N.; Bier, F. F. *Electroanal.* **2005**, *17*, 1043.
- (181) Patel, A. K.; Sharma, P. S.; Prasad, B. B. *Mat. Sci. Eng. C -Bio. S.* **2009**, *29*, 1545.
- (182) Prasad, B. B.; Tiwari, K.; Singh, M.; Sharma, P. S.; Patel, A. K.; Srivastava, S. *Chromatographia* **2009**, *69*, 949.

CHAPTER 2

A GENERALIZED PLATFORM FOR ANTIBODY DETECTION USING THE ANTIBODY CATALYZED WATER OXIDATION PATHWAY

Abstract

Infectious diseases such as influenza present a prominent global problem through a constant threat of pandemics. We report a new antibody sensor that can be specifically functionalized to detect a wide range of infectious diseases. This biosensor is based on electrochemical detection of hydrogen peroxide generated through the intrinsic catalytic activity of all antibodies: the antibody catalyzed water oxidation pathway. Our platform includes a polymer brush-modified surface where specific antibodies bind with high affinity and specificity to conjugated haptens. Hydrogen peroxide provides an electrochemical signal that is mediated by Resorufin/Amplex Red. We characterize the biosensor platform, using model anti-DNP antibodies, with the ultimate goal of designing a versatile device that is inexpensive, portable, reliable, and fast. We demonstrate detection of antibodies at concentrations that fall well within clinically relevant levels.

Introduction

Influenza pandemics have occurred every 10 to 50 years since 1580, often with

* This chapter has been submitted for review as an article to JACS.

tragic effects on human and livestock populations and their economies.¹ With escalating world population and global mobility, the challenges of preventing flu and other epidemics from proliferating are increasingly difficult. In event of an outbreak, costs to the world economy are predicted to be around \$2 - \$3 trillion, depending on severity.² Recent reports show that the avian A/H5N1 influenza virus can potentially be transmitted by aerosol or respiratory droplets between mammals.³⁻⁵ Mutations of only three or four nucleotides could develop within a single mammalian host thus posing the threat of transferring to humans and leading to a pandemic. Disease hosts can harbor a virus for several days before symptoms occur, allowing ample time for many others to become infected leading to a pandemic. Significantly improved detection of these diseases as they transfer through species would aid substantially in providing early warning of these threats. The host's immune response provides an important key for detection. When a viral or other pathogenic infection is met by an immune response, antibodies are generated that are specific for chemical groups (haptenes) on proteins or other pathogen components (antigens), and hence early discovery is often most easily accomplished by detection of these antibodies. Although sensitive antibody detection methods are currently available, these have limitations, and reliable new technologies are needed to meet the demand for rapid detection of highly contagious infections, especially in locations with limited laboratory access.

Currently, the most widely used methods for antibody detection are based on the enzyme-linked immunosorbent assay (ELISA). Selected haptic groups are immobilized on a surface, followed by addition of a sample (e.g., blood serum)

potentially containing antibodies, which bind to the hapten. Detection of these immobilized antibodies is carried out using a specially prepared secondary reagent, most often a secondary antibody specific for the analyte antibody. The secondary antibody is labeled with a tag such as a fluorescent molecule or an enzyme producing a colorimetric substrate. Requiring a secondary reagent increases the number of analytical and incubation steps and thus increases both the analysis time and the risk of nonspecific binding leading to false positives.

To overcome the limitations of the ELISA method, we developed a sensor platform based on the antibody-catalyzed water oxidation pathway (ACWOP) that takes advantage of the intrinsic capacity of single antibodies to catalyze the production of hydrogen peroxide (H_2O_2) from water in the presence of singlet oxygen ($^1O_2^*$), which can be generated by a photosensitizer (Figure 1B). Wentworth *et al.* first described the ACWOP and showed that it is independent of specificity, class, and species of antibody.⁶ The structural locus of this novel activity was found to be in the constant regions of immunoglobulins.⁷ The catalytic activity produces multiple mole equivalents of H_2O_2 per antibody (reportedly up to 500) to reach levels that can be detected and quantified using fluorescence.⁽⁶⁾ We confirmed the previous fluorescence method of ACWOP detection and have now successfully detected antibody generated H_2O_2 using electrochemical methods (Figure 1A).^{8,9} A primary advantage of the ACWOP is that it allows for direct detection of antibodies *via* H_2O_2 regardless of the antibodies' species and specificity, eliminating the need for specially prepared secondary reagents and mitigating other limitations of the ELISA approach. Our ultimate goal is to create a portable microfluidic platform for sensitive, rapid, and

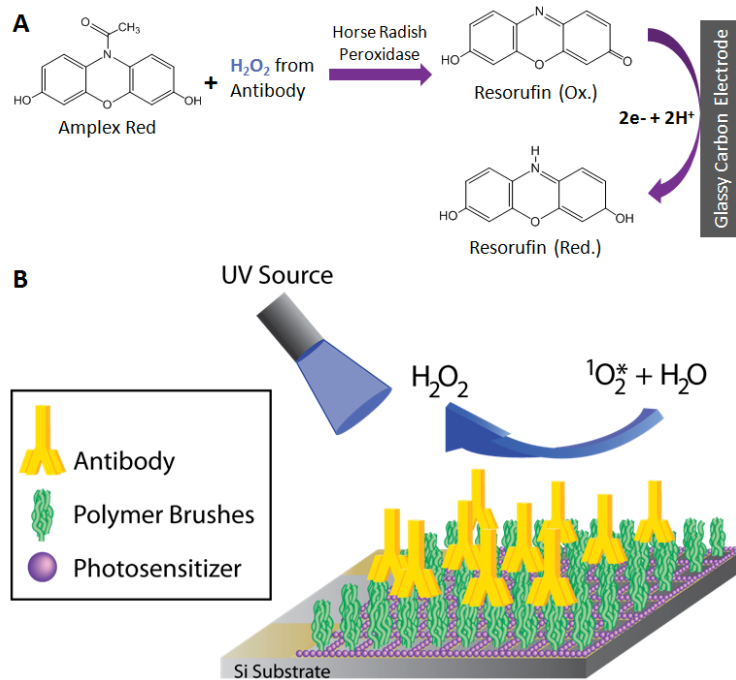


Figure 1. (A) Hydrogen peroxide produced from the antibodies reacts with Amplex Red in the presence of horseradish peroxidase to form resorufin, which is reduced at a glassy carbon electrode. (B) Schematic of biosensor platform based on the ACWOP process.

inexpensive detection of antibodies. Herein, we report key results towards fabricating and testing such a device.

Experimental Section

Materials: Allyl-2-bromo-2-methylpropionate, chlorodimethyl- hydrosilane, Pt on activated carbon (10 wt %), triethylamine, anhydrous toluene, 2,2'-bipyridine, 11-mercaptop-1-undecanol, 2-bromo-2-methylpropionyl bromide, anhydrous pyridine, copper (I) bromide (99.999%), copper (II) bromide(99.999%), copper (I) chloride (99.999%), poly(propylene glycol) methacrylate (POEGMA), N, N-diisopropylcarbodiimide (DIPC), dinitrophenol- ϵ -amino-*n*-caproic acid, dimethyl formamide (DMF), horseradish peroxidase (Type 1) (HRP), Amplex Red reagent, albumin from bovine serum (BSA) were purchased from Aldrich and used without further purification. Phosphate-buffered saline solution (PBS) was prepared from 0.1 M sodium phosphate buffer solution with 0.15 M sodium chloride and the pH adjusted to 6.0 or 7.2 using hydrochloric acid or sodium hydroxide. 4-(dimethylamino)pyridinium 4-toluene sulfonate (DPTS) was prepared from dimethyl amino pyridine and sodium p-toluene sulfonate following a literature procedure.¹⁰ Deionized water (18.2 MΩ•cm at 25°C) from Millipore's Milli-Q Synthesis A10 system was used to clean glassware and prepare aqueous solutions. All other solvents for rinsing and cleaning were purchased from Fisher Scientific.

Synthesis and Immobilization of Surface Initiators: Gold and silicon surface initiators were synthesized according to published procedures.^{11,12} Gold and silicon substrates were both cleaned using a Harrick Plasma Cleaner for 10 minutes, rinsed

with ethanol, and blown dry with nitrogen gas. The gold wafers were immersed in 1 mM initiator solution in anhydrous hexanes overnight under nitrogen. The silicon substrates were placed in a vacuum oven to ensure removal of all water particles before being placed in a 1 % (v/v) solution of the silane initiator in anhydrous toluene containing catalytic amounts of triethylamine for about 12 h at room temperature. After immobilization, both substrates were rinsed with anhydrous ethanol and dried under nitrogen.

Polymerization and Functionalization of POEGMA Brushes: The silicon substrates (1 cm × 2 cm) were placed in a dry Schlenk flask. Poly(propylene glycol) methacrylate (3.0 g, 8 mmol), CuCl (19.5 mg, 0.2 mmol), CuBr₂ (4.3 mg, 0.02 mmol), and 2,2'-bipyridine (76.0 mg, 0.49 mmol) were added to another 25 mL Schlenk flask equipped with a magnetic stir bar. Both flasks were evacuated and replaced with nitrogen four times. DI water (5.25 mL) was purged with nitrogen for at least 30 min and then transferred to the Schlenk flask containing the monomer via cannulation. The brown colored solution was stirred under nitrogen for about 10 minutes before being transferred into the flask containing the substrates. Polymerization was carried out at room temperature for 8-12 minutes, after which the substrates were rinsed with water and ethanol, blown dry under nitrogen gas, and characterized by ellipsometry. POEGMA brushes were functionalized by a similar method. A solution of dinitrophenyl-ε-amino-n-caproic acid (DNP) (37.5 mg, 1.12 mmol), DIPC (125 μL, 0.8 mmol), and DPTS (187.5 mg, 0.63 mmol) in anhydrous DMF (10 mL) was cannulated into the flask containing the substrates. The reaction was allowed to continue for 24 hours at 32°C. When finished, the substrates were washed with water

and ethanol and dried under nitrogen. Fluorescently labeled DNP-antibodies were used to confirm the functionalization of the DNP groups to the brushes.

Quantification of DNP Surface Coverage: The surface coverage, Γ , of DNP was determined using cyclic voltammetry (measurements carried out by Prof. Héctor Abruña's group, Department of Chemistry and Chemical Biology, Cornell University). Cyclic voltammetry was performed after the square wave voltammetry measurements because DNP groups are irreversibly reduced (near -0.4 V vs. Ag/AgCl) to hydroxylamine groups.¹³ The hydroxylamine group (+0.25 V vs. Ag/AgCl) is electrochemically reversible. The surface coverage of DNP was calculated by integrating the area of the anodic peak at +0.28 V vs. Ag/AgCl, assuming that each of the DNP groups is converted to a hydroxylamine group. The area is related to the charge, Q , of an electroactive species, in this case hydroxylamine, attached to an electrode. From Q , the surface coverage of the hydroxylamine is calculated from the following equation:

$$Q = nFA\Gamma \quad (1)$$

where n is the number of electrons passed per hydroxylamine ($n = 4$ in this case), A is the area of the electrode (0.43 cm^2 , which is one-fourth of the total electroactive area, 1.7 cm^2) and F is Faraday's Constant, 96485 C/mole e^- .⁹

Antibody adsorption measurements using Quartz Crystal Microbalance (QCM):

After functionalizing a gold-plated QCM crystal with DNP-modified brushes and photosensitizer, it was immersed in pH 7.2 PBS containing 60 mL of 1 mg/mL BSA controlled at 25 °C in a water jacket while the solution was stirred with a magnetic stirring bar (measurements carried out by Prof. Héctor Abruña's group, Department of

Chemistry and Chemical Biology, Cornell University). Once the frequency stabilized to a constant value, 100 μ L of 1 mg/mL rat anti-DNP IgG antibody solution (11 nM resultant concentration) was added to the PBS solution. By measuring the change in frequency, Δf , the surface coverage of antibodies adsorbed to the functionalized brushes was calculated using the Sauerbrey equation:

$$\Delta f = -C_f \cdot \Delta m \quad (2)$$

where C_f is the integral sensitivity factor, 56.6 Hz μ g⁻¹ cm² for a 5 MHz AT-cut quartz crystal and Δm is the change in mass in units of g cm⁻².¹⁴

Immobilization of Photosensitizer: The silicon wafer chip or QCM crystal containing polymer brush initiator was immersed in a 0.5 mM solution of photosensitizer, [Ru(v-bpy)₃](PF₆)₂, where v-bpy is 4-vinyl, 4'-methyl bipyridine, in 0.1 M tetrabutylammonium perchlorate in acetonitrile, and the solution was deaerated using nitrogen for 15 minutes. A coiled platinum wire and a silver wire were used as the auxiliary and reference electrodes, respectively. Potentials were calibrated using ferrocene, with $E_{1/2}$ +0.342 V vs. SCE.¹⁵ The potential was cycled for 10 cycles at a scan rate of 100 mV/s. After electropolymerization, the electrode was removed from the photosensitizer solution, rinsed with acetone and then acetonitrile, and then immersed in fresh electrolyte (immobilization carried out by Prof. Héctor Abruna's group, Department of Chemistry and Chemical Biology, Cornell University).

Hydrogen Peroxide Generation and Detection using SWV: We used square wave voltammetry (SWV) primarily for detecting hydrogen peroxide (H₂O₂) (measurements carried out by Prof. Héctor Abruna's group, Department of Chemistry and Chemical Biology, Cornell University). After immobilizing the antibody on the DNP-

functionalized brushes, the substrate (i.e., silicon wafer chip or QCM crystal) was placed in 3 mL of PBS, pH 7.2 and then irradiated with UV light for 60 minutes. Then, an aliquot of the irradiated solution was removed and diluted with PBS, pH 6.0 to a final volume of 5 mL in a three-electrode cell, followed by deaeration with N₂. 8.8 μL of 10 μM HRP in PBS and 10.0 μL of 0.1 mM Amplex Red reagent in DMSO were added (resultant concentration of 10 μM and 0.2 units/L, respectively) to the deaerated solution, and SWV was performed at a glassy carbon electrode (3 mm diameter) with amplitude 25 mV, step height 5 mV, and frequency 25 Hz. A Ag/AgCl reference electrode in a salt bridge (3% w/v agar with 0.2 M potassium nitrate) and a Pt coiled wire auxiliary electrode were used.

Device Fabrication: A checkerboard patterned device, consisting of 35 rows of sixteen 300 μm x 300 μm silicon oxide squares bordered by a gold lattice, was fabricated for signal amplification purposes. The silicon islands are surrounded by a continuous gold grid with lines 150 μm wide and enclosed by a 500 μm wide border. Conventional UV photolithographic methods were employed to pattern the electrodes used in this work. Silicon wafers were spun coated with lift-off resist (LOR 5A) and photoresist (SPR 220-3) and baked at 180°C for 3 min and 115°C for 90 sec, respectively. Soft contact exposure was performed on an EV620 contact aligner for 10 sec and a post-exposure bake was carried out at 115 °C for 90 sec. The wafers were developed by a Hamatech-Steag wafer processor using a double puddle process and then descummed for 4 minutes in a Branson P2000 barrel etcher. A CVC SC4500 e-beam evaporator was used to deposit 10 nm of Ti (adhesion layer) and 90 nm of Au. After metal deposition, the LOR/photoresist was removed by soaking the wafers in a

solution of Remover 1165 for a few hours.

QCM devices were also fabricated by conventional methods. Photoresist (SPR220-3) was spin coated on individual QCM devices and baked at 115°C for 90 sec. The samples were exposed for 10 seconds by an ABM Contact Aligner. After a post exposure bake at 115°C for 90 seconds, the devices were developed for 90 seconds in MIF 726 and then rinsed with water and dried under nitrogen. Using a Branson P2000 barrel etcher, the samples were descummed for 4 minutes. An ATRP initiator with a thiol functional group was used to attach to the gold surface.¹² The QCM substrates were kept in 1 mM initiator solution in anhydrous hexanes overnight under nitrogen. After immobilization, the remaining photoresist was removed by soaking the substrates in ethanol for 10 minutes and then rinsed with acetone and dried under nitrogen. The photosensitizer was then electrochemically immobilized on the newly exposed regions of the QCM gold surface (*vide infra*) and lastly polymer brushes was grown from the ATRP initiator sites.

Equipment: Quartz crystal microbalance (QCM) measurements were performed using a Model PM-740 plating monitor (Maxtek, Inc., Torrance, CA), and data were recorded using a custom LabWindows program. Stanford Research Systems (Sunnyvale, CA) and Tangidyne Corp. (Greenville, SC) were the sources for 5 MHz AT-cut quartz crystals, 1 inch diameter with Ti/Au. Square wave voltammetry (SWV) and cyclic voltammetry (CV) were performed using a Model 900 potentiostat from CH Instruments (Austin, TX) or an epsilon potentiostat (Bioanalytical Systems Inc., West Lafayette, IN). In some cases, such as the electropolymerization and DNP analysis, CVs were obtained using a Princeton Applied Research Model 173

Potentiostat-Galvanostat , a Model 175 Universal Programmer, and Model 176 Current Follower, and data were recorded using a custom LabVIEW program. For irradiating the samples a Model M-20V transilluminator (UVP LLC, Upland, CA) with emission in the midrange, 302 nm, was used. Radiant power at the sample was 0.7 mW/cm². Confidence intervals are reported to within 90 % confidence.

Results and Discussion

Our device incorporates three key elements: patterned polymer brushes to present selected haptic groups; cofactors required for ACWOP; and components for electrochemical detection and quantification of H₂O₂ (Figure 1B). Details about the materials and methods used and additional control experiments are given in the supporting information. A fundamental feature of our device is the use of poly(oligoethylene glycol methacrylate) (POEGMA) polymer brushes (Figure 2A) for anchoring a variety of hapten groups and for preventing non-specific adsorption of other biomolecules that may be present in the test sample. OEG moieties are known to be resistant to protein adsorption and have long-term stability due to their high packing characteristics.¹⁶ The dense packing of neighboring chains results in an increased entropic force which drives the brushes into a stretched state at high grafting densities and yields effective resistance to non-specific binding.¹⁷ To produce the necessary high grafting density, we employed atom transfer radical polymerization (ATRP) methods to grow brushes on either a silicon wafer chip or a gold-plated quartz crystal microbalance (QCM) crystal.¹³ By functionalizing the initiator end with either a silane or thiol group, we selectively bind the polymer brushes to silicon or gold

surfaces, respectively. Polymer brushes have the capacity to be modified with a broad range of haptens for corresponding detection of antibodies with a broad range of specificities.

For initial development and optimization of this platform, we used 2,4-dinitrophenyl (DNP) groups as a model hapten. This well-characterized hapten binds specific anti-DNP antibodies of several classes and species and can be conjugated to the ends of the brushes through a one-step process (Figure 2). The functionalized polymer brushes ranged in thickness from 13-35 nm, measured *via* ellipsometry, and two methods to confirm the presence of DNP groups were utilized. First, fluorescence imaging with fluorescently labeled anti-DNP IgG antibodies verified the presence of the DNP groups when compared to sample of unfunctionalized brushes (Figure 3A). Second, the electroactive DNP allowed measurement of its surface coverage through cyclic voltammetry by means of the reduction of nitro groups to the corresponding hydroxylamine (Figure 3B). The surface coverage of DNP was typically on the order of 10^{-11} mol/cm², with a maximum of 1.5×10^{-10} mol/cm².

Quartz crystal microbalance (QCM) measurements were used to determine the surface coverage of the antibodies (Figure 4A). The functionalized QCM crystal (Figure 4B) was placed in phosphate-buffered saline solution (PBS, pH 7.2), containing 1 mg/mL bovine serum albumin (BSA). The frequency was allowed to stabilize before the addition of a solution containing anti-DNP IgG antibodies (Figure 4A), and the Sauerbrey equation was used to relate the change in frequency to the mass of immobilized antibodies.¹⁸ The antibody surface coverage was typically $5(\pm 2)$ $\times 10^{-12}$ mol/cm². The POEGMA brushes were tested for non-specific adsorption in

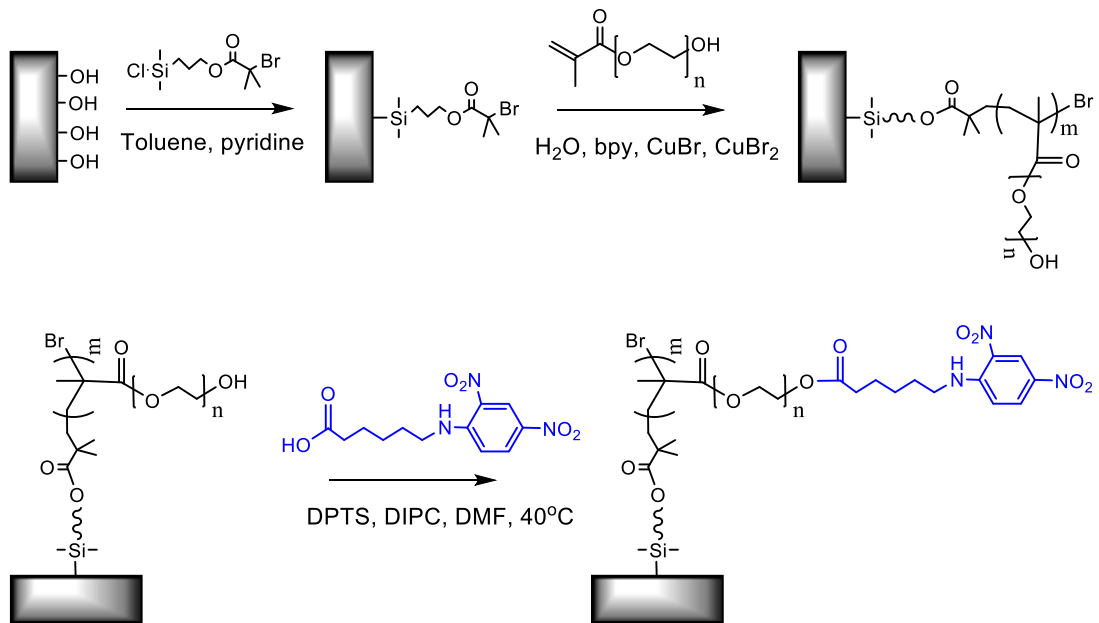


Figure 2: Synthesis of polymer brushes on a silicon substrate. Only the silicon surface is shown; gold surface modification using thiol based initiators was also carried out.

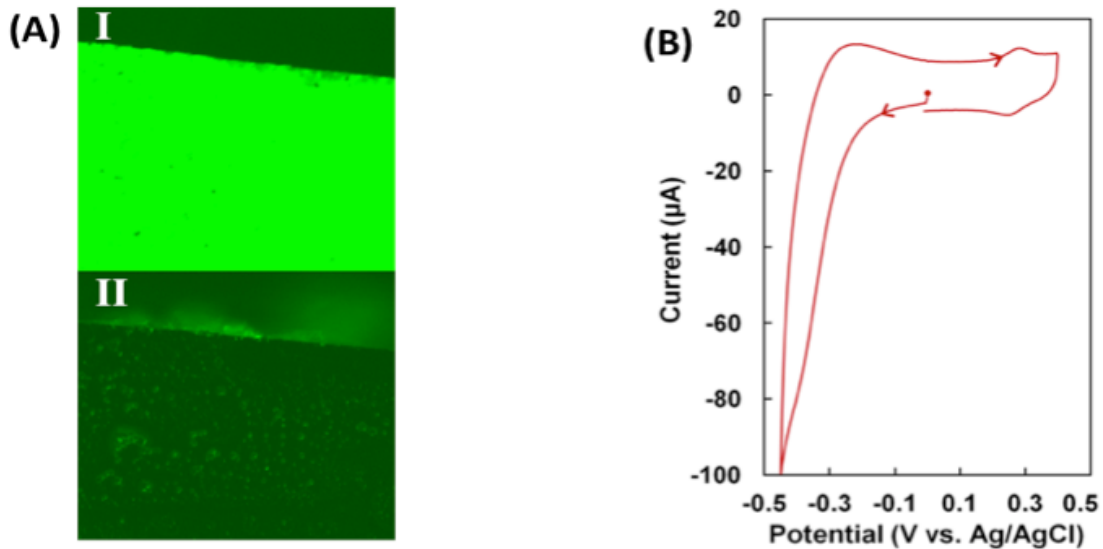


Figure 3: (A) Binding of AlexaFluor 488 (green) labeled anti-DNP IgE to POEGMA brushes functionalized, or not, with DNP. Brushes with DNP on the surface show green fluorescence (I). No fluorescence above background is observed on surfaces with POEGMA brushes without DNP functionalization under the same conditions of incubation with anti-DNP (II). (B) Cyclic voltammogram of DNP-functionalized polymer brush. Inset: Cyclic voltammogram of hydroxylamine formed upon reducing DNP. Supporting electrolyte, 0.1 M H_2SO_4 ; sweep rate, 100 mV/s.

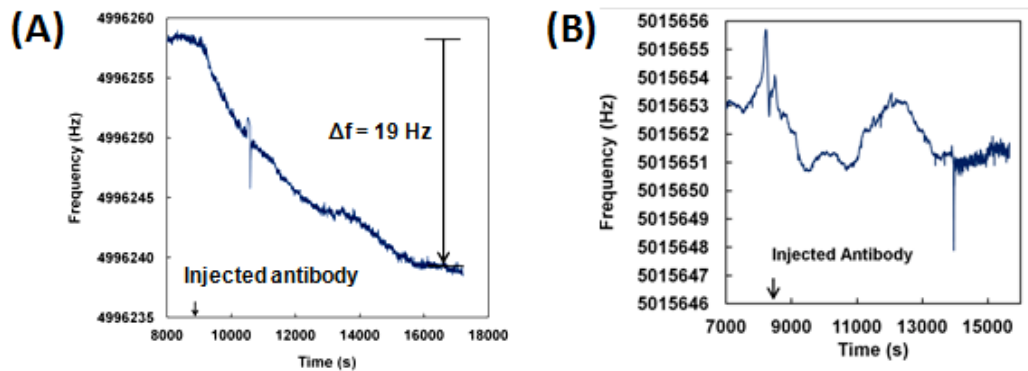


Figure 4: (A) Frequency response of QCM crystal platform in PBS, pH 7.2, containing 1 mg/mL BSA solution at 25°C. Rat anti-DNP IgG antibody solution (resultant concentration 11 nM) was added at 9000 s. (B) QCM frequency response to the addition of 100 μL of 1 mg/mL non-specific sheep IgG antibody (resultant concentration, 11 nM) to a 60 mL solution of PBS, pH 7.2 containing 1 mg/mL BSA solution at 25°C. The solution was stirred throughout the measurement.

control experiments by incubating the QCM crystals modified with POEGMA-DNP in a solution of non-specific antibodies. The DNP-polymer brush system on a QCM crystal was exposed to a solution of 10 nM non-specific sheep IgG antibody in 1 mg/mL BSA in PBS, pH 7.2. No significant change in the frequency was observed (Figure 4B), confirming that non-specific antibodies do not bind to the brushes. Furthermore, no significant increase in the amount of H₂O₂ was observed under these control conditions (*vide infra*).

Two types of platforms were used, one on silicon and another on a QCM crystal, in both cases presenting the polymer brushes adjacent to the photosensitizer on the same surface (Figure 5). Our ultimate device is designed to employ silicon chips. However, for calibration purposes, QCM crystals were used to quantify the mass of the bound antibodies. For the silicon chips, gold was evaporated onto 1 x 2 cm silicon wafer pieces in a grid pattern. The photosensitizer was electropolymerized on the gold (*vide infra*), whereas the polymer brushes, grown as depicted in Figure 2, were confined to the silicon oxide squares (Figure 5A). The same grid pattern was used for a QCM crystal (Figure 5B). However, because both the polymer brushes and photosensitizer were grown on a gold surface on the QCM crystal, a series of steps was employed to prevent the two films from overlapping. First, a photoresist was spin coated onto the QCM crystals to pattern the grid. Next, the thiol functionalized ATRP initiator was immobilized on the exposed gold surface, and the photoresist was subsequently removed. Finally, the photosensitizer was electropolymerized on the sections where the photoresist was removed, and polymer brushes were then grown from the regions containing the immobilized ATRP initiator. This specific order of

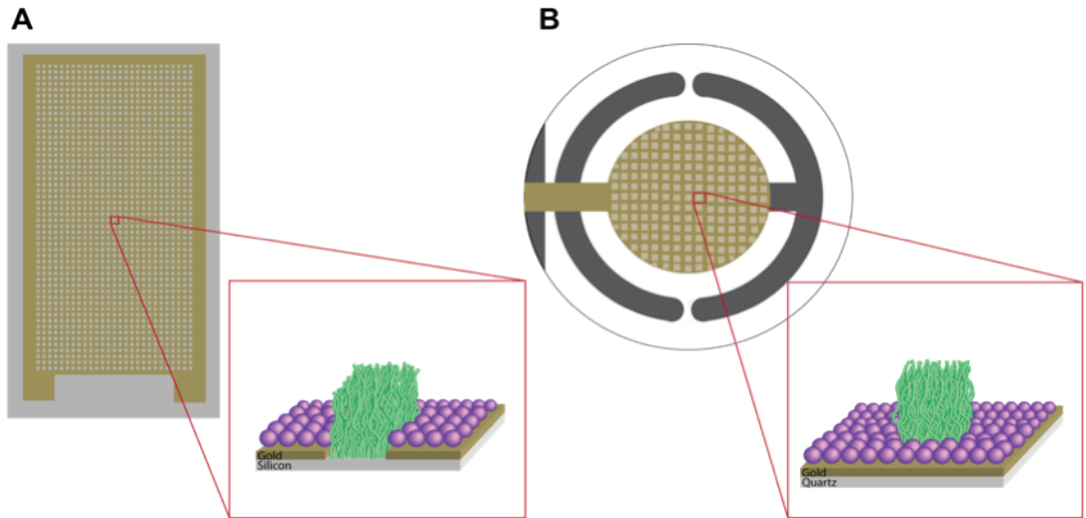


Figure 5. (A,B) Grid patterns of 150 μm wide lines surrounding 300 x 300 μm square areas on silicon (A) and gold electrode of a QCM crystal (B). Note that the figure is not drawn to scale. (C) Cyclic voltammograms of photosensitizer. Solid lines are for QCM crystal platform immersed in 0.5 mM $[\text{Ru}(\text{v-bpy})_3](\text{PF}_6)_2$, showing electropolymerization of photosensitizer upon reduction. Dashed lines are for an electropolymerized layer of $[\text{Ru}(\text{v-bpy})_3]^{2+}$ in fresh solution. Supporting electrolyte, 0.1 M TBAPF₆ in MeCN; sweep rate, 100 mV/s.

patterning and immobilization of the different components allowed for the maximum yield of both photosensitizer and polymer brushes on the same surface.

As described above, the ACWOP process requires singlet oxygen, ${}^1\text{O}_2^*$, which can be generated from ambient oxygen ${}^3\text{O}_2$ through the use of a photosensitizer, $[\text{Ru}(4\text{-vinyl},4'\text{-methyl}, 2,2'\text{-bipyridine})_3]^{+2}$ ($[\text{Ru}(\text{v-bpy})_3]^{+2}$) in our studies. We found that electropolymerized films of $[\text{Ru}(\text{v-bpy})_3]^{+2}$ (Figure 6)¹⁵ on the gold electrode immediately adjacent to the brushes maximized production of H_2O_2 . Typical coverage of photosensitzer was $1.5(\pm 0.5) \times 10^{-9} \text{ mol/cm}^2$, corresponding to a thickness of ca. 26 nm.

In addition to enhancing the signal to noise ratio, our results showed a significant increase in the ACWOP H_2O_2 signal for the adjacent, immobilized photosensitizer compared to photosensitizer in solution. This increase is likely the result of having the singlet oxygen generated in close proximity to the antibody. The lifetime of singlet oxygen in aqueous solution is in the range of 1-10 μs corresponding to a mean square distance (MSD) diffusion of less than 0.5 μm , assuming a diffusion coefficient of $2 \times 10^{-5} \text{ cm}^2/\text{s}$.^{19,20} Generating the singlet oxygen in close proximity to the antibody clearly enhances the sensitivity of the biosensor.

To generate ${}^1\text{O}_2^*$, and consequently H_2O_2 , the QCM crystal containing the immobilized antibodies and electropolymerized sensitizer was immersed in 3 mL of PBS (pH 7.2) and exposed to UV irradiation for 60 minutes. We found that 60 minutes with a broad wavelength source was optimal, as longer exposure times resulted in a decrease in signal and increase in background, possibly due to UV damage of the antibody.

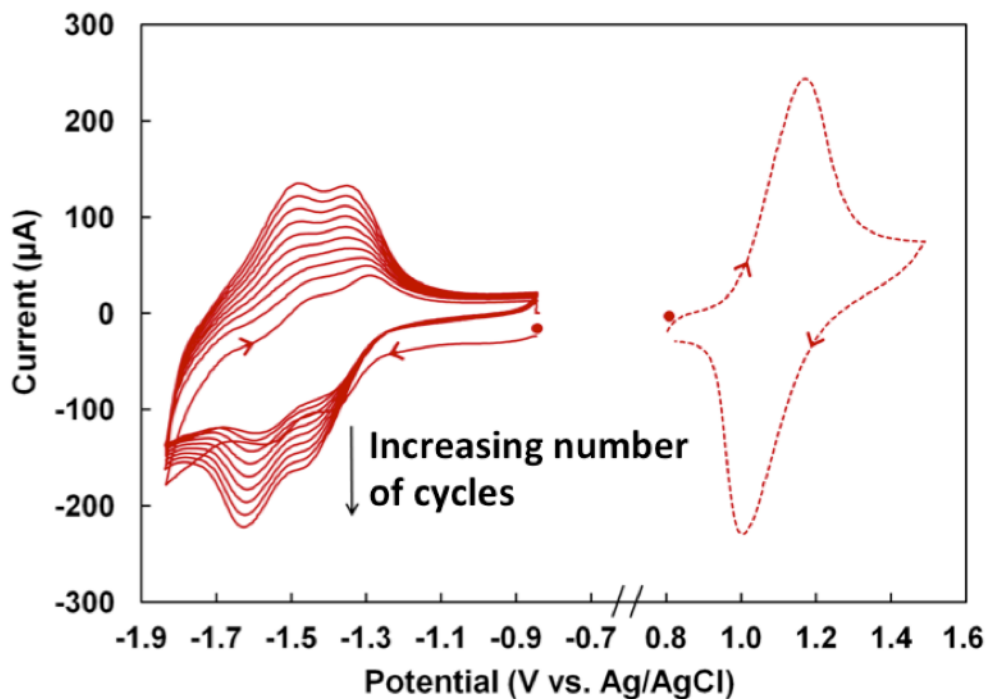


Figure 6. Cyclic voltammograms of photosensitizer. Solid lines are for QCM crystal platform immersed in 0.5 mM $[\text{Ru}(\text{v-bpy})_3](\text{PF}_6)_2$, showing electropolymerization of photosensitizer upon reduction. Dashed lines are for an electropolymerized layer of $[\text{Ru}(\text{v-bpy})_3]^{2+}$ in fresh solution. Supporting electrolyte, 0.1 M TBAPF₆ in MeCN; sweep rate, 100 mV/s.

The H₂O₂ generated was quantified using square-wave voltammetry (SWV) (Figure 7), which provides high sensitivity at low analyte concentrations.^{8,9,21} Amplex Red (N-acetyl-3,7-dihydrophenoxazine) reacts with H₂O₂ in a 1:1 ratio in the presence of horseradish peroxidase (HRP) to produce resorufin (7-hydroxy-3H-phenoxazin-3-one), which is fluorescent and exhibits a reversible redox response (Figure 1B).²² The lowest concentration of H₂O₂ detected with SWV was 0.33 nM (Figure 7 A,B). Assuming a surface coverage of antibodies of 5×10^{-12} mol/cm², and a liquid thickness of 100 μm (a value readily achievable in a microfluidic platform), a single turnover per immobilized antibody would give rise to a peroxide concentration of 500 nM, clearly well above our detection limit.

To quantify the number of mole equivalents of H₂O₂ generated per antibody, we evaluated H₂O₂ produced in the presence and absence of the immobilized antibody (Figure 7C). An aliquot of the irradiated solution was diluted with pH 6.0 PBS, followed by addition of Amplex Red and HRP. SWV was used to measure the amount of resorufin, which reduces near -0.2 V vs. Ag/AgCl, at a glassy carbon electrode. A readily quantifiable increase in reduction current (i.e., the amount of H₂O₂ produced) resulted from the presence of adsorbed antibody. Using a calibration curve, the mole ratio of H₂O₂ produced per antibody was determined. (Figure 7A,B). The ratio of H₂O₂ per antibody was 640 to 1200, which substantially exceeds the previously reported value.(6) Although this difference may be due, in part, to an increase in temperature, the biggest influence may be the generation of ¹O₂* in close proximity to the antibody (*vide supra*), such that this highly reactive species is more readily

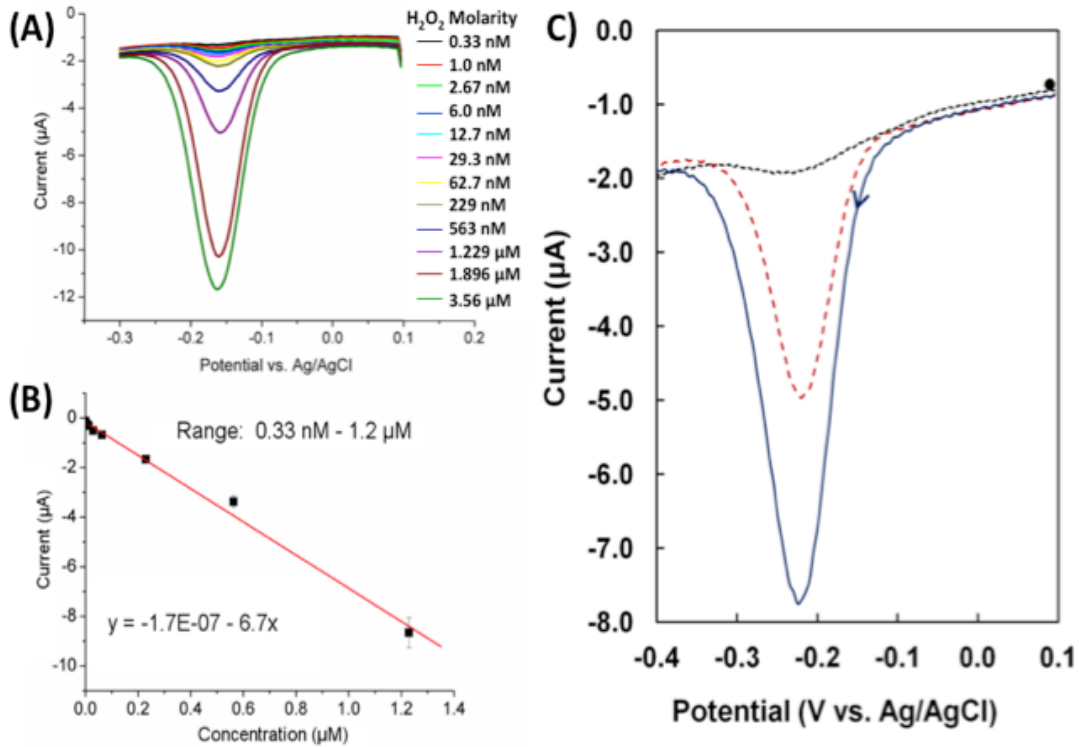


Figure 7. Square wave voltammetry (A) of 10 μM Amplex Red and 0.2 U/mL horseradish peroxidase (HRP) with varying concentrations of H_2O_2 to construct a calibration curve (B). Supporting electrolyte was PBS, pH 6.0. Step size, 5 mV; amplitude, 25 mV; frequency, 25 Hz. (C) Square wave voltammograms showing detection of H_2O_2 via reduction of resorufin at a 3 mm glassy carbon electrode after irradiation with UV light. Black short dashed line is 10 μM Amplex Red; red long dashed line is 10 μM Amplex Red with 0.2 U/mL HRP in the absence of antibody; blue solid line is 10 μM Amplex Red with 0.2 U/mL HRP in the presence of adsorbed antibody. Step size, 5 mV; amplitude, 25 mV; frequency, 25 Hz. A 1.5 mL aliquot of each irradiated solution in PBS, pH 7.2, was diluted to 5.0 mL using PBS, pH 6.0, and then Amplex Red and HRP solutions were added after deaerating the PBS.

intercepted by the antibody to generate H₂O₂. For any particular application, further calibration with a reference antibody solution will allow the concentration of antibodies in the test sample to be determined.

Conclusion

In summary, we have developed a general immunobiosensor platform, employing patterned polymer brushes with photosensitizer films, based on the electrochemical detection of H₂O₂ at clinically relevant concentrations generated through the ACWOP. We have shown that H₂O₂ at concentrations as low as 0.33 nM can be measured in a biosensor device. Antibodies at a surface coverage of 5×10^{-12} mol/cm² generate more than 25×10^{-10} mol H₂O₂/cm² (or >250 μM H₂O₂, assuming volume of 1cm x 1cm x 100 μm) in 60 min. These tests indicate that this device can detect lower than 3 pg antibodies in a 10 μL sample (2 pM). This compares quite favorably to the most sensitive ELISAs, which requires secondary agents and additional procedural steps. The use of secondary antibodies, as in the case for ELISA, is unnecessary, making our platform appealing for low cost applications. Moreover, since the ACWOP is a general characteristic of antibodies, our approach can, in principle, be applied to antibodies of virtually any specificity, class or species. We found results obtained from antibodies adsorbed on the platform on a silicon chip to be similar to those obtained using the QCM crystal (Figure S7). We are currently exploring the incorporation of this approach in microfluidic platforms and flexible electronics that would allow for widespread use and field deployment.

Acknowledgments

The authors would like to acknowledge the National Science foundation grant DMR-1105253 for support of this work. This work made use of the Cornell Center for Materials Research Shared Facilities which are supported through the NSF MRSEC program (DMR-1120296), the Nanobiotechnology Center shared research facilities at Cornell University, and was performed in part at the Cornell NanoScale Facility, a member of the National Nanotechnology Infrastructure Network, which is supported by the NSF (Grant ECS-0335765). All electrochemical measurements (Cyclic voltammogram of DNP-functionalized polymer brush, QCM measurements for surface coverage of antibodies, QCM measurements of non-specific adsorption, electrochemical polymerization of the photosensitizer, and square wave voltammograms for detection of H₂O₂) were conducted by Prof. Héctor Abruña's group, Department of Chemistry and Chemical Biology, Cornell University. Specific individuals include Nicole L. Ritzert, Hongjun Chen, and Michele E. Tague.

Antibody buffer solution and initial luminescent experiments for optimizing conditions were carried out by Prof. Barbara Baird's group, Department of Chemistry and Chemical Biology, Cornell University. Contributing members include Norah L. Smith, Devin Wakefield and Marcus Wilkes.

REFERENCES

- (1) Potter, C. W. *J. Appl. Microbiol.* **2001**, *91*, 572.
- (2) Burns, A.; van der Mensbrugghe, D.; Timmer, H.; The World Bank: 2006.
- (3) Herfst, S.; Schrauwen, E. J. A.; Linster, M.; Chutinimitkul, S.; de Wit, E.; Munster, V. J.; Sorrell, E. M.; Bestebroer, T. M.; Burke, D. F.; Smith, D. J.; Rimmelzwaan, G. F.; Osterhaus, A.; Fouchier, R. A. M. *Science* **2012**, *336*, 1534.
- (4) Russell, C. A.; Fonville, J. M.; Brown, A. E. X.; Burke, D. F.; Smith, D. L.; James, S. L.; Herfst, S.; van Boheemen, S.; Linster, M.; Schrauwen, E. J.; Katzelnick, L.; Mosterin, A.; Kuiken, T.; Maher, E.; Neumann, G.; Osterhaus, A.; Kawaoka, Y.; Fouchier, R. A. M.; Smith, D. J. *Science* **2012**, *336*, 1541.
- (5) Imai, M.; Watanabe, T.; Hatta, M.; Das, S. C.; Ozawa, M.; Shinya, K.; Zhong, G. X.; Hanson, A.; Katsura, H.; Watanabe, S.; Li, C. J.; Kawakami, E.; Yamada, S.; Kiso, M.; Suzuki, Y.; Maher, E. A.; Neumann, G.; Kawaoka, Y. *Nature* **2012**, *486*, 420.
- (6) Wentworth, P.; Jones, L. H.; Wentworth, A. D.; Zhu, X. Y.; Larsen, N. A.; Wilson, I. A.; Xu, X.; Goddard, W. A.; Janda, K. D.; Eschenmoser, A.; Lerner, R. A. *Science* **2001**, *293*, 1806.
- (7) Zhu, X. Y.; Wentworth, P.; Wentworth, A. D.; Eschenmoser, A.; Lerner, R. A.; Wilson, I. A. *P. Natl. Acad. Sci. U.S.A.* **2004**, *101*, 2247.
- (8) Lyon, J. L.; Stevenson, K. J. *J. Anal. Chem.* **2006**, *78*, 8518.
- (9) Bard, A. J.; Faulkner, L. R. *Electrochemical Methods: Fundamentals and Applications*; 2nd ed.; Wiley: New York, 2001.
- (10) Moore, J. S.; Stupp, S. I. *Macromolecules* **1990**, *23*, 65.

- (11) Shah, R. R.; Merreceyes, D.; Husemann, M.; Rees, I.; Abbott, N. L.; Hawker, C. J.; Hedrick, J. L. *Macromolecules* **2000**, *33*, 597.
- (12) Ramakrishnan, A.; Dhamodharan, R.; Ruhe, J. *J. Pol. Sci. .Pol. Chem.* **2006**, *44*, 1758.
- (13) Senaratne, W.; Takada, K.; Das, R.; Cohen, J.; Baird, B.; Abruna, H. D.; Ober, C. K. *Biosens. Bioelectron.* **2006**, *22*, 63.
- (14) Buttry, D. A.; Ward, M. D. *Chem. Rev.* **1992**, *92*, 1355.
- (15) Abruna, H. D.; Denisevich, P.; Umana, M.; Meyer, T. J.; Murray, R. W. *J. Am. Chem. Soc.* **1981**, *103*, 1.
- (16) Harder, P.; Grunze, M.; Dahint, R.; Whitesides, G. M.; Laibinis, P. E. *J. Phys. Chem. B* **1998**, *102*, 426.
- (17) Wang, R. L. C.; Kreuzer, H. J.; Grunze, M. *J. Phys. Chem. B* **1997**, *101*, 9767.
- (18) Sauerbrey, G. *Zeitschrift Fur Physik* **1959**, *155*, 206.
- (19) Salokhiddinov, K. I.; Byteva, I. M.; Gurinovich, G. P. *Zhurnal Prikladnoi Spektroskopii* **1981**, *34*, 892.
- (20) Merkel, P. B.; Kearns, D. R.; Nilsson, R. *J. Am. Chem. Soc.* **1972**, *94*, 1030.
- (21) Osteryoung, J. G.; Osteryoung, R. A. *Anal. Chem.* **1985**, *57*, A101.
- (22) Gajovic-Eichelmann, N.; Bier, F. F. *Electroanal.* **2005**, *17*, 1043.

CHAPTER 3

OECT GLUCOSE SENSOR WITH POLYMER BRUSHES

Abstract

Recently, there has been significant research in the area of organic electrochemical transistors (OECTs) due to their superior capabilities in chemical and biological sensing. Here we report for the first time the incorporation of glucose oxidase linked to polymer brushes grown directly on conducting polymer as the platform for a sensor. Polymer brushes were chosen for their biocompatibility and their ability to covalently tether enzymes and other biomolecules to selected surfaces. We fabricated OECTs made from the conducting polymer poly(3,4-ethylenedioxythiophene) doped with poly(styrene sulfonate), PEDOT:PSS, and polymerized from the electrode surface a mixed polymer brush of poly(glycidyl methacrylate) (PGMA) and poly(2-hydroxyethyl methacrylate) (PHEMA). The brushes were functionalized with glucose oxidase and demonstrated excellent performance in terms of glucose specific long-term stability and limit of detection.

Introduction

There are about 347 million diabetic patients worldwide and according to WHO reports, 3.4 million people died from diabetes related complications in 2010 alone.¹ Hyperglycemia, or raised blood sugar, is often a sign of uncontrolled diabetes, leading

* This chapter has been submitted for review as an article to Advanced Material.

to the recommendation that diabetic patients should check their glucose levels 2 to 4 times per day.¹ Continuous monitoring of glycemia enables one to inject insulin when needed, ultimately leading to an additional 5 years of life, 8 years of sight, 6 years without kidney disease, and 6 years safe from lower extremity amputation.²

Effective glucose sensors have been marketed for decades, but they are painful, costly and unsuitable for long term monitoring. Glucose is usually detected with a catalytic working electrode coated with glucose oxidase (GOx), a D-glucose specific enzyme. An ideal glucose sensor should be able to work in an aqueous environment during extended time periods, show good sensitivity and stability, be minimally invasive and be cost efficient. Organic electrochemical transistors (OECTs) satisfy most of these constraints since they can operate at low voltage in an aqueous environment and they can be easily fabricated at low cost.³ Based on conducting polymers, OECTs have shown large applications of chemical sensing including humidity sensors, lactate sensors and glucose sensors.^{4,5} OECTs make use of the change in current flowing in a conducting polymer electrode channel as a parameter to measure glucose concentrations.⁶ Poly(3,4-ethylenedioxythiophene) doped with poly(styrene sulfonate) (PEDOT:PSS) has been successfully used as the active layer of OECTs and has shown excellent results for biosensing due to its high conductivity, biocompatibility and stability in aqueous environment.^{7,8} Recent work on PEDOT:PSS OECT glucose sensors have demonstrated glucose detection limits from 5 nM to 100 mM range covering physiological and pathological blood, brain and saliva glucose ranges in human.⁹

In current OECT glucose sensors, the GOx is free in the electrolyte.^{10,11} However,

in vivo chronic monitoring of glucose requires the GOx to be bound to the electrode to prevent enzyme leakage and decrease of signal over time.⁶ Common methods of glucose binding include physical adsorption, covalent bonding, entrapment, and electropolymerization.¹²⁻¹⁵ With the exception of covalent bonding, these techniques are subject to enzyme leakage and lack the required immobilization stability. Covalent binding, on the other hand, anchors the enzyme to the surface while maintaining high activity. Different forms of chemical bonding have been suggested. Yang et al. used an organic-inorganic sol-gel silicate network with a primary amine functional backbone to provide a carbodiimide reaction with glucose oxidase.¹⁶ Others have covalently bound enzymes using supports such as copolymers of acrylonitrile¹⁷ and polyaniline (PANI) and chitosan-coupled carbon nanotubes (CS-CNTs).¹⁸ Here, we used polymer brushes as a scaffold to anchor glucose oxidase to our electrode surface.

Polymer brushes are polymer chains tethered at one end to a surface or substrate. “Grafting from” and “grafting to” are the typical forms of attachment.¹⁹ The “grafting to” method entails brushes first being polymerized in solution with an activated end group that can be covalently anchored to a surface. This technique leads to low density polymer brushes, in contrast to the “grafting from” method which produces high density polymer brushes. In this case, a self-assembled monolayer of an initiator molecule is covalently immobilized on a surface and the brush is grown from the surface through radical polymerization techniques such as atom transfer radical polymerization (ATRP) or nitroxide-mediated polymerization (NMP). It has been demonstrated that polymer brushes can effectively interface between biosensors and biological media in microelectronics, nanofluidic devices, biosensing, and other areas

of nanotechnology.²⁰⁻²³ Other advantages include control over chain length, and covalent attachment to a surface therefore preventing desorption of the polymer film.

We present the first example of polymer brushes anchored to a PEDOT:PSS surface. Utilizing biologically suitable polymer brushes in our devices enables the covalent attachment of GOx to provide high sensibility and stability of glucose sensing. We have focused on a mixed brush comprised of poly(glycidyl methacrylate) (PGMA) and poly(2-hydroxyethyl methacrylate) (PHEMA) which is a soft, flexible system that provides attachment points for the enzyme and is compatible with biological media. This technological choice provides optimal GOx attachment to our electrode device and shows stability over time.

Experimental Section

Materials: α -Bromoisobutyryl bromide, pyridine, copper (I) chloride, copper (II) dibromide, inhibitor remover, glycidyl methacrylate, 2-hydroxyethyl methacrylate, ethylene glycol, pyridine, d-glucose and glucose oxidase (type VII, >100,000 units/g) were purchased from Sigma Aldrich and used without purification unless stated otherwise. PEDOT:PSS (Clevios PH 1000) was purchase from Heraeus. Fe(III)tosylate and edot monomer were purchase from Yacoo Chemical Company. Parylene-c was purchase from SCS. Deionized water with a resistivity of 18.2 M Ω •cm at 25 °C was obtained from Millipore's Milli-Q Synthesis A10 system. All the other solvents were purchased from Fisher Scientific.

Pattern formation and deposition of PEDOT:PSS and PEDOT:TOS: The fabrication process of the conducting polymer electrodes is shown in Figure 1. Either

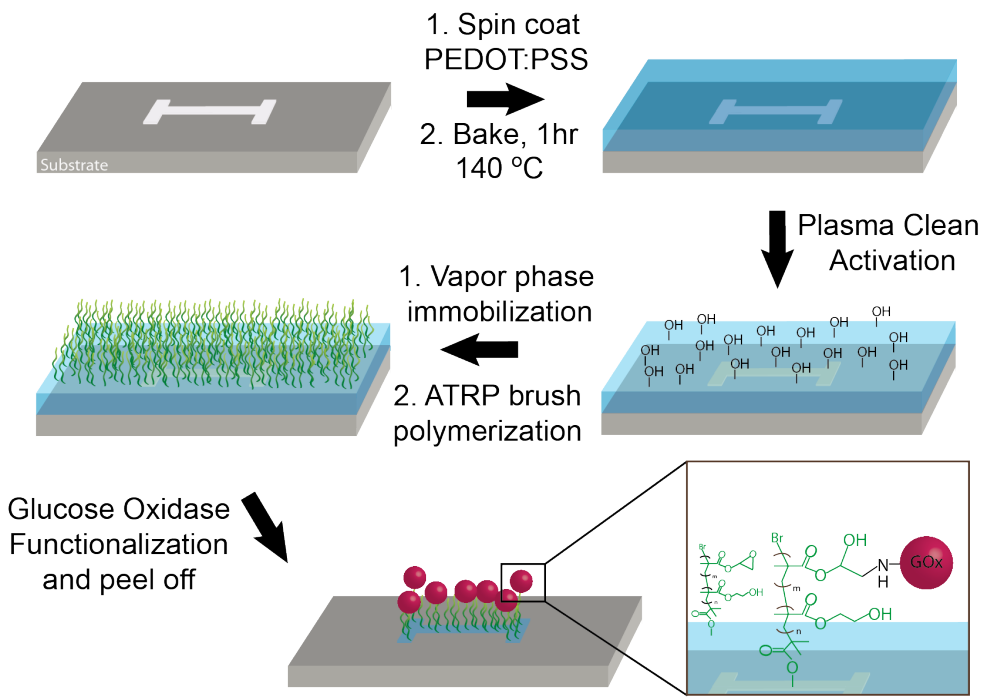


Figure 1. PGMA:PHEMA mixed polymer brush and glucose oxidase (GOx) fabrication on electrode device (A). Reaction cycles for detection of glucose in devices employing a Pt electrode (B).

PEDOT:PSS or PEDOT:TOS were used as the conducting polymer layer. Prior to coating, ethylene glycol was added to PEDOT:PSS in a volume ratio of 1:4 to increase conductivity. Dodecylbenzenesulfonic acid (DBSA) (0.5 μ L/mL) was added as a surfactant to improve film formation.²⁴ The two layers of PEDOT:PSS were respectively spun coated at 1200 rpm for 30 seconds and post baked 2 minutes at 110°C and spun coated at 650 rpm for 30 seconds and finally post baked for 1 hour at 140° C at atmospheric condition.

The PEDOT:TOS film was fabricated according to a previously published protocol.²⁵

The PEDOT based channel was patterned using a 2 μ m parylene-C sacrificial layer peel-off techniques,²⁶ resulting to a conducting polymer layer width of 0.1 mm. The defined active surface exposed to electrolyte was 1mm². The parylene-C sacrificial layer peel-off has been the very final part of the fabrication (after the brush growth and the GOx functionalization). An initial 2 μ m thick film of parylene-C was vapor deposited on silicon wafer and then used as substrate. Silane was added as a cross linker prior to initial parylene-C evaporation.

Plasma and Immobilization: PEDOT:PSS and PEDOT:TOS samples were oxidized using a Harrick Plasma Cleaner at 29.6 W for a range of times, 10 sec - 7 min. Once the surface was activated, the initiator was introduced in the vapor phase. A vial with 1ml of the initiator, α -bromoisobutyryl bromide, was placed in a glass reactor with the samples. The chamber was evacuated for 1 minute before removing the pump and sealing the reactor for 30-45 minutes. Afterward, the samples were

rinsed with ethanol and methanol to remove any physically absorbed ATRP starter.

Brush Growth: PGMA:HEMA brushes were prepared by placing two sample devices with immobilized initiator in a 25 mL Schlenk flask under an argon atmosphere. The flask was evacuated and backfilled with argon four times. CuCl (72.8 mg, 0.7 mmol), CuBr₂ (7.8 mg, 0.03 mmol), bipyridine (282 mg, 1.80 mmol) were taken in another 50 mL Schenk flask equipped with a magnetic stir bar. The air in the flask was evacuated and replaced with argon four times. Glycidyl methacrylate (2.60 g, 18 mmol), 2-hydroxyethyl methacrylate (3.085 g, 24 mmol), methanol (5 ml) and water (1.25 mL) was purged with argon for 25 minutes and cannulated into the flask containing the ligand and copper salts. The reaction mixture was stirred at room temperature for 30 min to ensure the formation of the copper-ligand complex. This solution was then transferred into the flask containing the initiator functionalized device samples and allowed to polymerize at 32 °C for different time lengths. After polymerization, the substrates were washed multiple times with dichloromethane and ethanol and dried under nitrogen gas.

OECT Functionalization by Glucose oxidase: Electrodes were first incubated in phosphate buffer (0.12M) at room temperature for 2 hours, then immersed in dimethylformamide (99.9%) (DMF) for 30 minutes at room temperature and finally the samples were incubated in glucose oxidase (GOx) (10 mg GOx for 10ml buffer) and DMF (0.1ml) solution, under agitation for 48 hours at room temperature. Every 12 hours the GOx/DMF solution was replaced. After the last incubation the samples were washed out with saline (0.9%) and again with Phosphate buffer (0.12M).²⁷ Electrodes were stored in phosphate buffer at 4°C.

Electrochemical: The electrochemical measurements were performed before and after brush formation and the GOx functionalization of the transistor in order to verify the electric parameters of the electrode.

The transistors were characterized using phosphate buffer (0.12M) as electrolyte. The gate electrode was a platinum wire with a volume 10:1 relative to the recorded conducting polymer. The total surface of conducting polymer functionalized by GOx was 10:1 relative to the recorded conducting polymer. The transistor were optimally biased and the drain and gate currents were recorded.

For the glucose measurements, the bias was applied for 180 seconds and a 180 seconds delay between biases was performed. These durations were found to be sufficient to reach steady-states. The drain current responses were normalized to the responses at 0 glucose concentration and has been described in previously published paper.²⁸ Each response was an average of 100 data points at a steady state (with and without glucose).

The stability measurements experiments were performed in 10mM of glucose electrolyte relative to 0mM of glucose electrolyte during 23 days under optimal biasing.

Tools: Polymer brushes were characterized by AFM (Veeco Icon) and NEXAFS. NEXAFS experiments were carried out on the U7A NIST/Dow materials characterization end station at the National Synchrotron Light Source at Brookhaven National Laboratory (BNL). The general underlying principles of NEXAFS spectroscopy and a description of the beamline at BNL have been reported elsewhere.^{29,30} The X-ray beam was elliptically polarized (polarization factor = 0.85),

with the electric field vector dominantly in the plane of the storage ring. The photon flux was approximately 1×10^{11} photons per second at a typical storage ring current of 750 mA. A spherical grating monochromator was used to obtain monochromatic soft X-rays at an energy resolution of 0.2 eV. The C 1s NEXAFS spectra were acquired for incident photon energies in the range of 270–320 eV. The incidence angle of the X-ray beam, measured from the sample surface, was set to 120° to maximize the Auger electron emission angle, making the measurement most surface-sensitive. The partial electron yield (PEY) signal was collected using a channeltron electron multiplier with an adjustable entrance grid bias (EGB) that was set at –150 V for these experiments. The channeltron PEY detector was positioned at an angle of 36° relative to the incoming X-ray beam in the plane defined by the sample normal and the X-ray beam and at an angle of 35° out of that plane.

Parylene-C was deposited using an SCS labcoater 2. Pattern were defined thru photomask with a SUSS MJB4 contact aligner and a reactive Ion etching O₂ plasma (160W, 50 sccm O₂, 15 min) using an Oxford 80 plus.

The electrochemical measurements were performed with a Keithley 2612A dual SourceMeter to bias the transistor and record the drain and gate currents.

Results and Discussion

There are numerous ways of depositing GOx on a surface. The major benefits of using polymer brushes include varying the length (distance between surface and enzyme) and covalent attachment, which prevents leakage of the enzyme from the surface. Because PEDOT:PSS is an unconventional surface for polymer brush

growth, characterization techniques must be carefully considered. After polymerization, a surface color change is observed due to brush growth and chemical changes can be confirmed via Near Edge X-Ray Absorption Fine Structure (NEXAFS). NEXAFS is a type of absorption spectroscopy that measures the photoabsorption cross-section for the excitation or photoionization of tightly bound core electrons. This is an ideal tool for probing bonding and orientation of molecules or molecular fragments on a surface. The presence of polymer brushes on a PEDOT:PSS surface can therefore be confirmed. Figure 2A shows a NEXAFS spectrum of PEDOT:PSS without functionalization (red line), where the C 1s- $\pi^*_{C=C}$ resonance appears at \sim 285.5 eV. This peak is characteristic of the aromatic π bonds found in PEDOT:PSS. Brush polymerization alters the chemical composition of the surface. Spectra of PGMA brushes on PEDOT:PSS (green and blue line) show the emergence of the C 1s- $\pi^*_{C=O}$ near 289.1 eV. This can be attributed to the carbonyl structures present in the backbone of the polymer brushes. The thicker the brush (blue), the greater the intensity of the carbonyl peak and the lower the intensity of the PEDOT:PSS peak, thus confirming a higher surface coverage. This observation is discussed further below.

The most conventional method of measuring brush thickness is ellipsometry. However, it becomes very difficult to model the PEDOT:PSS layer and accurately calculate the brush layer thickness. Instead, we used AFM. Figure 2B shows a scratch in the film that was measured before and after polymerization. Results confirmed an increase in film thickness on the order of 20 nm, which is congruent with the expected brush growth. For consistency, brush lengths were kept in this region for all

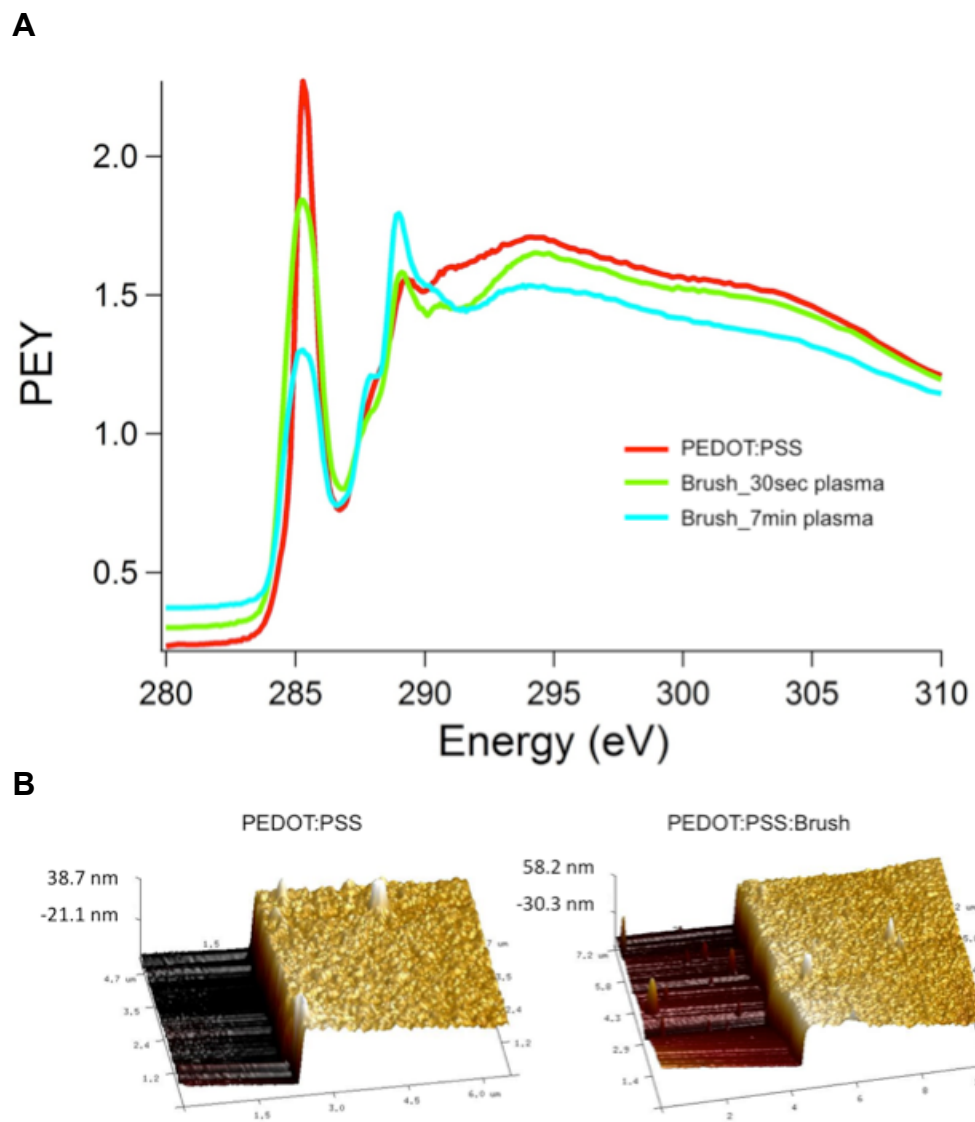


Figure 2. NEXAFS data confirming presence of polymer brush on PEDOT:PSS. Samples shown were acquired at an X-ray incidence angle of 60° (A). AFM image of a scratch in the PEDOT:PSS film before and after polymer brush growth (B). A height increase around 20 nm is observed due to brush polymerization.

electrochemical measurements.

Different types of polymer brushes can be grown from PEDOT:PSS surfaces as long as the polymerization environment does not destroy or lift off the film from the surface. The ATRP conditions used for our device (MeOH:H₂O 4:1), do not affect the film or conductivity of PEDOT:PSS. PGMA and PHEMA brushes were selected because they both can be grown under these conditions and previous studies have shown these polymers are compatible with GOx in biological environments.^{27,31} PGMA contains epoxy groups which can undergo a ring opening reaction when in the presence of a primary amine group. It has been shown that available amine groups on the GOx enzyme will undergo this reaction and attach to the polymer.³² PHEMA, on the other hand, swells in water and becomes soft and flexible. When immersed in an enzyme buffered solution, the combination of both as a mixed polymer brush produces a swollen system in which the enzyme can diffuse into and attach to available epoxy groups. Results indicated that without incorporation of the PHEMA, homogeneous PGMA brushes were likely in a glassy state and too rigid to react with and incorporate the glucose oxidase. The PEDOT:PSS/PGMA OECT previously loaded in GOx were responding to an increase of glucose only when GOx was added to the electrolyte revealing an insufficient anchoring of the enzyme to the PGMA brushes. By adding PHEMA as comonomer and swelling the brushes to expose more functional groups within the system, a much higher loading capacity is achievable.

Conventional polymer brush ATRP initiator immobilization conditions consist of anhydrous toluene solutions reacting with the surface for long periods of time (12 to 24 hours).³³ Long exposures to such severe environments can damage the

PEDOT:PSS; therefore, alternate methods to immobilize the initiator were established. By activating the surface with OH groups, an initiator can instead be attached in the gas phase. The ATRP starter bromoisobutyrylbromide has a vapor pressure of 2.8 mbar (ACD PhysChem Simulation) under ambient conditions, which makes it ideal for gas phase functionalization. Vapor immobilization allows for shorter reaction times (30-45 min) without direct contact to harsh solvent systems. The PEDOT:PSS films remained intact and retained conductivity after immobilization in the vapor phase and thus this method was preferred over the standard immobilization in solution process.

Just like standard silicon wafers, the PEDOT:PSS surface must first be primed before the initiator can be introduced. A mild plasma oxidation clean can provide the required functional groups on the surface, but caution must be taken because over exposure can damage the conductivity of the PEDOT:PSS. NEXAFS data (figure 2A) illustrates the effects of polymer brush growth associated with plasma oxidation priming. Short plasma oxidation times result in thinner brushes (green line) due to fewer initiating sites available; however longer plasma oxidation times render more functional groups available for initiator immobilization. Greater initiator surface coverage yields thicker, higher density polymer brushes (blue line). The tradeoff is the effect on conductivity. While long plasma etches may produce thicker brushes, extended exposure reduces PEDOT:PSS conductivity. Results show that shorter plasma oxidation times, 10 - 30 seconds, retain conductivity while still generating a thin polymer brush layer. For our purposes of covalent GOx attachment, a short brush has enough available functional groups to suffice. Therefore we have optimized our

process to short etch periods in order to obtain a thin brush and still maintain a high level of conductivity.

Enzymatic glucose sensors work via a cascade of reactions induced by the interaction between glucose and its enzyme, the GOx (figure 3). This cascade begins by the transformation of D-glucose into D-gluconolactone in the presence of GOx. The GOx reduced by the initial reaction gets reoxidized by oxygen, leading to peroxidase production. When interacting with the catalytic electrode, peroxidase gives rise to hydrogen and oxygen and transfers electrons to the catalytic working electrode (here a platinum electrode). As a result, the biasing of the PEDOT based channel is changed proportionally to the concentration of glucose. We compared modulations induced by platinum gate bias to current flowing into the PEDOT:PSS channel (I_{sd}). After the initial brush growth fabrication step and the glucose oxidase functionalization, an average decrease of $5.6 \mu\text{A}$ ($n=8$) of the negative I_{sd} was measured at a V_{sd} of -0.7 Volts and a platinum gating of 0.7 Volts. This reveals that the electric performances of the PEDOT:PSS are maintained.

We reproduced this experiment with PEDOT doped with tosylate (PEDOT:TOS). This conductive polymer is also a very promising candidate with a high conductivity characterized as 1000 S/cm for a film formed by vapor phase deposition and keeps most of the properties of the PEDOT.³⁴ Increases of the resistance and large decreases of the modulation of current flowing into the channel (I_{sd}) to different Ag/AgCl gate voltage bias relative to similar OECT prior to the initial brush growth fabrication step were observed. Those modulations decreased dramatically after the polymer brush growth. This led to almost no I_{sd} modulation when biased by a platinum electrode

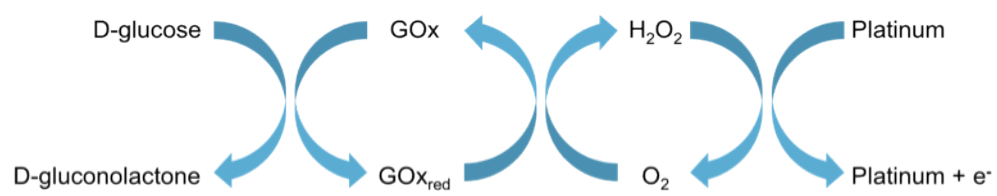


Figure 3. Reaction cycles for detection of glucose in devices employing a Pt electrode (B).

signifying that PEDOT:TOS is not appropriate as a glucose sensor with this technique.¹⁰ This is explained by the fact that platinum is not polarized contrary to Ag/AgCl. We thus chose PEDOT: PSS as conductive polymer.

After the functionalization with GOx, the PEDOT:PSS/PGMA/PHEMA/GOx (PPPG) electrode response to glucose was investigated (figure 4). The steady-state Isd are normalized to similar bias Isd without glucose. This normalization provided a range of response from no glucose (zero) to highest glucose concentration (more doped channel). When the PPPG had not been incubated in a solution with DMF before the functionalization (red line), the normalized response was small and showed significative response only at high concentration of glucose (up to 10 mM). The relative values are superior to 0.1 only from 10 mM of glucose to 100 mM (0.36 to 0.4, respectively).

Conversely, when the PPPG had been incubated before the functionalization step (black line) the normalized responses were already high for small concentrations of glucose (0.95 at 10 µM), increasing dramatically up to the highest concentration (3.84 at 100 mM). This range covers the physiological and pathological blood, brain and saliva glucose range in human. For comparison, the non-functionalized PGMA electrode was used as a glucose sensor with free glucose oxidase in the electrolyte (5 µl at 50mg/10ml in 50µl of 0.12M phosphate buffer) at 10mM of glucose (blue triangle). These results show that DMF helps the functionalization of the electrode by relaxing the polymer brush chains such that GOx can more readily diffuse into the system and covalently attach to a greater degree.

PPPG electrodes were also tested for their stability over time (figure 5). Four

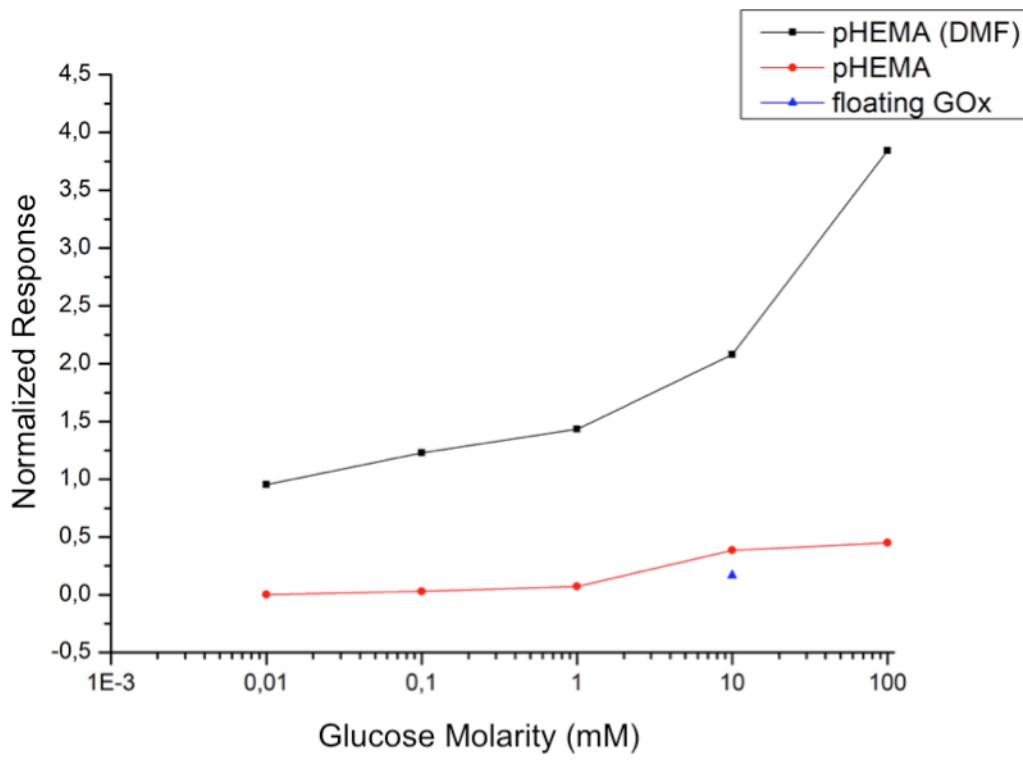


Figure 4. Normalized response to glucose of PEDOT:PSS/PGMA/pHEMA/GOx electrode. Black line represents electrode initially incubated in DMF, red line represents electrode not incubated in DMF, blue triangle corresponds to free Glucose oxidase in electrolyte.

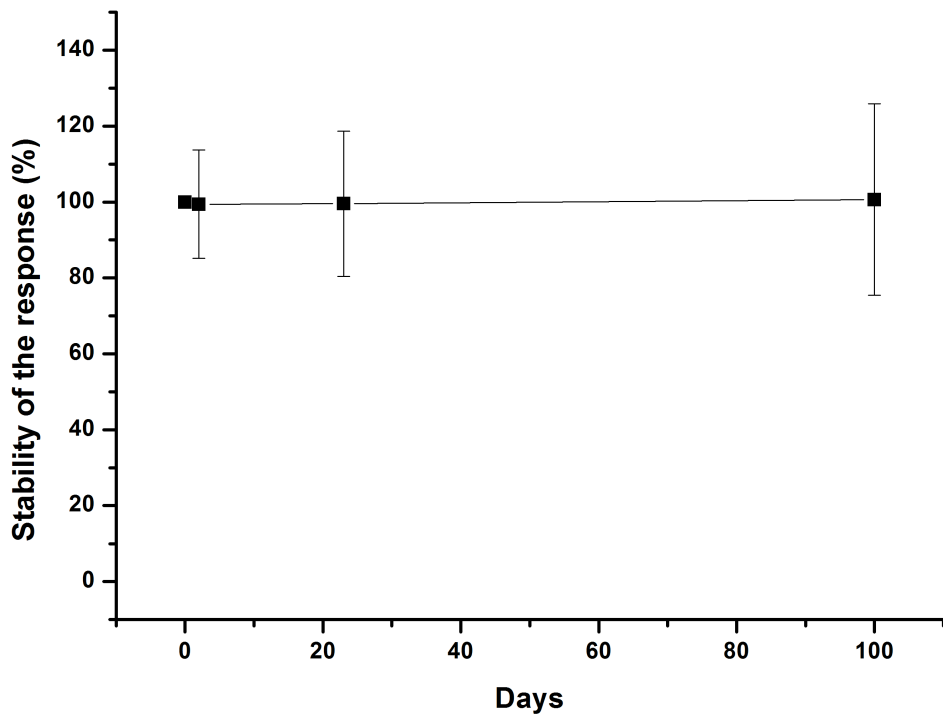


Figure 5 Stability versus time for PEDOT:PSS transistors with PGMA:HEMA brushes and functionalized with GOx.. Measurements were performed at optimal bias for 10mM of glucose in phosphate buffer (0.12M)

devices were tested over a period of 100 days. The stability was calculated relative to the response of the same transistor on the first day of measurement. Measurements were performed at a concentration of 10 mM. For reference, transistors incubated with GOx (non-covalently bound, incubation time of 60 min in PBS) showed an almost immediate decrease in response, reaching zero response within after a few days. With covalent bonding, the devices retain 100% of their response over 100 days, with only a small increase in standard deviation, from 14% on day 2 to 25% at 100 days. This is a remarkable stability over an extended time period.

Conclusion

Although glucose sensors have been around for decades, the incorporation of OECTs has taken the technology to a new level as part of a more complex sensing device. Simple fabrication, biocompatibility, flexibility, low operational voltage and the ability to operate in aqueous environments make these materials ideal surfaces to interface with biological media. Going one step further, we have demonstrated polymer brushes can be integrated into the system as a scaffolding to anchor glucose oxidase without compromise to the electrical performance of the PEDOT:PSS conducting substrate. Covalently binding the GOx to the brushes prevents enzyme leakage and thus loss of signal over time. Such functionalization methods, as well as ATRP initiator immobilization and subsequent brush polymerization, does not alter the conductivity of the transistor. Additionally, GOx functionalized polymer brush electrodes showed remarkable stability over time periods up to 23 days. These new probes may constitute the basis for future local multimodal recording.

Acknowledgements

The authors would like to acknowledge the National Science foundation grant DMR-1105253 for support of this work. This work made use of the Nanobiotechnology Center shared research facilities at Cornell University and was performed in part at the Cornell NanoScale Facility, a member of the National Nanotechnology Infrastructure Network, which is supported by the NSF (Grant ECS-0335765). We thank Prof. E. J. Kramer and Dr. Daniel A. Fisher for help with NEXAFS analysis and gratefully acknowledge the use of beamline U7A at the NSLS, part of Brookhaven National Laboratories. PEDOT:PSS transistor fabrication, GOx functionalization and all electrochemical measurements (device's normalized response to glucose and stabilization data) were conducted by Prof. George Malliaras and his student Thomas Doublet, Department of Bioelectronics, Centre Microélectronique de Provence, Ecole Nationale Supérieure des Mines de Saint Etienne.

REFERENCES

- (1) WHO Diabetes Fact Sheet. *World health Organization* Fact sheet N°312 (2013).at <<http://www.who.int/mediacentre/factsheets/fs312/en/index.html>>
- (2) Nathan, D. M. *J. A. M. A.* **1996**, 276, 1409.
- (3) Bernards, D. A.; Malliaras, G. G. *Adv. Funct. Mater.* **2007**, 17, 3538.
- (4) Nilsson, D. *Sensor Actuat. B-Chem.* **2002**, 86, 193.
- (5) Yang, S. Y.; DeFranco, J. A.; Sylvester, Y. A.; Gobert, T. J.; Macaya, D. J.; Owens, R. M.; Malliaras, G. G. *Lab Chip* **2009**, 9, 704.
- (6) Vaddiraju, S.; Burgess, D. J.; Tomazos, I. ; Jain, F.C.; Papadimitrakopoulos, F. *J. Diabetes Sci. Tech.* **2010**, 4, 1540.
- (7) Khodagholy, D.; Doublet, T.; Quilichini, P.; Gurfinkel, M.; Leleux, P.; Ghestem, A.; Ismailova, E.; Herve, T.; Sanaur, S.; Bernard, C.; Malliaras, G. G. *Nat. Commun.* **2013**, 4, 1575.
- (8) Mabeck, J. T.; DeFranco, J. A.; Bernards, D. A. ; Malliaras, G. G. ; Hocdé, S. ; Chase, C. *J. Appl. Phys. Lett.* **2005**, 87, 013503.
- (9) Tang, H. ; Yan, F. ; Lin, P. ; Xu, J. ; Chan, H. L. W. *Adv. Funct. Mater.* **2011**, 21, 2264.
- (10) Zhu, Z. T.; Mabeck, J. T.; Zhu, C.; Cady, C. N.; Batt, C. A.; Malliaras, G. G. *Chem. Commun.* **2004**, 13, 1556.
- (11) Macaya, D. J.; Nikolou, M.; Takamatsu, S.; Mabeck, J. T.; Owens, R. M.; Malliaras, G. G. *Sensor Actuat. B-Chem* **2007**, 123, 374.

- (12) Ekanayake, E. M. I. M. ; Preethichandra, D. M. G. ; Kaneto, K. *Biosens. Bioelectron.* **2007**, 23, 107.
- (13) Wang, Z. ; Zhou, X. ; Zhang, J. ; Boey, F. ; Zhang, H. *J. Phys. Chem. C* **2009**, 113, 14071.
- (14) Li, J. ; Lin, X. *Biosens. Bioelectron.* **2007**, 22, 2898.
- (15) Dai, Z. ; Bao, J. ; Yang, X. ; Ju, X. *Biosens. Bioelectron.* **2008**, 23, 1070.
- (16) Yang, X. ; Hua, L. ; Gong, H. ; Tan, S. N. *Anal. Chim. Acta* **2003**, 478, 67.
- (17) Godjevargova, T. ; Nenkova, R. ; Konsulov, V. *J. Mol. Catal. B-Enzym.* **2006**, 38, 59.
- (18) Wan, D. ; Yuan, S. ; Li, G. L. ; Neoh, K. G. ; Kang, E. T. *ACS Appl. Mater. Inter.* **2010**, 2, 3083.
- (19) Zhao, B. ; Brittain, W. *Prog. Polym. Sci.* **2000**, 25, 677.
- (20) Stuart, C.; Huck, W. T. S.; Genzer, J.; Müller, M.; Ober, C. K.; Stamm, M.; Sukhorukov, G. B.; Szleifer, I.; Tsukruk, V. V.; Urban, M.; Winnik, F.; Zauscher, S.; Luzinov, I.; Minko, S. *Nat. Mater.* **2010**, 9, 101.
- (21) Welch, M. ; Rastogi, A. ; Ober, C. K. *Soft Matter* **2011**, 7, 297.
- (22) Chiang, E. N. ; Dong, R. ; Ober, C. K. ; Baird, B. *Langmuir* **2011**, 27, 7016.
- (23) Hollmann, O. ; Gutberlet, T. ; Czeslik, C. *Langmuir* **2007**, 23, 1347.
- (24) Jimison, L. H. ; Tria, S. A.; Khodagholy, D.; Gurfinkel, M.; Lanzarini, E.; Hama, A.; Malliaras, G. G.; Owens, R. M. *Adv. Mater.* **2012**, 24, 5919.
- (25) Jimison, L. H. ; Hama, A.; Strakosas, X.; Armel, V.; Khodagholy, D.; Ismailova, E.; Malliaras, G. G.; Winther-Jensen, B.; Owens, R. M. *J. Mater. Chem.* **2012**, 22, 19498..

- (26) Khodagholy, D. ; Doublet, T.; Gurfinkel, M.; Quilichini, P.; Ismailova, E.; Leleux, P.; Herve, T.; Sanaur, S.; Bernard, C; Malliaras, G. G. *Adv. Mater.* **2011**, 23, 268.
- (27) Arica, M. Y. ; Hasirci, V. *J. Chem. Technol. Biot.* **1993**, 58, 287.
- (28) Shim, N. Y. ; Bernards, D. A.; Macaya, D. J.; DeFranco, J. A.; Nikolou, M.; Owens, R. M.; Malliaras, G. G. *Sensors* **2009**, 9, 9896.
- (29) Paik, M. Y. ; Krishnan, S.; You, F.; Li, X.; Hexemer, A.; Ando, Y.; Kang, S. H.; Fischer, D. A.; Kramer, E. J.; Ober, C. K. *Langmuir* **2007**, 23, 5110.
- (30) Genzer, J.; Sivaniah, E.; Kramer, E. J.; Wang, J.; Körner, H.; Char, K..; Ober, C. K.; DeKoven, B. M.; Bubeck, R. A.; Fischer, D. A.; Sambasivan, S. *Langmuir* **2000**, 16, 1993.
- (31) Schulz, B. ; Riedel, A. ; Abel, P. U. *J. Mol. Catal. B-Enzym.* **1999**, 7, 85.
- (32) Bayramoğlu, G. ; Akgöl, S. ; Bulut, A. ; Denizli, A. ; Yakup Arıca , M. *Biochem. Eng. J.* **2003**, 14, 117.
- (33) Welch, M. E. ; Ohm, C. ; Ober, C. K. *J. Chem. Technol. Biot.* **2012**, 25, 53.
- (34) Winther-Jensen, B. ; West, K. A *Macromolecules* **2004**, 37, 4538.

CHAPTER 4

CHARACTERIZATION OF POLYMER BRUSH MEMBRANES VIA HF LIFTOFF TECHNIQUE

Abstract

Surface modification using end-tethered polymer brushes is an attractive, versatile and effective method of tailoring the surface properties of a material. However because the chains are covalently attached, characterization of these films is limited. When polymer brushes are detached in their native state, as opposed to fabricating a crosslinked initiator support, additional analytical techniques can be employed. We report lifting off patterned polymer brush membranes from a silicon oxide surface via a hydrofluoric acid etch. This method allows examination of polymer brushes via TEM and thus provides information regarding the perfection of initiator self assembled monolayer formation, brush growth as well as the effect of different crosslinking procedures.

Introduction

In recent years polymer brushes have garnered much attention because of their ability

*Reproduced with permission from M. Elizabeth Welch and Christopher K. Ober. Characterization of Polymer Brush Membranes via HF Etch Liftoff Technique. ACS Macro Letters **2013**, 2 (3), pp 241–245. Copyright 2013 American Chemical Society.

to alter surface properties on a scale of just a few nanometers. A surface can be modified with polymer brushes to create an interface compatible with biological environments.^{1,2} Such properties lead to applications in fields including bioelectronics, responsive surfaces, protein resistant surfaces, and biosensors.³⁻⁸

Polymer brushes are polymer chains tethered to a surface or substrate. There are two common methods of attachment, “grafting from” and “grafting to”. The grafting to technique involves first polymerizing the chain and attaching an anchor group to the chain that can then bind to the surface. However, due to steric repulsion between incoming chains and chains already attached, the grafting density can be rather low. The grafting from method, on the other hand, can produce high density polymer brushes by first immobilizing an initiator molecule on the surface and subsequently growing chains through polymerization techniques such as atom transfer radical polymerization (ATRP), nitroxide-mediated polymerization (NMP), and reversible addition fragmentation chain transfer (RAFT).^{9,10}

Since the chains are covalently attached to a substrate, characterization of the film may be difficult or provide an incomplete picture of the brush. Brushes are commonly characterized by water contact angle, IR/FTIR (chemical content), ellipsometry (thickness) and AFM (surface roughness). IR, contact angle and ellipsometry measurements evaluate large areas and provide information about the brush averaging over this region. AFM instead looks at much smaller regions, but it is limited to surface characterization and provides little information about the sub-surface of the brush film. None of these methods can give much insight into the effect of localized chain stretching or packing density of the brush regions. Much more information could be

obtained if the brush were not bound to a surface. In order to characterize the film itself, a polymer brush film removed from a surface enables additional types of detailed study. This new field of polymer brush analysis is just beginning to be explored. Amin et al. have prepared polymer carpets by depositing an electron-beam crosslinking self assembled monolayer (SAM) of biphenyl on a support and subsequently growing polymer brushes from it through surface initiated polymerization of vinyl monomers.¹¹ Then this layer was removed for analysis. Other researchers have expanded on this method of a crosslinked initiator surface and transferred polymer carpets to a graphene surface as a way of chemical functionalization.¹² Due to the biocompatibility of polymer brushes,¹³ applications in other fields such as biosensors and Janus membranes could be well suited for use of these polymer brush films.

We have developed a straightforward technique to remove patterned sections of polymer brushes, using polystyrene (PS) and poly(glycidyl methacrylate) (PGMA) brushes to test our approach. Both crosslinked and uncrosslinked polymer brushes (the latter as a control) were detached and subsequently analyzed by transmission electron microscopy (TEM). Our initial reasoning was that the polymer brushes should be crosslinked in order to retain physical integrity. The different crosslinking processes used were investigated to gain a better understanding of the resulting polymer brush membrane's physical and chemical characteristics. Previous work on polymer brush nanochannels led us to recognize the surprising strength of bridging brush layers stretched over distances ranging from 100 nm to a few microns.¹⁴ Therefore we have developed a method of detaching polymer brush films that enables their further

exploration (Figure 1).

Experimental Section

Materials: Allyl-2-bromo-2-methylpropionate, chlorodimethyl-hydrosilane, Pt on activated carbon (10 wt %), ethylenediamine, potassium hydroxide, trifluoromethanesulfonic acid, 2,2'-bipyridine, N,N,N',N',N"-pentamethyldiethylenetriamine (PMDETA), pyridine, copper (I) bromide, copper (I) chloride, copper (II) dibromide, inhibitor remover, anhydrous toluene, N,N-dimethylformamide, triphenylsulfonium nonaflate (TPS-Nf), hydrofluoric acid, glycidyl methacrylate, styrene (S) were purchased from Sigma Aldrich and used without purification unless stated otherwise. S was passed through basic alumina to remove the inhibitor before use. Deionized water with a resistivity of 18.2 MΩ•cm at 25 °C was obtained from Millipore's Milli-Q Synthesis A10 system. All the other solvents were purchased from Fisher Scientific.

Synthesis of Silane Initiator and Immobilization: Hydrosilylation of allyl 2-bromo-2-methylpropionate was carried out using a literature procedure to obtain the ATRP initiator, 3-(chlorodimethylsilyl)propyl 2-bromo-2-methylpropionate.¹⁵ Wafer pieces with a 2 μ m silicon oxide layer were oxidized using a Harrick Plasma Cleaner for ten minutes, rinsed with ethanol, and heated to remove all traces of water. In a glove box, the wafer pieces were immersed in a toluene solution of the initiator (varying concentrations) and pyridine (0.05 mM) overnight at room temperature. The substrates were then removed from the solution and washed with water, ethanol, and dichloromethane (DCM) sequentially and sonicated for ten minutes in DCM. Wafers were given a final rinse of dichloromethane and blown dry under nitrogen gas.

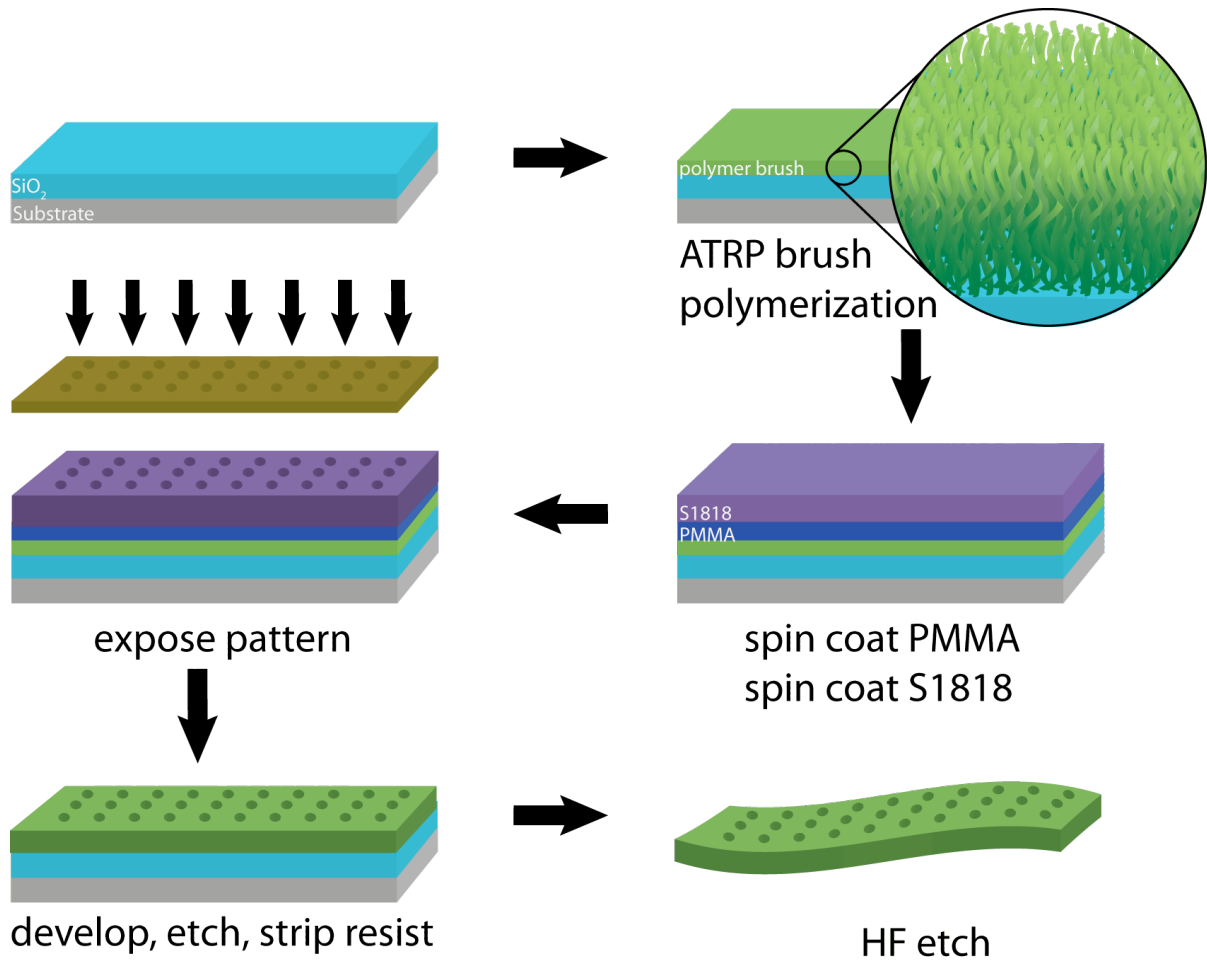


Figure 1. Detachment scheme producing membranes that can be transferred to TEM grids.

PGMA Brush Polymerization: PGMA brushes were prepared by placing two wafer pieces with immobilized initiator on the surface in a 25 mL Schlenk flask under an argon atmosphere.

The flask was evacuated and back filled with argon four times. CuCl (72.8 mg, 0.7 mmol), CuBr₂ (7.8 mg, 0.03 mmol), bipyridine (282 mg, 1.80 mmol) were taken in another 50 mL Schenk flask equipped with a magnetic stir bar. The air in the flask was evacuated and replaced with argon four times. Glycidyl methacrylate (10.42 g, 73 mmol), methanol (8ml) and water (2 mL) was purged with argon for about twenty minutes and cannulated into the flask containing the ligand and copper salts. The reaction mixture was stirred at room temperature for 20 min to ensure the formation of the copper-ligand complex. This solution was then transferred into the flask containing the initiator coated wafer pieces and allowed to polymerize at 32 °C for different time lengths. After polymerization, the substrates were washed with dichloromethane and ethanol and dried under nitrogen gas.

PS Brush Polymerization: Polystyrene was prepared by degassing via vacuum freeze-pumping a solution of styrene (14 mL, 148 mmol, inhibitor removed), PMDETA (130 µL, 0.9 mmol) and anhydrous anisole (5 mL) for five times. The solution was then transferred to an argon-purged 25 mL Schlenk tube loaded with CuBr (50 mg, 0.3 mmol). The mixture was stirred for 15 minutes and then cannulated to another Schlenk tube (also argon-purged) with initiator coated wafers. The reaction was kept at 110 °C for a certain period of time. Finally, the substrates were rinsed with dichloromethane and ethanol and dried under nitrogen gas.

Polymer Brush Patterning: PGMA brush samples were first spin coated with 5.5% PMMA in anisol and baked for 3 minutes at 90 °C. Both PS and PGMA brush wafers were then spin-coated with positive tone photoresist S1818 (Shipley) and baked for 90 seconds at 90 °C. The samples were exposed to UV light ($\lambda = 405$ nm) for ten seconds using an ABM contact aligner with a patterned mask of individual membranes containing 20 μm holes 190 μm apart. After a post exposure bake (PEB) for the same length of time and temperature as before, substrates were developed in MIF 726 for 1.5 minutes. Next the wafer pieces were etched for 4 minutes with a standard oxygen etch recipe using a PT72 Etcher. Remaining photoresist was removed by acetone, dichloromethane and ethanol.

Brush Crosslinking: To crosslink the PS polymer brush, the samples were flood exposed with the same UV source but for a duration of 10 minutes. Lastly, a PEB of 1.5 minutes at 90 °C followed. PGMA brushes were crosslinked by both chemical and lithographic means. Lithographically, a 3 wt-% solution of photo-acid generator, triphenylsulfonium nonaflate (TPS-Nf), in propylene glycol methyl ether acetate (PGMEA) was spin coated on patterned PGMA brush samples and baked for 1.5 minutes at 110 °C. The substrates were then exposed to UV light ($\lambda = 405$ nm) for 1.5 minutes and then baked for 1.5min at 90 °C. Patterned PGMA brushes were chemically crosslinked three ways. First, samples were placed in a solution of 1M ethylenediamine at room temperature overnight and subsequently rinsed with water, dichloromethane and ethanol. Another method tested was 1M KOH in DMF and toluene at 60 °C for 1.5 hours. Third, patterned samples were placed in a 1M toluene

solution of triflic acid and kept at room temperature for 1.5 hours.

Membrane Liftoff: The brush films were removed from the surface by etching the silicon oxide layer with a 48 wt. % solution of HF. The detached, floating films were rinsed twice with water before being transferred to a copper grid for transmission electron microscopy (TEM).

Characterization: Polymer brushes were characterized by ellipsometry, AFM and transmission electron microscopy. Thicknesses of the brushes were measured using an Imaging Ellipsometer - Nanofilm EP3 with a 532 nm laser starting at a 50° angle and ending at 60°. A PMMA_450 model (PMMA_450/SiO₂/Si substrate) was used to fit the data, in which the PMMA layer was representative of the polymer brush. A FEI T12 TWIN TEM was used to acquire optical images of the films. FTIR data was obtained using a Bruker Optics – Vertex 80v with an ATR germanium crystal.

Results and Discussion

Membrane Fabrication. A 2 μm silicon oxide (SiO₂) layer thermally grown on a standard silicon wafer was selected for brush polymerization for two reasons. First, in terms of brush growth, it is chemically equivalent to the silicon wafer surface and thus initiator immobilization and brush polymerization environments will not affect or remove the oxide film. As a result, we are not limited to the type of polymer brushes that can be investigated with this technique. Second, SiO₂ can be dissolved by hydrofluoric (HF) acid. HF etches oxides but it does not harm polymers and therefore will not affect the polymer brush membranes. The brush films can then be rinsed repeatedly with water to remove HF and transferred to TEM grids for further

characterization.

Instead of using a crosslinked SAM layer as noted above, our method of detachment employs a HF acid etching process which preserves the initiator layer in its uncrosslinked state and allows for analysis of initiator immobilization uniformity (figure 1). Results show initiator immobilized at low concentrations produces lower density, patchy brushes whereas initiator immobilized at high concentrations generates high density, homogeneous brushes. This finding is in accordance with previous investigations regarding the mechanism of SAM formation.^{16,17} They show that at room to low temperature, island domains will nucleate in the plane of the surface (figure 2).¹⁸⁻²¹ Experimental parameters found to have a high impact on the mechanism included water content, deposition time, and temperature.^{18,22} We have determined that initiator concentration also influences the quality of initiator layer formed and thus polymer brush film growth. Our method of membrane liftoff provides the opportunity to analyze initiator quality, immobilization conditions, and optimization parameters.

Image Analysis. A first topic of study was the uniformity of the polymer brush layer. The quality of this layer is indicative of the homogeneity of the initiator immobilization step. As noted above, the SAM formation process involves assembly of islands prior to formation of a complete and uniform layer. Typical characterization of the SAM island formation includes AFM, optical ellipsometry, scanning tunneling microscopy (STM), and lateral force microscopy (LFM).²³⁻²⁵ However, SAMs of our ATRP initiator can also be characterized via analysis of the polymer brushes grown from them. The coverage density of polymer brushes is largely dependent on the

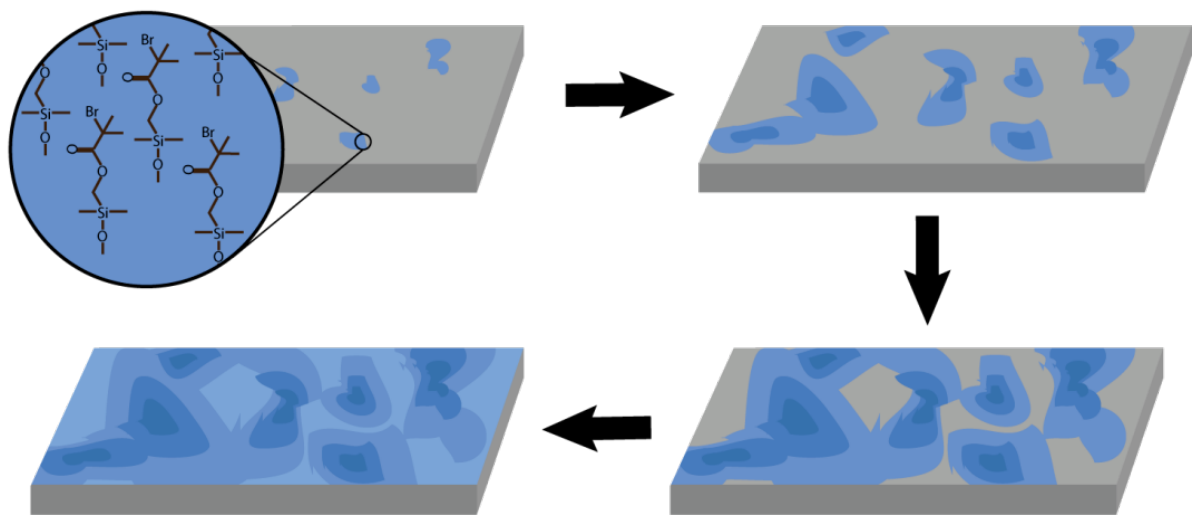


Figure 2. Illustration of initiator SAM formation via island mechanism.

quality of the initiator surface. A closely packed initiator surface allows for polymerization of high grafting density brushes. Therefore by examining the density of the polymer brushes, we can acquire information regarding our initiator deposition via TEM bright field mode. Previous studies have used AFM to distinguish buckling and folding; however it is extremely difficult to do AFM on detached films. TEM is important because we need a way to visualize detached membranes. This technique can probe fine detail and provide contrast information, which to a first approximation may be modeled by Beer's law. The enhanced sensitivity and additional contrast formation data provides clear indications of how dense our polymer brushes are and what regime we are working in (patchy brushes vs. uniform brushes). It is important to establish growth conditions because, for example, when exploring the concept of brush stretching and expansion (discussed later) we only use the high density, uniform brush conditions.

Figure 3 shows TEM images of PS and PGMA membranes at different initiator concentrations. On average, we find initiator immobilization concentrations less than 2 mM generate "patchy" brushes. The brushes appear to be less dense in some areas and denser in others. We speculate this is because our initiator immobilization follows the island formation mechanism where domains will nucleate and eventually grow together instead of proceeding by homogeneous deposition. At low initiator concentrations, complete coverage cannot be achieved. However, when the initiator concentration is increased, these irregular regions are no longer observed and instead a uniform membrane is produced. AFM results support these TEM findings. Figure 4 shows uncrosslinked PGMA brush films removed from the substrate and allowed to

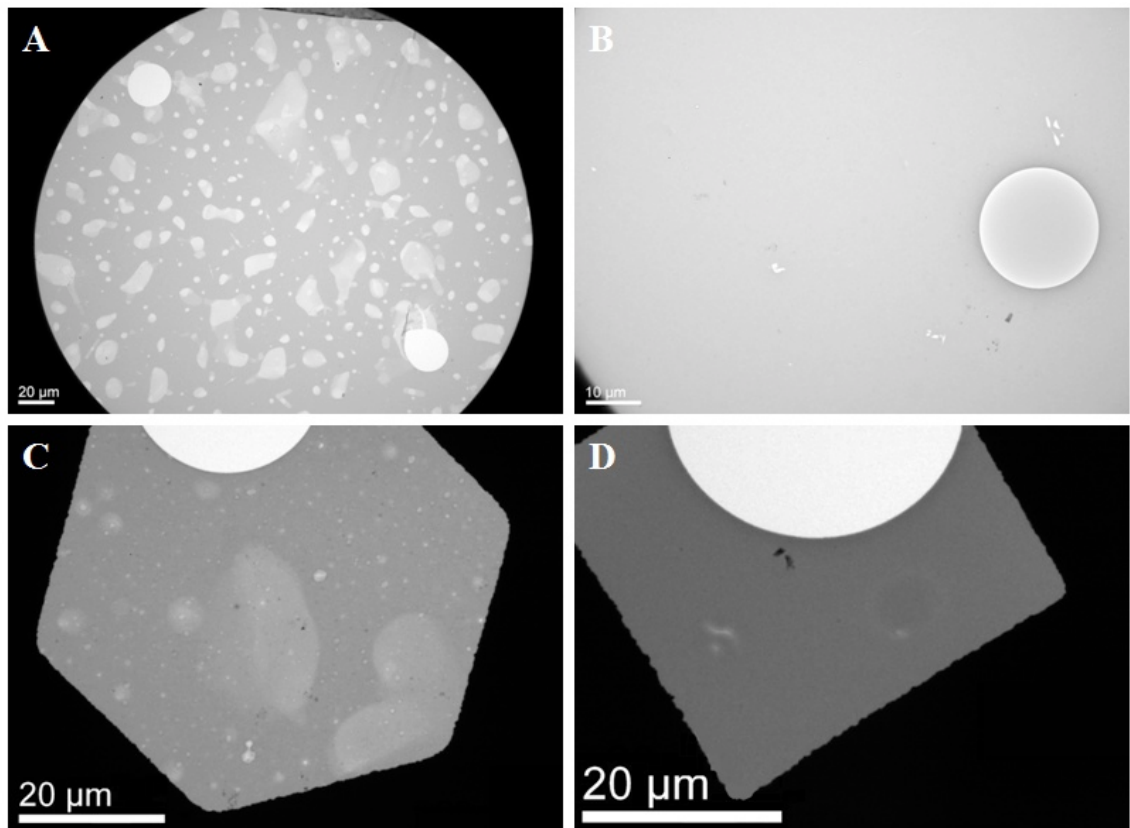


Figure 3. (A) TEM image of crosslinked PS brush membrane at 1mM initiator immobilization concentration and (B) 20mM. (A) shows a brush membrane with irregular thickness caused by heterogeneous deposition of initiator while the higher concentration in (B) leads to a uniform brush membrane. (C) Uncrosslinked PGMA brush membrane at 1mM and (D) 8mM initiator immobilization concentration. As above, the lower concentration of initiator in (C) leads to brush thickness variations. See Supporting Information for analysis of heterogeneous brush.

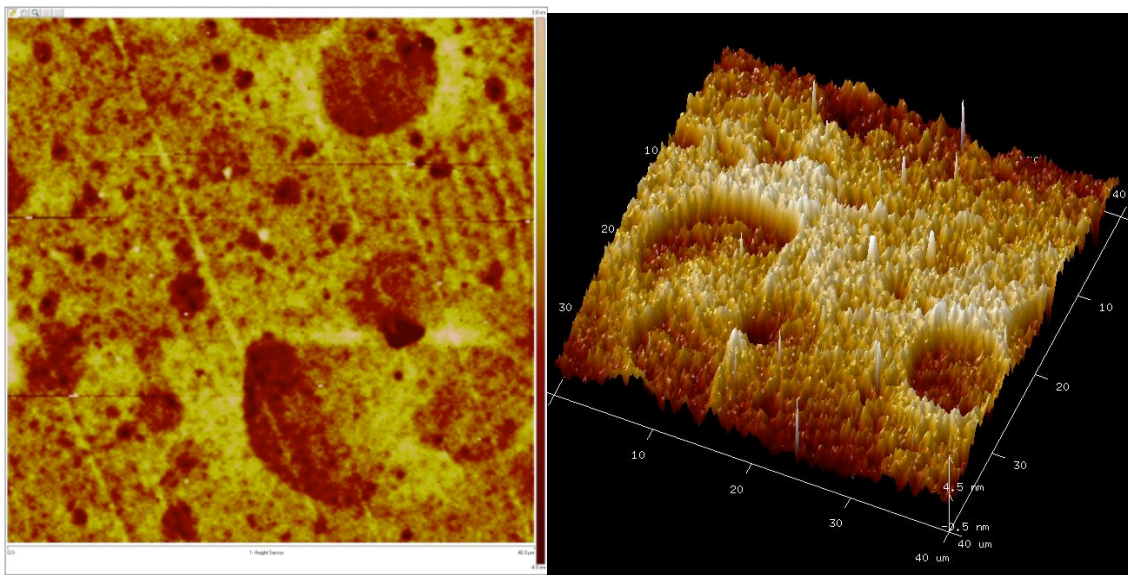


Figure 4. AFM of uncrosslinked PGMA film height image (a) and 3D image (b).

settle back down on the surface for AFM characterization. Just as before, at low initiator immobilization concentrations we noticed patchy, irregular brushes. The height difference between these regions is 2-6 nm and confirms our TEM data observations.

Using imaging processing software, we were able to further analyze the patchy films and the approximate densities of the irregular regions. To evaluate the relative thickness of the resulting brush films an analysis developed by Lauterwasser and Kramer²⁶ for the study of crazing on thin polymer films was used in which the optical density (ϕ) of an area can be calculated from a ratio of the ϕ_{hole}/ϕ_{film} . TEM images of the brush films taken on TEM grids showed that some of the brush films were not of uniform thickness caused by a variation in the initial initiator deposition step. The use of low concentrations of ATRP surface initiator or using initiator that had aged and was no longer effective could cause the variation. In one sample TEM image (Figure 5), a brush film with a fold and a hole which showed regions one, two and three layers thick was used to evaluate this method. Using the optical density of the hole image as reference and the average film thickness determined by ellipsometry, the three layer thicknesses were compared using the relationship for relative optical density to determine film thickness, equations 1 and 2.

$$\text{Eqn 1: } \phi_{hole} = M_0$$

$$\text{Eqn 2: } \phi_{film} = M_0 \exp(-t \cdot \rho_{film}/\lambda_{eff} \rho_0)$$

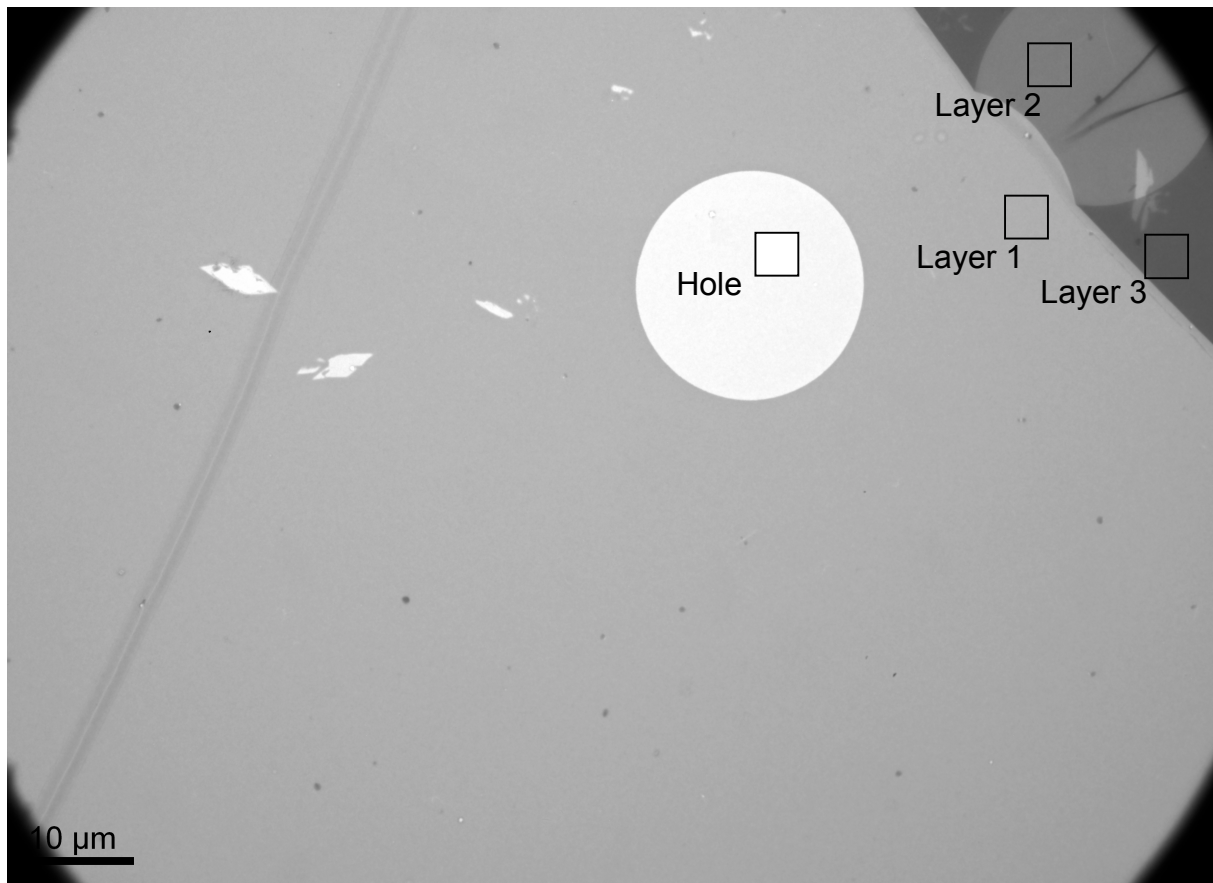


Figure 5. Brush layer showing uniform layer and folded region. Optical densities were taken from 1 (1 layer), 2 (2 layers) and 3 (3 layers).

where ϕ is optical density, t is thickness, λ_{eff} is effective electron scattering length and ρ is density.

Assuming the film density is uniform, then the film thickness (t_{film}) scales as:

$$\text{Eqn 3: } t_{\text{film}} \propto -\ln \left(\frac{\phi_{\text{film}}}{\phi_{\text{initiator}}} \right)$$

As can be seen in Table 1, this approach to determining relative layer thickness shows the correct relationship between the number of layers and the thickness of each section. Once this method was established with confidence, it was used to assess the thickness variation in films that lacked a uniform initiator density in the sample.

In addition, using ImageJ 1.47g freeware available from NIH, the relative coverage of thin regions in various brush films was evaluated. The image threshold was adjusted to separate the region of uniform and maximum film thickness from regions with lower thickness (less initiator) in the sample. ImageJ, and its built-in function to Analyze and Measure, was used to determine the fraction of area covered in the micrograph by the uniform thick brush. Numerous points of observation including the marker hole, homogeneous sections, and thin regions were selected and measured. For a PS film that was 76 nm thick in the dense brush region, the thin regions were shown to vary between 50 to as few as 10 nm. These films had breaks between the thick brush and thin regions, so measurements of surface properties would show the surface characteristics of polystyrene, even though the brush varied greatly from region to region. Calculations were carried out to give the relative thickness of the regions

# Layers	$\phi_{n\text{-film}}$	$\ln(\phi_{n\text{-film}}/\phi_{\text{hole}})$	Thickness (nm)
1	165	0.40	76
2	106	0.80	152
3	72	1.2	228

Table 1. The optical density of the hole (ϕ_o) had a measured value of 246. The film thickness for one layer was found to be 76 nm by ellipsometer, so films of 2 and 3 layers were scaled accordingly.

which, coupled with binary imagery processing, can provide overall area coverage. Analysis of the PS TEM images using ImageJ (Figure 6) and PGMA (not shown) illustrates the overall coverage by full thickness brushes to be ~ 75% in both cases indicating the quality of the brush is determined by the initiator monolayer and not the nature of the monomer. This demonstration justifies the utility of this liftoff method as a means of better understanding the type of brush regime and coverage being produced. Moreover, it should be noted that this trend seems to be independent of polymer brush type and different polymerization environments. Thus by lifting polymer brush films from a substrate and characterizing them via TEM, we can determine the quality and coverage of brushes our system is producing as well as the immobilization efficiency of our ATRP initiator.

Crosslinking Methods. Different polymer brush thicknesses have been explored with this technique ranging from 30-190 nm. Regardless of thickness, all films have proven to be surprisingly robust. Both crosslinked and uncrosslinked polymer brush membranes were preserved after detachment and had a tendency to fold, wrinkle or buckle instead of tearing or fracturing. They also maintain their structure and composition under high vacuum in the TEM. This is consistent with our original study of polymer brush bridges spanning over nanochannel distances of a few microns without collapse or breakage. Huck has also shown that it is possible to electrochemically detach brush films and that these brush layers remain intact.²⁷ These observations imply that such films can potentially undergo further

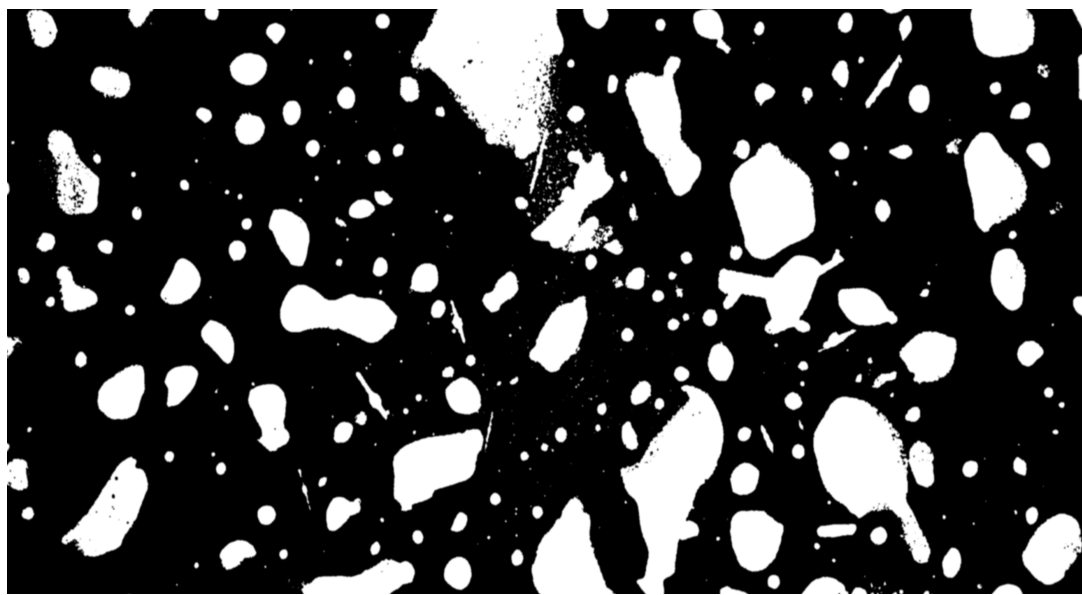


Figure 6. Patchy film of PS brushes. TEM image assigned threshold using ImageJ to highlight full thickness regions and subsequently Analysis and Measure commands used to calculate coverage of full thickness brush of 75% of total area in image.

functionalization and remain whole.

Further exploration of the effect of crosslinking polymer brushes before removal from the surface was investigated by both lithographic and chemical methods (Figure 7). After the polymer brushes were grown from the silicon oxide layer, they were patterned into individual membranes with holes 20 μm in diameter spaced 180 μm apart. These shapes and dimensions were chosen to serve as points of reference for TEM and optical microscopy, although other patterns and dimensions are possible as well. Results showed patterned holes of uncrosslinked membranes expanded to diameters of 30-32 μm , but if a crosslinking process was applied, the films retained shapes closer to that of the original 20 μm diameter pattern. We do not believe this expansion is due to the swelling of the polymer brushes. During our patterning and liftoff procedure residual solvents are extracted, generating polymer brush membranes in the glassy state. The observation of change in dimension is then due to the chain relaxation from substrate release and not from swelling. Other studies have suggested stress relaxation associated with high surface packing and chain concentration (leading to Eigen strain), is a significant contributing factor to the mechanical properties of polymer brushes.²⁸ Such strain drives the release process in both crosslinked and uncrosslinked films. In order to prevent this expansion, we have looked into various forms of crosslinking. Polystyrene is known to crosslink under prolonged exposure to UV radiation through UV-generated free radicals.^{29,30} To ensure full crosslinking, patterned PS samples were exposed to UV radiation for 10 minutes before the HF etch step. TEM images confirmed the original circles maintained their 20 μm diameter thus establishing that this method of crosslinking is successful for PS.

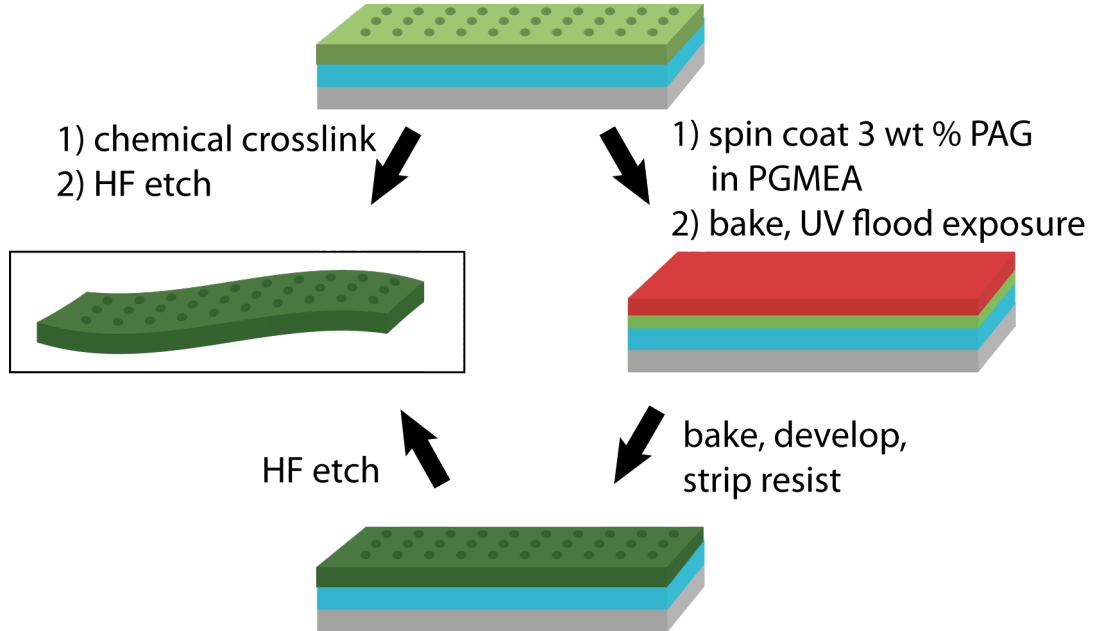


Figure 7. Schematic of chemical and lithographic methods of crosslinking polymer brushes.

Different techniques of crosslinking were explored for PGMA brushes. First, both acid and base reactions were tested using triflic acid, KOH, and ethylenediamine to cause crosslinking. FTIR of the strong acid and strong base crosslinking reactions was analyzed to verify the chemical change (figure 8). Results showed an increased presence of absorption peaks consistent with the formation of ether bonds, thus suggesting the epoxy ring opened up to form new linkages with neighboring chains.

The same crosslinking effect is demonstrated via TEM characterization. Table 2 summarizes the results by examining the expansion of the patterned regions. As shown, more vigorous acids and bases are required to effectively crosslink the epoxide side groups; however, it should be noted that high concentration and long exposure times of these strong acid and bases can destroy the brush. Concentrations over 2 M, and overnight reaction times lead to the polymer brushes being stripped from the surface and dissolved in solution. Lower concentrations (1 M) and reaction times under 2 hours lead to polymer brush crosslinking without damage. In addition to chemical crosslinking, lithographic techniques can also be employed. Introducing a photoacid generator (PAG) and using UV radiation is a promising method. Typical PAGs are compounds added to a spin coating solution that decompose upon exposure to yield free radicals or cations. A standard PAG (1-3 wt%) was added to PGMEA solvent and spin coated directly on the polymer brushes. The substrate was then exposed to UV radiation for 1.5 minutes, baked, and developed. The generated strong acid can diffuse into the brushes, open the epoxy rings, and crosslink the brushes similar to triflic acid. As shown in Table 2, both the triflic acid and PAG approaches produce similar crosslinking results. By lifting the polymer brush membranes from

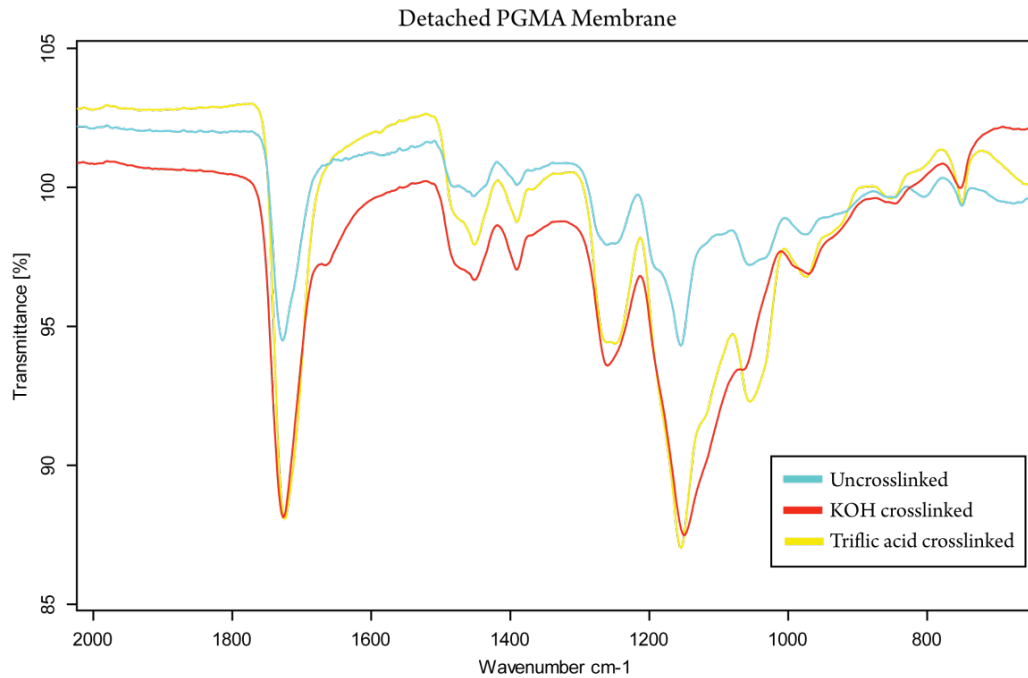


Figure 8. shows IR spectra of a detached PGMA film. The blue curve represents an uncrosslinked detached PGMA film, the yellow and red curves are from triflic acid and KOH crosslinking treatments, respectively. The peaks are similar except around 1150 cm^{-1} which shows significant increase and broadening. This is due to the epoxide ring opening and formation of aliphatic ether bonds with neighboring chains.

Crosslinking method	Patterned hole diameter (μm)	Hole diameter after liftoff (μm)	Film Expansion Strain (%)
1 M KOH	20	20	0
1 M triflic acid	20	23	15
1 M ethylene diamine	20	27	35
Photoacid generator	20	23	25

Table 2. Expansion of hole diameter after liftoff was measured by TEM. Film expansion strain is the nominal strain or change in hole diameter relative to the starting dimension.

the surface and analyzing the expansion of the patterned features, the efficiency of various crosslinking techniques can be investigated. We have developed a method of removing polymer brush membranes from a surface for detailed characterization. Polymerizing polymer brushes via ATRP from silicon oxide and employing an HF etch to lift off the film allows numerous types of brushes to be analyzed. Because silicon oxide is chemically stable in organic solvents, we are not limited to a particular type of brush. Additionally, HF only etches oxides; hence the polymer membranes are not chemically sacrificed. Analysis by TEM provides more information about the initiator immobilization and brush polymerization process. At low initiator immobilization concentrations, polymerization leads to patchy brushes comprised of isolated areas of decreased brush density. We believe this observation is indicative of the island formation mechanism for SAMs in general and this method can provide insight into polymer brush initiator immobilization parameters and the types of brushes that can be produced. Heterogeneous brush formation takes place under conditions that have been reported in the literature that are assumed to form uniform brush layers. AFM is unlikely to reveal this irregularity unless this is being specifically looked for.

Conclusions

As we expected, crosslinked brushes can be removed from the Si substrate to produce robust polymer films that retain the original patterned dimension. By first patterning the polymer brushes, we establish reference points from which to base our findings after membrane liftoff. Patterned circles of a specific diameter were

examined before and after film removal and brush film size was analyzed to confirm the effectiveness of different crosslinking processes. Surprisingly when uncrosslinked brush layers are removed, they remain intact and expand in the x-y plan due to chain relaxation caused by Eigen strain release first introduced during the original brush growth process. Overall this polymer brush film removal system can provide information regarding initiator immobilization, brush polymerization/functionalization methods, and answer questions about the nature of these brush films.

Acknowledgments

The authors would like to acknowledge the National Science foundation grant DMR-1105253 for support of this work. This work made use of the Cornell Center for Materials Research Shared Facilities which are supported through the NSF MRSEC program (DMR-1120296), the Nanobiotechnology Center shared research facilities at Cornell University, and was performed in part at the Cornell NanoScale Facility, a member of the National Nanotechnology Infrastructure Network, which is supported by the NSF (Grant ECS-0335765).

REFERENCES

- (1) Jancar, J.; Douglas, J. F.; Starr, F. W.; Kumar, S. K.; Cassagnau, P.; Lesser, A. J.; Sternstein, S. S.; Buehler, M. J. *Polymer* **2010**, *51*, 3321.
- (2) Yuan, J. Y.; Xu, Y. Y.; Muller, A. H. E. *Chem. Soc. Rev.* **2011**, *40*, 640.
- (3) Welch, M.; Rastogi, A.; Ober, C. *Soft Matter* **2011**, *7*, 297.
- (4) He, H. T.; Jing, W. H.; Xing, W. H.; Fan, Y. Q. *Appl. Surf. Sci.* **2011**, *258*, 1038.
- (5) Ionov, L.; Minko, S. *ACS Appl. Mater. Inter.* **2012**, *4*, 483.
- (6) Rodriguez-Emmenegger, C.; Brynda, E.; Riedel, T.; Houska, M.; Subr, V.; Alles, A. B.; Hasan, E.; Gautrot, J. E.; Huck, W. T. S. *Macromol. Rapid Comm.* **2011**, *32*, 952.
- (7) Tria, M. C. R.; Grande, C. D. T.; Ponnappati, R. R.; Advincula, R. C. *Biomacromolecules* **2010**, *11*, 3422.
- (8) Zhu, L.; Zhao, B. *J. Phys. Chem. B* **2008**, *112*, 11529.
- (9) Edmondson, S.; Osborne, V. L.; Huck, W. T. S. *Chem. Soc. Rev.* **2004**, *33*, 14.
- (10) Pyun, J.; Kowalewski, T.; Matyjaszewski, K. *Macromol. Rapid Comm.* **2003**, *24*, 1043.
- (11) Amin, I.; Steenackers, M.; Zhang, N.; Beyer, A.; Zhang, X. H.; Pirzer, T.; Hugel, T.; Jordan, R.; Golzhauser, A. *Small* **2010**, *6*, 1623.
- (12) Steenackers, M.; Gigler, A. M.; Zhang, N.; Deubel, F.; Seifert, M.; Hess, L. H.; Lim, C.; Loh, K. P.; Garrido, J. A.; Jordan, R.; Stutzmann, M.; Sharp, I. D. *J. Am. Chem. Soc.* **2011**, *133*, 10490.

- (13) Andruzzi, L.; Senaratne, W.; Hexemer, A.; Sheets, E. D.; Ilic, B.; Kramer, E. J.; Baird, B.; Ober, C. K. *Langmuir* **2005**, *21*, 2495.
- (14) Paik, M. Y.; Xu, Y. Y.; Rastogi, A.; Tanaka, M.; Yi, Y.; Ober, C. K. *Nano Lett.* **2010**, *10*, 3873.
- (15) Shah, R. R.; Merreccyes, D.; Husemann, M.; Rees, I.; Abbott, N. L.; Hawker, C. J.; Hedrick, J. L. *Macromolecules* **2000**, *33*, 597.
- (16) Schreiber, F. *Prog. Surf. Sci.* **2000**, *65*, 151.
- (17) Onclin, S.; Ravoo, B. J.; Reinhoudt, D. N. *Angew. Chem. Int. Edit.* **2005**, *44*, 6282.
- (18) Bierbaum, K.; Grunze, M.; Baski, A. A.; Chi, L. F.; Schrepp, W.; Fuchs, H. *Langmuir* **1995**, *11*, 2143.
- (19) Brzoska, J. B.; Benazouz, I.; Rondelez, F. *Langmuir* **1994**, *10*, 4367.
- (20) Parikh, A. N.; Allara, D. L.; Azouz, I. B.; Rondelez, F. *J. Phys. Chem.* **1994**, *98*, 7577.
- (21) Brzoska, J. B.; Shahidzadeh, N.; Rondelez, F. *Nature* **1992**, *360*, 719.
- (22) Reiniger, M.; Basnar, B.; Friedbacher, G.; Schleberger, M. *Surf. Interface Anal.* **2002**, *33*, 85.
- (23) Stranick, S. J.; Parikh, A. N.; Tao, Y. T.; Allara, D. L.; Weiss, P. S. *J. Phys. Chem.* **1994**, *98*, 7636.
- (24) Liu, Y.; Wolf, L. K.; Messmer, M. C. *Langmuir* **2001**, *17*, 4329.
- (25) Dinh, D. H.; Vellutini, L.; Bennetau, B.; Dejous, C.; Rebiere, D.; Pascal, E.; Moynet, D.; Belin, C.; Desbat, B.; Labrugere, C.; Pillot, J. P. *Langmuir* **2009**, *25*, 5526.

- (26) Lauterwasser, B. D.; Kramer, E. J. *Philos. Mag. A* **1979**, *39*, 469.
- (27) Edmondson, S.; Frieda, K.; Comrie, J. E.; Onck, P. R.; Huck, W. T. S. *Adv. Mater.* **2006**, *18*, 724.
- (28) Annabattula, R. K.; Huck, W. T. S.; Onck, P. R. *Journal of the Mechanics and Physics of Solids* **2010**, *58*, 447.
- (29) Knudsen, D.; Harnish, B.; Toth, R.; Yan, M. D. *Polym. Eng. Sci.* **2009**, *49*, 945.
- (30) Mu, B.; Shen, R. P.; Liu, P. *Nanoscale Res. Lett.* **2009**, *4*, 773.

CHAPTER 5

EXPANSION AND STRETCHING OF DETACHED POLYMER BRUSH
MEMBRANES

Abstract

Polymer brushes have been an area of great interest in the past decade due to the broad range of applications including bio-related and medicinal research. Most recently, the possibility of lifting them from the surface to create ultra thin membranes is being explored. We report a novel technique for the fabrication of detached polymer brush membranes. To date, the stretching of neutral polymer brushes has been explored almost entirely by theoretical means. The advantage of etching polymer brushes to free them from a surface enables comparison of the dimensional changes of the polymer chains before and after detachment. The resulting freed patterned polymer films showed stability and unique expansion behavior. Our observations and experimental data have provided insight into the conformational changes that take place in brush films after detachment that can be correlated to theoretical predictions.

Introduction

Polymer chains that are densely packed and attached at some point to a surface are termed polymer brushes. First used to stabilize colloidal particles, polymer brushes have been recognized as a research topic since the 1950s. They are currently implemented in many fields including biotechnology, engineering, and material science and have applications in microelectronics, nanofluidic devices, biosensing,

and other areas of nanotechnology.¹⁻⁴ In addition to the ever increasing forms of applications, theory has also played its role in brush history providing a better understanding of the nature of these materials.

The first description of a polymer brush system was proposed by Alexander and de Gennes and was comprised of a scaling argument for free energy and height of the brush layer.^{5,6} Their approach treated each polymer as a sequence of “blobs” or hard spheres whose uniform size is determined by the confinement of neighboring chains. In the case of a moderately dense brush, the radius of the blobs must be on the order of the distance between anchor points, assuming weakly interacting chains. These authors make another assumption that the free chain ends are confined to the top of the grafted layer and that the vertical polymer profile is a step function, all chains behaving identically.

This theory was improved by Milner et al. by employing a self-consistent field (SCF) approximation.⁷ Here chains are regarded to be in the strongly stretched state; however, the chain ends are no longer restricted exclusively to the brush surface, they are instead determined self-consistently. The only significant contributing chain configurations are those that follow the classical path (those of least action or free energy) between the chain end points. Thus rather than a step function density profile, this model predicts a parabolic concentration profile.

One potential limitation of this theory is that the excluded volume interactions are accounted for using only the second virial coefficient, making this approach applicable only to low density brushes. Wang *et al.* further investigated this aspect for thin versus thick brush systems.⁸ They demonstrated that the density profiles are, for the

most part, well predicted by the Milner model. This result is due to a weak dependence on grafting density and because the linear dependence of the brush height on the polymerization index is independent of the number of terms in the virial expansion. So for brushes with a degree of polymerization of several hundred or more, scaling calculated by the second virial approach is suitable. However, they did find that shorter chains, degree of polymerization of 50 or less, required a more detailed treatment to predict brush energies and aspects such as the lateral pressure. Our brush lengths are greater than this regime.

While theory has provided a great deal of insight into the behavior of polymer brushes, experimental data regarding the stretching of these systems is less straightforward. Most commonly, the stretching and swelling of brushes has been investigated in terms of polyelectrolyte brushes (PE). Electrostatic interactions between the charged groups inside the PE brushes dominate the driving force for swelling. As a consequence, their physicochemical properties are greatly dependent on factors that can alter the electrostatic interactions such as pH and ionic strength of the solution, grafting density, and type of ionizable groups. Good understanding of the swelling behavior and changes in thickness of these PE systems has been achieved by analysis through techniques including dynamic light scattering (DLS), atomic force microscopy (AFM), ellipsometry, and neutron reflectometry.⁹⁻¹²

However, the stretching of neutral brushes is a different matter. Because neutral brushes don't respond to stimuli like PE brushes, their stretching characteristics cannot easily be experimentally quantified. The fact that polymer brushes are covalently attached to a surface, a feature normally considered an advantage, limits the types of

characterization methods available for analysis. Standard forms of characterization of polymer brushes include ellipsometry, FTIR, water contact angle, and AFM. However, data acquired by the first three techniques is an average over a large sample area. AFM provides more detail, but is limited to the surface. None of these methods gives insight into the stretching nature of polymer brushes or the packing density of neighboring chains. In order to better understand the strain in these brush systems experimentally, a novel characterization technique must be realized.

In the last decade a few groups have started to investigate the concept of detached brushes. Huck *et al.* chemically crosslinked poly(glycidyl methacrylate) (PGMA) brushes grown from a patterned gold electrode surface.¹³ By applying a short pulse to the electrode, the bond between the end of the chain and the gold surface was weakened enough allowing the film to buckle and in some cases detach. The authors note that domes formed by the buckled film take into account the eigenstrain such that the chains arrange to minimize the elastic energy in the overall film. Although buckling patterns observed were theorized to be due to relief of internal stress first introduced during the polymerization process, without detaching the entire film it is difficult to fully analyze the system free from additional variables.

Here we introduce the notion of completely detaching polymer brushes and analyzing the free membranes via AFM and transmission electron microscopy (TEM). We have developed an etching method to lift off patterned polymer brush membranes. Analysis of the patterned features before and after detachment provides insight into the stretching properties of densely packed polymer brushes. Comparison between crosslinked and uncrosslinked brushes confirms a membrane expansion is observed in

the uncrosslinked brushes when detached from the surface. This poses the question of what is the nature of such growth in the x-y plane. Two possibilities can be considered; first dimensional change is anisotropic and the system is not behaving as an ideal elastomer. Compared to polymers in solution, dense polymer brushes are in a stretched, less entangled state and thus it is not unreasonable that some of their physical properties may vary in different directions. That might suggest that the system undergoing relaxation is therefore not isovolumetric and the glass transition temperature (T_g) would be greatly affected. On the other hand, the expansion could also be isovolumetric as is usually predicted by theory. In this case, physical changes would be related to a shrinkage in the z-direction which is attributed to chain relaxation and the simultaneous increase in dimension of chains in the x-y plane going to more of a random coil conformation. By investigating details of the films dimensional changes, T_g , and relating experimental observations to current brush theory, we believe this study gives insight to help answer questions about the nature of neutral brushes.

Experimental Section

Materials: Allyl-2-bromo-2-methylpropionate, chlorodimethyl-hydrosilane, Pt on activated carbon (10 wt %), 2,2'-bipyridine, pyridine, copper (I) bromide, copper (II) dibromide, copper (1) chloride, glycidyl methacrylate, methyl methacrylate, inhibitor remover, anhydrous toluene, *N,N*-dimethylformamide, hydrofluoric acid, were purchased from Sigma Aldrich and used without purification unless stated otherwise. Methyl methacrylate was passed through a short column of inhibitor

remover beads before use. Deionized water with a resistivity of 18.2 MΩ•cm at 25 °C was obtained from Millipore's Milli-Q Synthesis A10 system. All the other solvents were purchased from Fisher Scientific.

Synthesis of Silane Initiator and Immobilization: Hydrosilylation of allyl 2-bromo-2-methylpropionate was carried out using a literature procedure to obtain the ATRP initiator, 3-(chlorodimethylsilyl)propyl 2-bromo-2-methylpropionate.¹⁴ Wafer pieces with a 2 μ m silicon oxide layer were oxidized using a Harrick Plasma Cleaner for ten minutes, rinsed with ethanol, and heated to remove all traces of water. In a glove box, the wafer pieces were immersed in a toluene solution of the initiator (varying concentrations) and pyridine (0.05 mM) overnight at room temperature. The substrates were then removed from the solution and washed with water, ethanol, and dichloromethane (DCM) sequentially and sonicated for ten minutes in DCM. Wafers were given a final rinse of dichloromethane and blown dry under nitrogen gas.

Brush Polymerization: PMMA brushes were prepared by placing two wafer pieces with immobilized initiator on the surface in a 25 mL Schlenk flask under an argon atmosphere. The flask was evacuated and back filled with argon four times. CuBr (142.4 mg, 1.0 mmol) and bipyridine (312 mg, 2.0 mmol) were taken in another 50 mL Schenk flask equipped with a magnetic stir bar. The air in the flask was evacuated and replaced with argon four times. Methyl methacrylate (10.0 g, 100 mmol), methanol (8 ml) and water (2 mL) were purged with argon for about twenty minutes and cannulated into the flask containing the ligand and copper salt. The reaction mixture was stirred at room temperature for 30 min to ensure the formation of the copper-ligand complex. This solution was then transferred into the flask

containing the initiator coated wafer pieces and allowed to polymerize at 32 °C for different time lengths. After polymerization, the substrates were washed with dichloromethane and ethanol and dried under nitrogen gas. PGMA brushes were prepared via the same procedure but instead using CuCl (72.8 mg, 0.7 mmol), CuBr₂ (7.8 mg, 0.03 mmol), bipyridine (282 mg, 1.80 mmol), glycidyl methacrylate (10.42 g, 73 mmol), methanol (8ml) and water (2 mL).

Polymer Brush Patterning: PMMA brush samples were first spin coated with positive tone photoresist S1818 (Shipley) and baked for 90 seconds at 90 °C. The samples were exposed to UV light ($\lambda = 405$ nm) for ten seconds using an ABM contact aligner with a patterned mask of individual membranes containing 20 μm holes 190 μm apart. After a post exposure bake (PEB) for the same length of time and temperature as before, substrates were developed in MIF 726 for 1.5 minutes. Next the wafer pieces were etched for 4 minutes using a standard oxygen etch recipe using a PT72 Etcher. Remaining photoresist was removed with acetone and the patterned features were then characterized by AFM.

Membrane Liftoff: The brush films were removed from the surface by etching the silicon oxide layer with a 48 wt. % solution of HF. The detached, floating films were rinsed twice with water before being transferred to a copper grid for transmission electron microscopy (TEM) or allowing to settle back to the surface for further characterization.

Ellipsometry: Thicknesses of the brushes were measured using an Imaging Ellipsometer - Nanofilm EP3 with a 532 nm laser starting at a 50° angle and ending at 60°. A PMMA_450 model (PMMA_450/SiO₂/Si substrate) was used to fit the data, in

which the PMMA layer was representative of the polymer brush. For T_g data, a thermal stage was mounted to the ellipsometry and samples were measured every 2° over a range of 70° - 130° . For the first data point collected, a 10 point measurement was acquired starting at a 50° angle and ending at 60° . For every subsequent set a 3 point measurement was acquired starting at a 58° angle and ending at 60° .

Characterization: Polymer brushes were characterized by ellipsometry, AFM (Veeco Icon) and transmission electron microscopy. A FEI T12 TWIN TEM was used to acquire optical images of the films.

Results and Discussion

Due to the limited forms of characterization available for covalently attached polymer brushes, we have proposed an innovative method of detaching brush membranes for further examination. Polymer brushes were grown via atom transfer radical polymerization (ATRP) from a silicon oxide surface. The oxide is beneficial because it is chemically identical to a regular silicon wafer, the standard surface for brush growth, and because it can be etched away by hydrofluoric acid (HF). Because of its chemical stability, any type of polymer brush can be grown from this surface and investigated regardless of polymerization environments. By applying a hydrofluoric acid (HF) etch; the oxide will be dissolved while the polymer brushes are thus lifted off from the surface generating free standing thin membranes that can then be transferred to a TEM grid (figure 1) or allowed to settle back to the surface for AFM characterization.

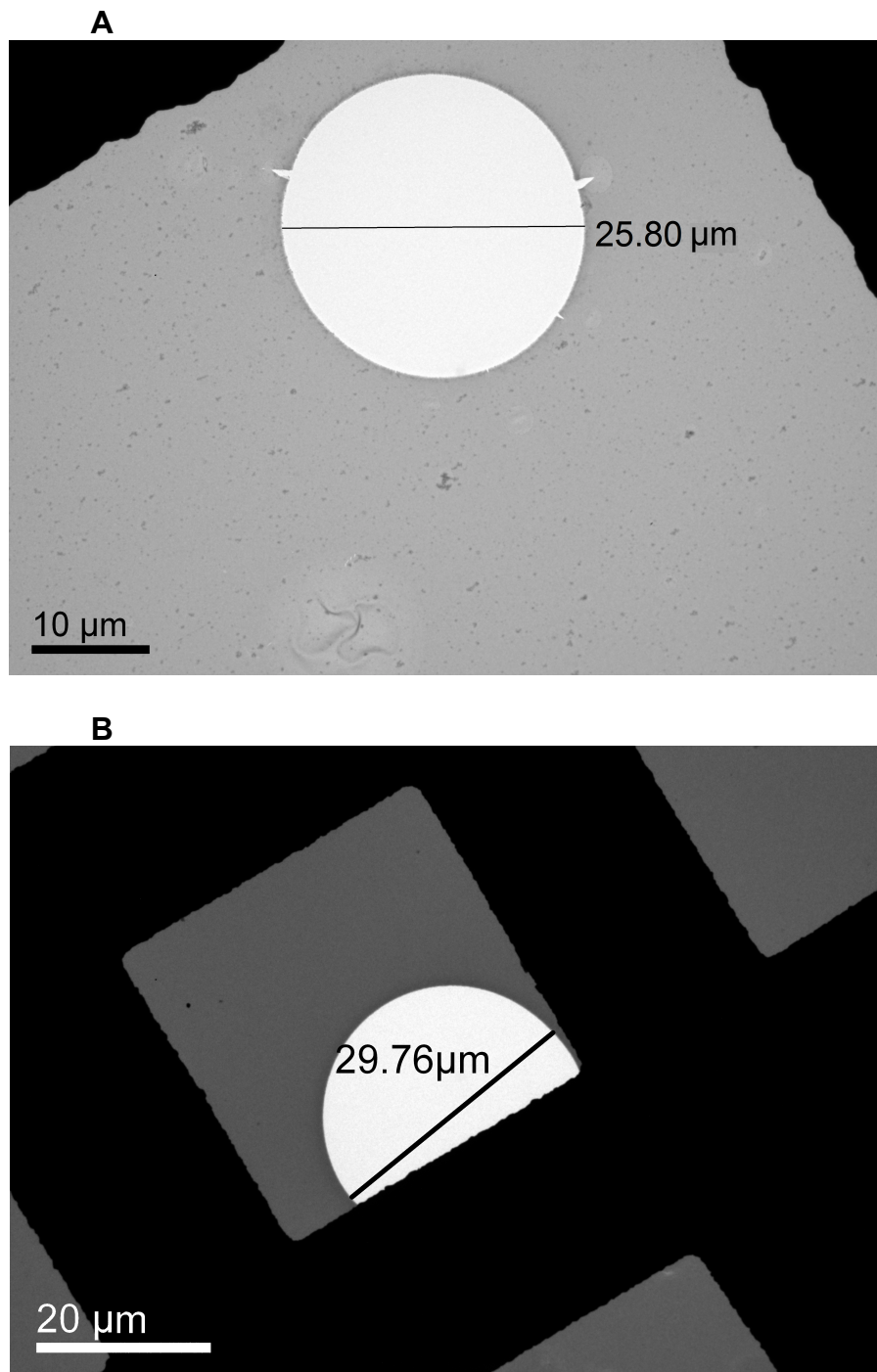


Figure 1. TEM images of PMMA (A) and PGMA (B) confirm brush membranes are thick, homogeneous films. This technique also shows the expansion properties of the membranes after being removed from the surface.

PMMA and PGMA brushes were grown and patterned into individual membranes with 20 μm diameter holes spaced 180 μm apart. The holes were important for two reasons, first they allowed for rapid diffusion of HF to the oxide surface for etching (discussed later) and second they have the benefit of acting as markers for dimensional changes in the brush films. AFM of the patterned holes before etching confirmed both the dimensions (20 μm diameter) and the thickness of the brush while in its original, stretched state.

If before HF etching an effective crosslinking process is applied, such as a basic reaction of KOH to the PGMA brushes, the removed films retain the patterned spacing and size of the holes or are close to those dimensions (see Chapter 4). This indicates that crosslinking can fix the overall shape and form of brushes in their initial polymerized structure. Perhaps the more interesting observations come into effect when the brush membranes have not been crosslinked.

Both PMMA and PGMA uncrosslinked brushes have been explored and in each case a characteristic increase in the diameter of the hole is observed (20-30% increase in x-y dimensions) as well as a reduction in the thickness. TEM and AFM indicate the same findings although thickness was not measured for the TEM samples (table 1). Results indicate that when the membranes are lifted off and the surface attachment constraints are removed, the chains are able to relax. It should be noted that the films are not exposed at any point during the process to solvent systems that might swell or soften the brushes; therefore another driving force must be the reason for the chain relaxation. Such relaxation in the z-direction, causing a growth in the x,y plane, was evaluated to determine whether the change was isovolumetric (figure 2). The probable

Sample	Original Hole Diameter (μm)	Post-removal Diameter (μm)	Original Thickness (nm)	Etched Thickness (nm)	Thickness Decrease (%)	Calculated Thickness (nm)	Calculated Diameter (μm)
PMMA 1	20	26.3	58.6	30.3	48.3	33.8	27.8
PMMA 2	20	25.0	105	67.0	36.2	67.2	25.0
PMMA 3	20	24.5	82.0	61.2	25.4	54.5	23.2
PGMA	20	25.1	152	94.7	37.7	96.3	25.3

Table 1. PMMA and PGMA film thickness were measured before and after membrane detachment by AFM. Calculated thickness is theoretical height of brushes based on the measured hole diameter using the equation for volume of a sphere, $V = \pi r^2 h$ and $h = \frac{V}{\pi r^2}$ where r_n is the new measured hole radius. Calculated diameter is theoretical hole expansion based on the measured thickness of the brushes after detachment. The same equation for volume of a sphere is used as well as $r = \sqrt{\frac{V}{\pi h_n^2}}$ where h_n is the measured brush height after detachment.

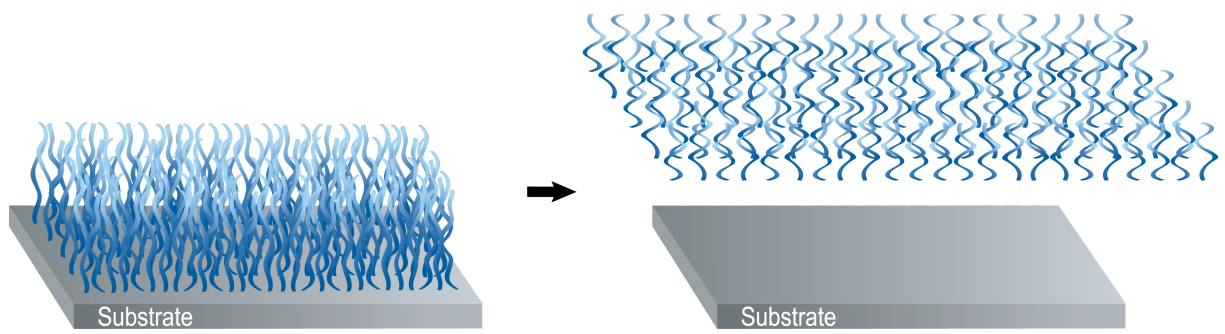


Figure 2. Illustration of isovolumetric film expansion. After detachment, brushes relax in the z-direction and result in a simultaneous expansion in the x,y-plane.

driving force is eigen strain or residual stress in the z-direction caused by the polymerization induced stretching of the polymer chains. While these findings are consistent with the theoretical view that the polymer brush chains are behaving like elastomers, a closer inspection of the polymer brush system suggests other characteristics should also be taken into consideration. We can gain insight into stretching properties by considering just an individual chain. The force of a single polymer chain can be calculated using the theory of rubber elasticity. For a single strand,

$$f = \frac{dF}{dr} = -\frac{TdS}{dr} = 3k_b T \frac{r}{\langle R^2 \rangle}$$

where $\frac{r}{\langle R^2 \rangle}$ is a measure of the chain extension of the stretched brush, f is force, F is the Helmholtz free energy, T is temperature, and r is the rms end-to-end distance. When a chain is in a fully stretched state, the entropy is significantly reduced because there are fewer possible conformations. If the external force is removed, an entropy driven restoring force will cause the chain to return to its equilibrium state, usually a random coil. Polymer brushes grown from the surface by a radical polymerization method at high grafting density exist in a stretched state. When the film is detached and the restrictive anchor points are removed, some restorative force exists in which collapse in the z-direction is permitted. However, because the chains are under conditions of high grafting density, neighboring chains prevent complete chain relaxation. In other words, detached membranes do not go from a constrained brush regime all the way to an unrestricted mushroom regime. But why is this so?

This raises the further questions as to how the chains are held together and why they don't just separate and allow the brush film to disintegrate? Furthermore, the expansion takes places in the x-y plane. What enables the films to stretch but then causes them to stop at about the same degree of strain? We expect the film robustness to be due to entanglements. Although in a very dense brush the chains are in a highly stretched state, the system is not perfect and there will be entanglements and chain overlap. It is not due to a residual crosslinked layer where the brushes were formerly attached. This is supported by the observation that the membranes maintain a planar shape on removal from the substrate. If crosslinking of a sublayer was taking place during the brush film removal process, then more curvature would be seen in the film. Crosslinking the bottom (or top) section of a preexisting film can lead to a contraction which is commonly known to result in rolling or bending deformation. Our planar membranes suggest uniformity throughout the brush film and thus no localized constraint at the bottom. Therefore we suggest that homogeneous entanglements throughout the brush film prevent the brushes from completely separating upon release and still permit some restorative force to act on chain relaxation. Although it is beneficial to realize the importance of chain entanglement and the effect it has on the brush system, a deeper investigation must be carried out.

The relaxation of the brush films suggests that they are under conditions above the glass transition temperature of the polymer brushes. Perhaps the brush microstructure naturally produces a low T_g material? In order to gain a better understanding of the behavior of these polymers, we have evaluated the T_g of the thin film material. Keddie *et al.* investigated PMMA spin coated thin films on silicon oxide and gold

using spectroscopic ellipsometry.¹⁵ By identifying the discontinuity in thermal expansion of the films, the T_g could be identified. They report higher T_g values for PMMA on silicon oxide (397 K) compared to gold (386 - 390 K) due to restricted chain mobility at the interface attributable to hydrogen bonding between PMMA and the surface hydroxyl groups. They also note that their value for bulk T_g (390 K) is higher than a previously reported value of 378 K.¹⁶ We measured a T_g for our attached polymer brushes in a similar manner and found the samples to be on the order of 378 - 383 K, significantly lower than reported by Keddie but still well above our process conditions. Figure 3 shows a typical scan of a PMMA brush system where there are two regions with differing slopes where thickness increases with temperature. These results are not unreasonable considering the fact that our brush system is in a stretched state and thus chain interactions with the oxide interface is negligible. Our brushes are behaving as PMMA in a bulk film, free from exterior surface interactions.

What then enables mobility of the brushes and permits the relaxation process to occur? An important aspect to consider is the etching step itself. Although the reaction of HF with silicon oxide is exothermic,



it is unlikely that there are large thermal transients associated with the etch step. Any heat generated by the reaction would almost certainly dissipate directly into the silicon wafer due to its large thermal mass and high conductivity. Also, because the reaction is so rapid (membranes lift off virtually instantaneously) a temperature increase as the

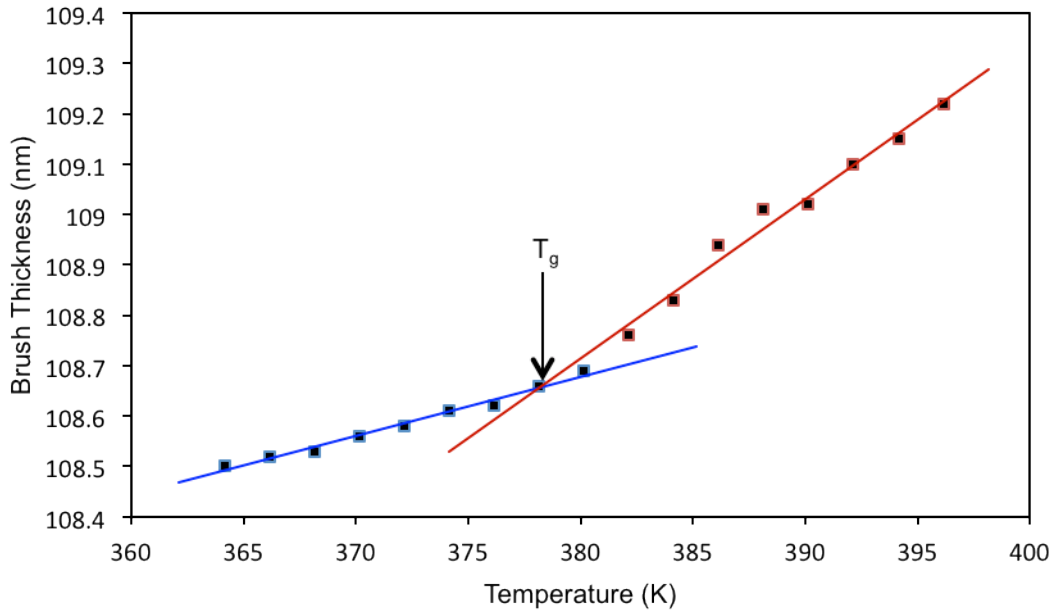
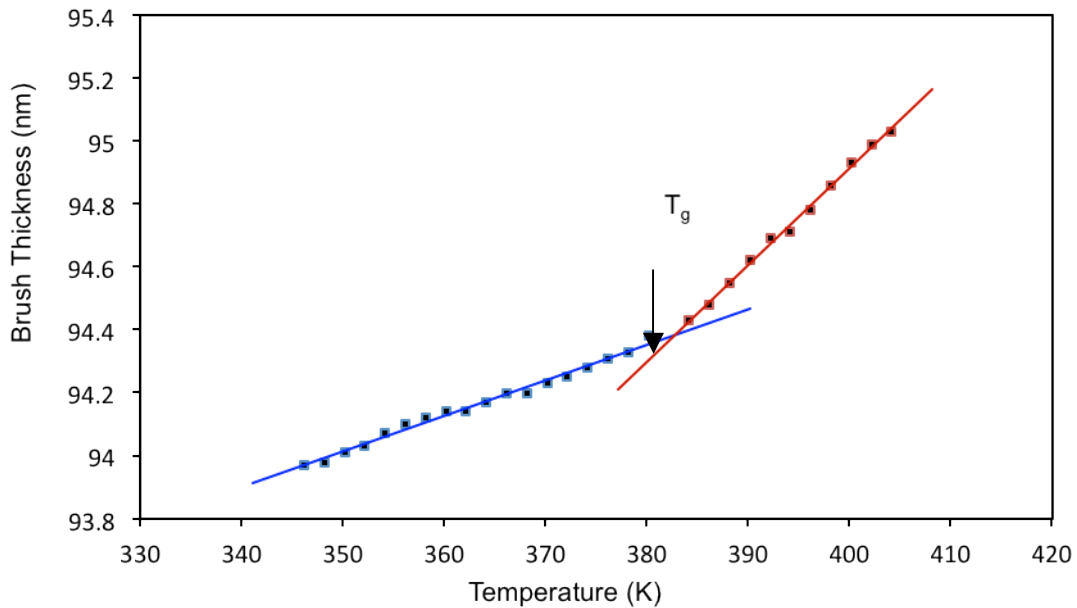
A**B**

Figure 3. Measured thickness as a function of temperature for a 108 nm and 93 nm thick PMMA brush on a silicon wafer, A and B respectively. The intersection of the trendlines indicate a glass transition near 378 K and 382.5 K, respectively.

source of detachment is improbable. However, this observation of fast detachment is worth closer examination. One of the initial reasons membranes were patterned with 20 μm holes approximately 180 μm apart was to provide sufficient access points for the HF to etch the oxide and therefore decrease the time required to detach the films. Surprisingly though, when exposed to HF most of the membranes lift off almost instantaneously. Such a rapid response suggests the HF is directly penetrating through the brushes and immediately cleaving the attachment points instead of undercutting through the patterned holes. If this is the case, and HF is diffusing into the brushes, then it brings into question if the acid could be interacting with the PMMA. To respond to this issue we need to consider what we already know. First, we observe the polymer membranes are expanding in the x,y-direction after the etch step which suggests a transition from the glassy state to a mobile state has taken place. For this switch to take place either the brushes must be heated to reach their T_g or their T_g must be lowered. Since the etching step takes place at room temperature and since it is the case that the reaction itself does not produce enough heat to increase the temperature of the polymer film, it is unlikely that the membranes are reaching their original T_g values. What is more probable is that the T_g is being lowered and permitting chain motion at room temperature. Such an effect may be the result of the HF interactions with the brushes; essentially the HF may be acting as a plasticizer. Membrane expansion has been observed for every sample tested. Although exposure times have varied, the HF component has always been consistent, thus strongly suggesting it is the more significant contributing factor and likely the source responsible for the chain

mobility and relaxation.

What causes the expansion to stop considering that the freed films are still in a stretched state? Since the brush stretching is almost instantaneous, then this suggests the brushes naturally relax to a certain strain and stop. Again we can speculate that entanglements in the brushes that enable a limited stretching in the x-y plane before they provide a counterforce to the relaxation taking place in the z-direction. After several seconds, the HF is removed when removal of the oxide layer is complete. Once the HF is removed, then plasticization is done and the chains are locked in.

Conclusion

The detachment of polymer brushes from surfaces is a very new field and one that is generating a great deal of interest. The ability to tailor and functionalize a polymer film attached to a surface and then lift it off to generate ultra thin free membranes is attractive in many fields such as ultra fine filtration and purification, microfluidics, and the formation of Janus particles. Here we have shown that detached polymer brushes can also give insight to the nature of these materials. Until now, the stretching of neutral polymer brushes has been primarily investigated through theoretical means. Numerous models based on scaling arguments and SCF approximations have been proposed which give light to brush behavior in terms of such properties as solvent and grafting density. By examining polymer brushes as a covalently attached system and then comparing them after a lift off process, the nature of their stretching properties can be experimentally investigated.

By utilizing an HF etching process to release polymer brushes, they can be

investigated in terms of a change in brush height and membrane dimensions. Detached films can be scooped onto TEM grids for detailed characterization of film homogeneity as well as membrane expansion information. AFM results show a reduction in thickness and a film growth in the x,y-direction. When the anchor points are cleaved from the surface, the external force is released, a restorative force allows the chains to relax into a more unstretched conformation. The chains will not reach equilibrium (a random coil), however, due to high grafting density and the fact that some entanglement exists within the brushes. This also prevents the membranes from separating and completely disintegrating. There are enough entanglements to preserve the film as a whole and provide a degree of robustness.

The source of this observed film expansion in the x-y plane seems to be driven by polymerization induced chain stretching but is also attributable to the etching step and HF acting as a plasticizer. In order for the polymer membranes to expand, the chains must go from a glassy state to a mobile state. Since there is no heat source during this process, this transition can only take place by lowering the T_g . A conceivable source for this decrease is the incorporation of a plasticizer. The extremely fast membrane release implies that HF is diffusing directly through the brushes in order to immediately cleave the attachment points. This observation establishes the fact that HF has an opportunity to interact with the brush chains immediately after exposure and possibly affect the physical properties of the material. Regardless of the source, the fact that we can observe the isovolumetric stretching properties of neutral brushes is a new concept aspect of these materials. Theoretical predictions have provided insight for these stretching properties, but this is the first example of a method to

experimentally verify such calculations. Moreover, this process can lead to a comparison study of a variety of polymer brushes and their stretching capabilities based on chemical composition as well as other factors.

Acknowledgments

The authors would like to acknowledge the National Science foundation grant DMR-1105253 for support of this work. This work made use of the Cornell Center for Materials Research (CCMR) shared Facilities which are supported through the NSF MRSEC program (DMR-1120296), the Nanobiotechnology Center shared research facilities at Cornell University, and was performed in part at the Cornell NanoScale Facility (CNF), a member of the National Nanotechnology Infrastructure Network, which is supported by the NSF (Grant ECS-0335765).

REFERENCES

- (1) Welch, M.; Rastogi, A.; Ober, C. *Soft Matter* **2011**, *7*, 297.
- (2) Stuart, M. A. C.; Huck, W. T. S.; Genzer, J.; Muller, M.; Ober, C.; Stamm, M.; Sukhorukov, G. B.; Szleifer, I.; Tsukruk, V. V.; Urban, M.; Winnik, F.; Zauscher, S.; Luzinov, I.; Minko, S. *Nat. Mater.* **2010**, *9*, 101.
- (3) Chiang, E. N.; Dong, R.; Ober, C. K.; Baird, B. A. *Langmuir* **2011**, *27*, 7016.
- (4) Tam, T. K.; Pita, M.; Trotsenko, O.; Motornov, M.; Tokarev, I.; Halamek, J.; Minko, S.; Katz, E. *Langmuir* **2010**, *26*, 4506.
- (5) Alexander, S. *Journal De Physique* **1977**, *38*, 977.
- (6) Degennes, P. G. *Macromolecules* **1980**, *13*, 1069.
- (7) Milner, S. T. *Science* **1991**, *251*, 905.
- (8) Martin, J. I.; Wang, Z. G. *Journal of Physical Chemistry* **1995**, *99*, 2833.
- (9) Lu, Y.; Mei, Y.; Schrinner, M.; Ballauff, M.; Moller, M. W. *Journal of Physical Chemistry C* **2007**, *111*, 7676.
- (10) Azzaroni, O.; Brown, A. A.; Cheng, N.; Wei, A.; Jonas, A. M.; Huck, W. T. S. *Journal of Materials Chemistry* **2007**, *17*, 3433.
- (11) Biesalski, M.; Johannsmann, D.; Ruhe, J. *Journal of Chemical Physics* **2002**, *117*, 4988.
- (12) Tran, Y.; Auroy, P.; Lee, L. T. *Macromolecules* **1999**, *32*, 8952.
- (13) Edmondson, S.; Frieda, K.; Comrie, J. E.; Onck, P. R.; Huck, W. T. S. *Adv. Mater.* **2006**, *18*, 724.
- (14) Shah, R. R.; Merreccyes, D.; Husemann, M.; Rees, I.; Abbott, N. L.; Hawker,

- C. J.; Hedrick, J. L. *Macromolecules* **2000**, *33*, 597.
- (15) Keddie, J. L.; Jones, R. A. L.; Cory, R. A. *Faraday Discussions* **1994**, *98*, 219.
- (16) Rogers, S. S.; Mandelkern, L. *Journal of Physical Chemistry* **1957**, *61*, 985.

CHAPTER 6

SUMMARY AND FUTURE DIRECTIONS

Electrochemical Biosensor: This project involves a unique union of experts from a diverse background including biophysics, electrochemistry, immunology, and material science. Over the past few years the project has seen substantial progress and development. The polymer brushes have been redesigned and optimized, the photosensitizer (which was originally added to the analyte solution) has been electrochemically immobilized on a surface, and the device platform has been reinvented into individual patterned electrodes. These improvements have elevated this project to a new level. The collaborative work illustrated in chapter 2 has demonstrated excellent device fabrication and sensitivity for our system.

At this point, there are two directions which can be explored. First, novel antibodies can be tested. The results and techniques demonstrated in chapter 2 were based on a model approach using DNP-antibodies, a convenient and well understood system. However, in order to illustrate the potential of this biosensor for mainstream usage, it must first be shown to be successful using high impact antibodies. Viruses such as H5N1 and H1N1 are well known by the general population thanks to continuous media coverage. If peptides specific for antibodies associated with these flu viruses can be immobilized on the brushes and detected at low levels, this may draw a great deal of interest from industry and enable the possibility of a startup company.

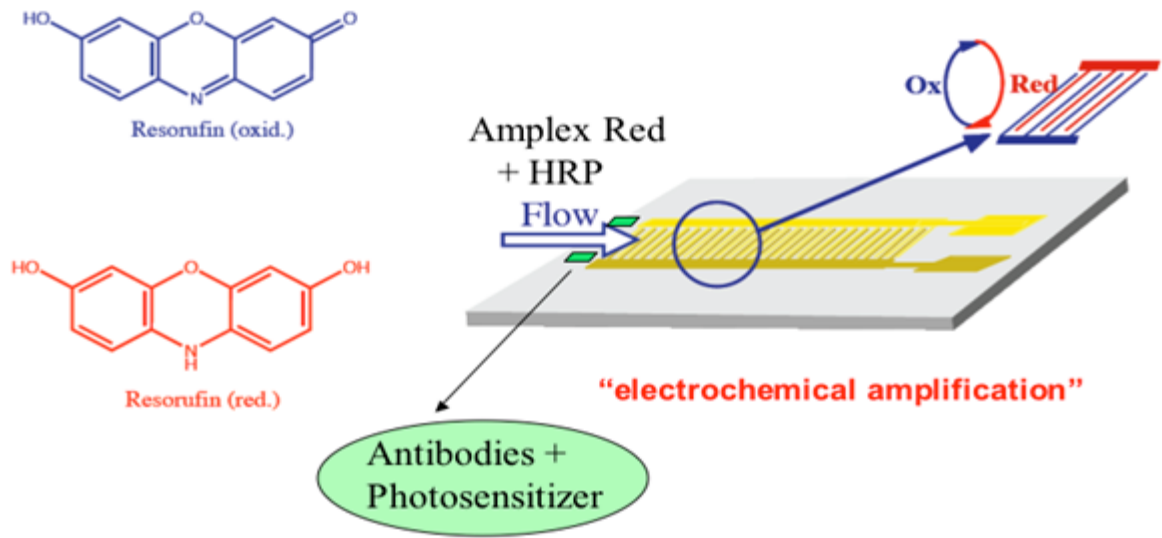


Figure 1. Construction of an interdigitated system for detection amplification.

Another point of interest and next direction is the need for a portable device capable of directly identifying infected live stock in the field. Our current system has already demonstrated exceptional levels of detection; however, this can readily be incorporated into microfluidic devices (figure 1). Even employing standard microchannels (for example 200 μm high and 500 μm wide) and an interdigitated array of perhaps 1000 electrodes could possibly lead to several orders of magnitude amplification. Additionally, with growing emphasis on flexible substrates, such interdigitated microfluidic systems could be constructed on plastics. In a previous chapter we demonstrated our capability of polymerizing brushes from a conjugated polymer surface. This capability could lead to novel device platforms that could be mass produced at low cost. Overall, the fabrication of amplified electrodes functionalized for target viruses would allow for widespread use and field deployment.

OECT Glucose Sensor: Here we have demonstrated the ability to polymerize brushes from an unconventional surface, PEDOT:PSS. This novel immobilization technique has the potential to be transferred to a plethora of other unique polymer surfaces such as other conductive polymer substrates or flexible electronics. Additionally, the initiator immobilization process is less time consuming (1 hour compared to 12 hours of standard immobilization in solution) and does not use any harsh solvents, and the initiator can be easily purchased instead of synthesized. Overall this method can open up new avenues for polymer brush applications.

Chapter 3 illustrates the fabrication and characterization of the polymer brushes on PEDOT:PSS and the optimization necessary for retention of the polymer's conductivity. It was also established that the polymer brushes sufficiently bound glucose oxidase without hindering the enzyme's activity for periods of up to 23 days. Results confirmed the incorporation of the polymer brushes scaffold enhanced the longevity of the glucose detecting electrode and suggested the new platform may constitute the basis for future local multimodal recording.

Having established a working electrode with brushes, the next step is merging this new scaffolding idea with the current *in vivo* electrocorticography (ECoG) technology. Present electrodes make use of the ability to record both neurological signal (unit activity of neuron as rhythm of networks of neurons) and metabolic activity (Glucose) (figure 2). Until now, one major issue with these devices was the leakage of the glucose oxidase enzyme required for the metabolic activity detection of glucose. Polymer brushes may be the answer to this problem. PEDOT:PSS electrodes will be fabricated such that 3 mm will be implanted into the brain of a rat while leaving 5 mm for connection and fixation out of the brain. Sections of the electrode will allow for polymer brush polymerization and functionalization of the enzyme. If successful, a large amount of data can be recorded during one implantation. Both neurological signals and metabolic activity may be documented at the same time with only one probe, thus eliminating the use of multiple highly intrusive probes into the delicate tissue.

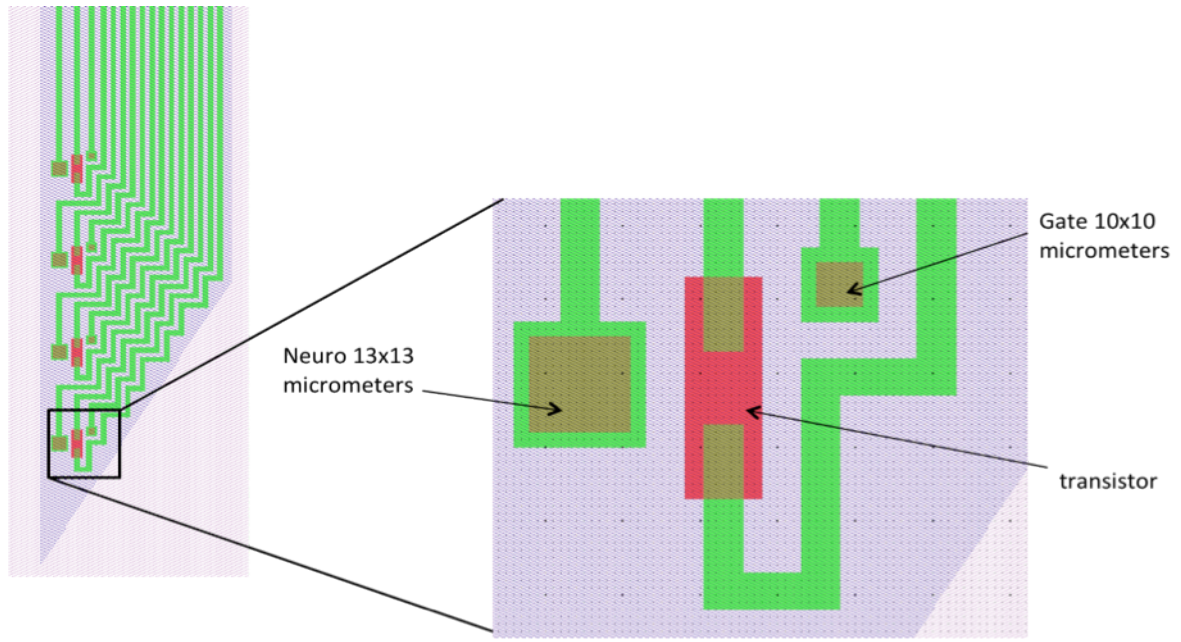


Figure 2. Illustration of an electrode that can record both neurological signal (unit activity of neuron as rhythm of networks of neurons) and metabolic activity (glucose).

Polymer Brushes for Cellular Motility: This relatively new project explores the use of polymer brushes as a scaffolding platform for quantitative temporal and spatial analysis of specific protease activities on the surface of living, motile cells. The advantage of polymer brushes is that they can be functionalized with a plasmin-specific, peptide (D-val-leu-lys)-containing a fluorogenic plasmin substrate. The idea is that when a cell moves across the functionalized surface, it will cleave off the peptide leaving a trail that can be visualized under fluorescence microscopy.

Thus far, the peptide-dye has been synthesized, a mixed brush system has been recognized, and the attachment of the dye molecule to the brushes has been successfully achieved and characterized by FTIR and Fluorescent imaging. In addition we have started the process of testing the polymer brush biocompatibility with the cells as well as developing and optimizing a “scratch assay” to watch the migration of the cells. Although significant progress has been made in a short period of time, the ultimate goal has still not been achieved.

Issues have arisen regarding the enzyme mediated cleavage of the peptide from the coumarin dye. Polymer brushes functionalized with the peptide dye have been incubated with different types of enzymes at various temperatures for both long and short periods of time, but a change in fluorescence is never seen. Solution tests with a fluorescence spectrometer have also been carried out and showed similar results. Fluorescence after enzyme exposure only provides 1.5 orders of magnitude increase in fluorescence. Ideally, we need to be in the range of a 1000 times increase in fluorescence such that a difference can be visualized on the polymer surface. This

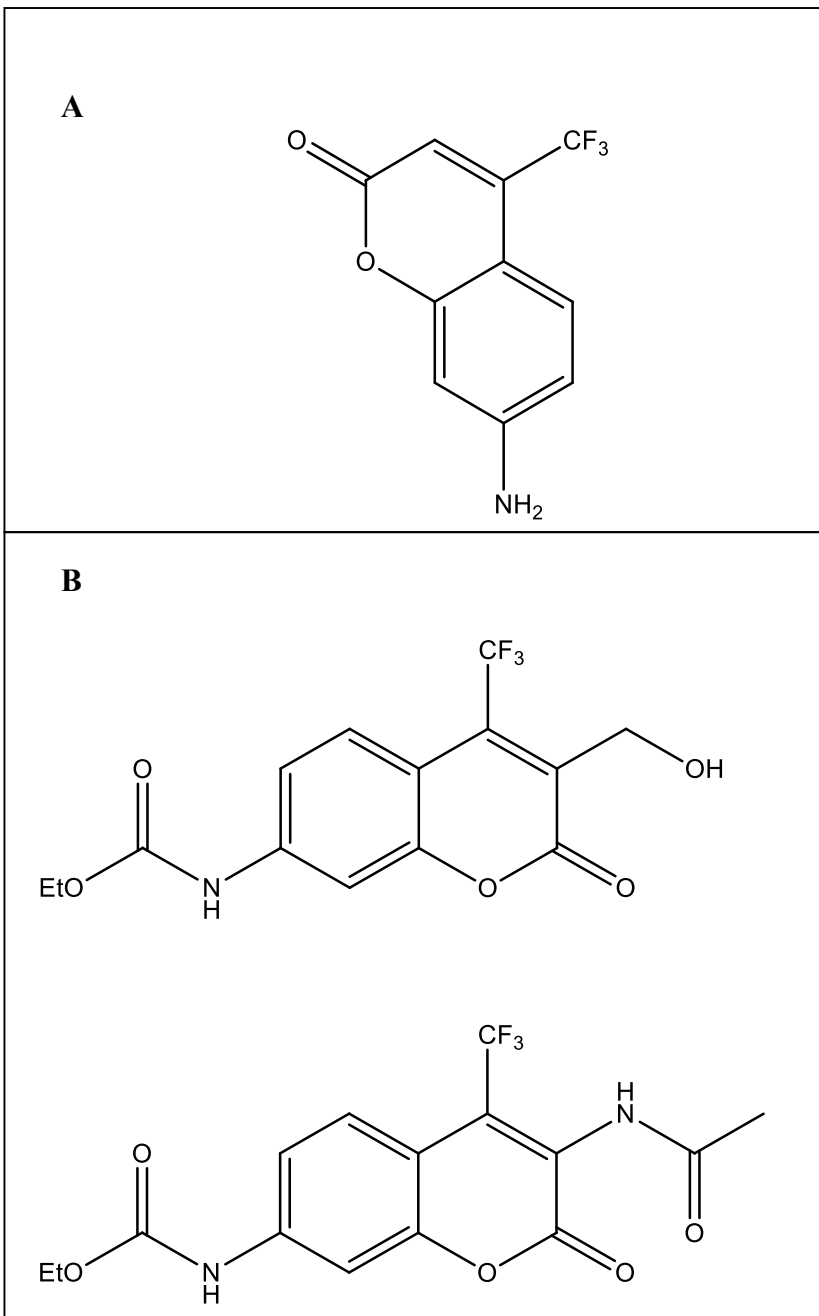


Figure 3. Structure of the original coumarin dye (A). Possible structures for new dye that incorporates CF_3 moiety (B).

suggests the enzyme is unable to effectively cleave the peptide from the dye and thus a closer inspection of the chemical bonding may be necessary.

Taking a step back to the original coumarin dye structure, it should be noted that a CF₃ group resides on the second ring (figure 3). This group was initially eliminated because it was synthetically challenging to incorporate; however, it may be a key feature not only for fluorescence amplification but also enzyme efficiency. By adding such a highly polar group, perhaps electron density can be pulled away from the amide bond which links the peptide to the dye and makes it more susceptible to enzyme attack.

Another possibility might be to increase the length of the linkage between the coumarin dye and the peptide. This would help provide better access for the enzyme as well as give more tunability to the peptide attachment bond/point. However, this would bring into question if the linker molecule would continue to quench the fluorescence of the dye even after enzyme exposure. With a few synthetic tweaks, the fluorescentce of the peptide substrate in solution and attached to the brushes after peptide cleavage will be great enough to allow for cellular motility visualization.

Polymer Brush Membrane Detachment: In chapters 5 and 6 a process is detailed of removing polymer brushes directly from a surface to generate ultra thin free standing membranes. Unlike other polymer carpet examples in the literature, this etching technique allows for characterization methods not available in the attached form. TEM images provide information on initiator immobilization conditions, polymer brush film homogeneity, crosslinking efficiency, and answer questions about the nature of these brush films. The most interesting observation that has surfaced

from this work is the expansion properties seen after an uncrosslinked brush is detached. Chapter 6 goes into more detail relating the relaxation of chains in the z-direction and growth in the x,y plane to current brush theory and isovolumetric behavior. It is proposed a plasticizing effect during the HF etch step may be the source for the film expansion. However more knowledge is required to fully understand the behavior of the material.

A significant source of information could be in determining the molecular weight of the polymer brush. Because polymer brushes are covalently attached to a surface, measuring the molecular weight is quite difficult. Some people put sacrificial initiator into the polymer brush reaction vessel and consider the polymer that is generated in solution to be the same molecular weight as the brushes grown from the surface. It has not yet been experimentally confirmed if this assumption is accurate; however, this may be where detaching polymer brush films could answer those questions. The difficulty is producing enough polymer brush material for the GPC to detect. Brushes are thin films to begin with, and since they are generally grown on small areas, the amount of polymer etched free is not even a weighable quantity. Consequently it might be that the best and only approach is by manipulating highly advanced techniques of spectroscopy such as MALDI and light scattering. This data would aid in calculating degree of stretching and justify the speculations laid out in chapter 6.

Further down the road additional applications could be imagined for detached polymer brush films. There are multiple methods for ultra thin membrane fabrication. However the advantage of using polymer brushes is the ability to easily tailor thickness, grafting density, and functionality. We foresee that this work and the

tailored shaping of brush films and nanoparticles could find application as encapsulation agents or as very small scale building blocks. Additionally by creating diblock copolymer brushes it is possible to create Janus membranes, where each face has different properties capable of interfacing with biological media.

Overall polymer brushes have come a long way since first emerging in the mid 1950s. Theoretical and experiment studies of brushes have lead to advanced technological developments in a variety of fields including bioelectronics, sensors, micro engineering, and material science. Great progress has been made, but more can be realized. We are only limited by our lack of creativity, and it is my hope that this thesis has generated enthusiasm for this topic and incited inspiration for projects to come.

APPENDIX

POLYMER BRUSHES AS SURFACE SCAFFOLDS FOR CELLULAR MOTILITY

Abstract

Protease enabled, growth factor-directed cell migration is fundamental to many biological processes such as angiogenesis. However it is still unknown how the amalgamation of effects on cell mobility and effects on extrinsic matrix properties results in cellular migration. Current technology does not allow us to image the cell surface protease activity. To overcome this limitation, we have developed a technique that will allow quantitative temporal and spatial analysis of specific protease activities on the surface of living, motile cells. Polymer brushes have been incorporated into our system to act as a scaffold support because they can be functionalized with fluorescent peptide moiety (annexin A2-mediated) that will become activated when enzymatically cleaved. The interaction between polymer brushes and human umbilical vein endothelial cells has been investigated in terms of brush thickness and different plating environments.

Introduction

On the surface of cells reside numerous types of proteases, enzymes which catalyze the hydrolytic cleavage of peptide bonds in proteins, which control a variety of biological processes such as cell motility, invasion, tissue remodeling, wound healing, and signal transduction, leading to rapid and dynamic changes in cell function. Of particular importance is protease enabled, growth factor-directed cell

migration which has been demonstrated to be a major contributor in angiogenesis.¹ Angiogenesis is the process in which new blood vessels are formed from pre-existing vasculature.² Endothelial cells that form the blood vessels secrete matrix metalloproteases to carve a pathway through provisional and mature extracellular matrix. Protein fragments generated from the degradation, as well as angiogenic growth factors, foster the migration and proliferation of endothelial cells, which re-associate to create new tubular structures and recruit stabilizing mural cells such as pericytes. Other plasma membrane-associated proteolytic systems that play a role in angiogenesis include receptor-associated urokinase, and the annexin A2 fibrinolytic system.³ While significant genetic, biochemical, and pharmacological work has been carried out to examine the signaling scheme for individual cell migration, little is known regarding the genes and mechanisms driving cellular movement. Currently there are few methods for imaging cell surface protease activity under dynamic, real-time conditions. A surface with the capability of visualizing protease interaction would aid in the understanding of cellular activity by providing a clear temporal and spatial record of single cell protease activity in response to specific biologic, chemical, or physical stimuli both *in vitro* and *in vivo*.

We believe a surface ideal for such methodology is a polymer brush film, that is, polymer chains covalently tethered to a surface.⁴ The number of chains attached per unit area of surface, the grafting density, determines the structure and conformation of the brush layer. When neighboring chains are sparsely assembled such that they do not influence one another, the brush is said to be in a “mushroom” state.⁵ However, at sufficiently dense coverage the chains experience steric or electrostatic repulsion from

neighbors and stretch away from the surface in a “brush-like” formation. Polymer brushes have many desirable characteristics such as providing excellent surface coverage, a suitable mechanical interface, and the molecular attachment sites needed to bind biomacromolecules such as peptides, antibodies or dye molecules, while preventing non-specific binding.^{6,7} In the past few years they have acquired much attention for their involvement in microelectronics, nanofluidic devices, biosensing, and other areas of nanotechnology.⁸⁻¹²

For our platform we generated random copolymer brushes composed of poly(2-hydroxyethyl methacrylate) (*PHEMA*) and poly(glycidyl methacrylate) (*PGMA*) and functionalized them with a plasmin-specific, peptide (D-val-leu-lys)-containing fluorogenic plasmin substrate (VLKF). This specific peptide was chosen such that the cell moves across the brush surface, cell surface plasmin will cleave the peptide and activate the fluorescent tag, thus revealing the path of the cell via fluorescence microscopy (figure 1).

Experimental Section

Materials: Allyl-2-bromo-2-methylpropionate, chlorodimethyl-hydrosilane, Pt on activated carbon (10 wt %), pyridine, copper (I) chloride, copper (II) dibromide, inhibitor remover, glycidyl methacrylate, 2-hydroxyethyl methacrylate, *N,N*-diisopropyl carbodiimide (DIPC), dimethyl formamide (DMF), and phosphate buffered saline (PBS, pH=7.4) were purchased from Sigma Aldrich and used without purification unless stated otherwise. Fibronectin and Phalloidin Alexa 647 were purchased from Invitrogen. Deionized water with a resistivity of 18.2 MΩ•cm at

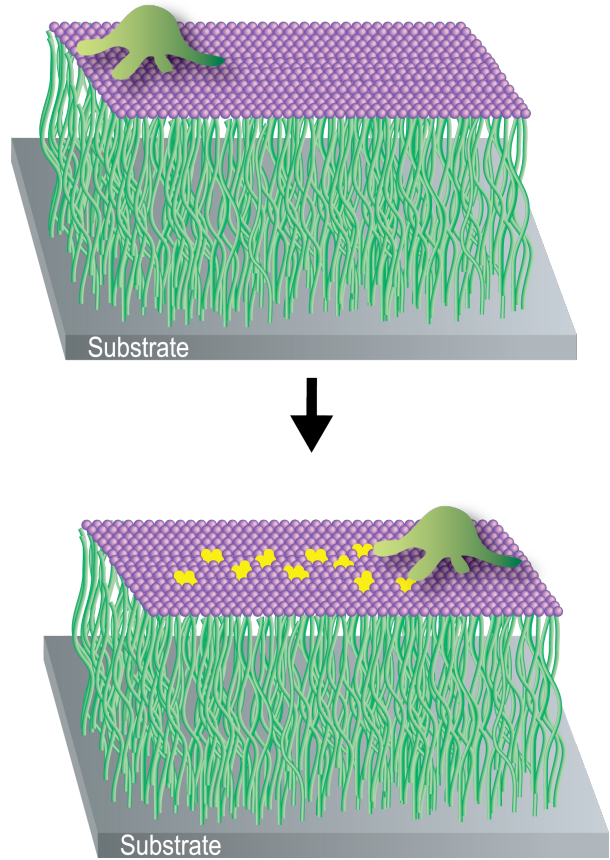


Figure1. Illustration of a cell moving across a peptide-fluorescent dye functionalized polymer brush surface (not to scale – brush length is exaggerated).

25°C was obtained from Millipore's Milli-Q Synthesis A10 system. 4-(dimethylamino)pyridinium 4-toluene sulfonate (DPTS) was prepared from dimethyl amino pyridine and sodium p-toluene sulfonate following a published procedure.¹³ All the other solvents were purchased from Fisher Scientific.

Synthesis of Silane Initiation and Immobilization: Hydrosilylation of allyl 2-bromo-2-methylpropionate was carried out using a published procedure to obtain the ATRP initiator, 3-(chlorodimethylsilyl)propyl 2-bromo-2-methylpropionate.¹⁴ Round, glass microscope coverslips (12 mm diameter) were oxidized using a Harrick Plasma Cleaner for ten minutes, rinsed with ethanol, and heated to remove all traces of water. In a glove box, the glass disks were immersed in a toluene solution of the initiator (2 mM) and pyridine (0.05 mM) overnight at room temperature. The substrates were then removed from the solution and washed with water, ethanol, and dichloromethane (DCM) sequentially and sonicated for ten minutes in DCM. Wafers were given a final rinse of dichloromethane and blown dry under nitrogen gas.

Brush Growth: PGMA:PHEMA brushes were prepared by placing two glass cover slips with immobilized initiator in a 25 mL Schlenk flask under an argon atmosphere. The flask was evacuated and backfilled with argon four times. CuCl (72.8 mg, 0.7 mmol), CuBr₂ (7.8 mg, 0.03 mmol), bipyridine (282 mg, 1.80 mmol) were taken in another 50 mL Schenk flask equipped with a magnetic stir bar. The air in the flask was evacuated and replaced with argon four times. Glycidyl methacrylate (2.60 g, 18 mmol), 2-hydroxyethyl methacrylate (3.085 g, 24 mmol), methanol (5 ml) and water (1.25 mL) was purged with argon for 25 minutes and cannulated into the flask containing the ligand and copper salts. The reaction mixture was stirred at room

temperature for 30 min to ensure the formation of the copper-ligand complex. This solution was then transferred into the flask containing the initiator functionalized device samples and allowed to polymerize at 32 °C for different time lengths. After polymerization, the substrates were washed multiple times with dichloromethane and ethanol and dried under nitrogen gas.

Brush Functionalization: Brushes were functionalized with ethylenediamine (1M solution) at room temperature overnight and the glass slides subsequently rinsed with water, dichloromethane and ethanol. The fluorogenic plasmin substrate was attached to the PHEMA-PGMA-NH₂ brushes in one step. Samples were placed in a 25 mL Schlenk flask under argon atmosphere. The flask was evacuated and back filled with argon three times. A solution of fluorogenic plasmin substrate (150 mg, 101 mM), DIPC (125 µL, 0.19 mM), and DPTS (187.5 mg, 0.15 mM) in anhydrous DMF (2.5 mL) plus a few drops of DMSO was cannulated into the flask containing the substrates. After reacting for 48 h at 32 °C, the substrates were washed with dichloromethane and anhydrous ethanol.

Cell Culture: PGMA-NH₂ brushes were grown on cover slips and placed into a 24 well plate. Samples were sterilized with 70% ethanol for 40 minutes and rinsed 3 times with 1X phosphate buffered saline (PBS). *HUVEC cells were harvested with 0.05% trypsin/0.53 EDTA for 2 minutes and plated 30,000 cell/well/500µl.* The plates were monitored over a time frame of 10 days. For fibronectin samples, the same procedure above was followed except before the cells were plated, the brushes were coated with 7mg/ml of fibronectin in 1X PBS for 30 mintues at 37 °C.

Cell Staining: The integrity of the cytoskeleton of the HUVEC cells was checked by staining them with phalloidin. Cells were rinsed with 1X PBS CaCl₂ and MgCl₂ (C/M) twice and fixed with 4% *paraformaldehyde* for 30 minutes and then rinsed again with 1X PBS C/M 3 times. Phalloidin Alexa 647 (1:50, invitrogen) was applied for 1.5 hours at room temperature and then rinsed with 1X PBS C/M 3 times. DAPI (1:10K) was applied for 10 minutes at room temperature and again rinsed with 1X PBS C/M 3 times. To observe cell mobility, 70% confluent HUVEC cells were stained with DiIC12 for 1 hour, rinsed with 1X PBS, and cultured for 2 days. After, cells were split and cultured for another five days before being split whereby 15,000 cells were plated onto the 26.5 nm PGMA-NH₂ brush sample for 2 days. The brush sample was then transferred to the dish with the fibrin/VEGF gel and cell mobility was monitored on a Zeiss LSM 5 Live confocal Microscope

Characterization: Polymer brushes were characterized by ellipsometry, FTIR, and fluorescent microscopy. Thicknesses of the brushes were measured using an Imaging Ellipsometer - Nanofilm EP3 with a 532 nm laser starting at a 50° angle and ending at 60°. A PMMA_450 model (PMMA_450/SiO₂/Si substrate) was used to fit the data, in which the PMMA layer was representative of the polymer brush. FTIR data was obtained using a Bruker Optics – Vertex 80v with an ATR germanium crystal. Fluorescent images were taken using an Olympus BX51 upright fluorescence microscope, equipped with a Roper Cool Snap hx CCD camera and using a DAPI filter set 340-380 nm excitation and 435-485 nm emission.

Results and Discussion

Both homopolymer brushes of PGMA and random copolymer brushes of PHEMA and PGMA were investigated as a platform for our system. The PGMA segments are important because the epoxy group can be functionalized with a diethylamine molecule that can then be used to covalently attach VLKF (figure 2). The nucleophilic ring-opening of the oxirane side chain groups was successfully carried out in both aqueous media and organic solvents. XPS measurements (figure 3) were taken of a PGMA brush (control) and a PGMA brush functionalized with diethylamine to chemically determine if the amine was being incorporated into the polymer brushes. The N (1s) signal at 395 eV confirms the existence of the amine groups on the surface. PHEMA, on the other hand, swells in water and becomes soft and flexible. When immersed in an aqueous solution, the combination of both as a mixed polymer brush produces a swollen system in which molecules can readily diffuse into and attach to available epoxy groups. Results indicate homopolymer brushes of PGMA can reach an acceptable degree of functionalization; however, the incorporation of PHEMA may further increase loading capacity.

For initial proof of concept, the fluorescent substrate without the peptide, a coumarin dye, was first attached to the PGMA-PHEMA-NH₂ brushes and characterized. The primary amine moiety on the dye was capped with an Fmoc protecting group in order to prevent secondary reactions and inverse binding to the brushes. Additionally, *N*-hydroxysuccinimide (NHS) was used to activate the compound's carboxylic acid group so that it could form amide linkages with the functionalized brushes. Figure 4 shows the FTIR spectra of the brush system

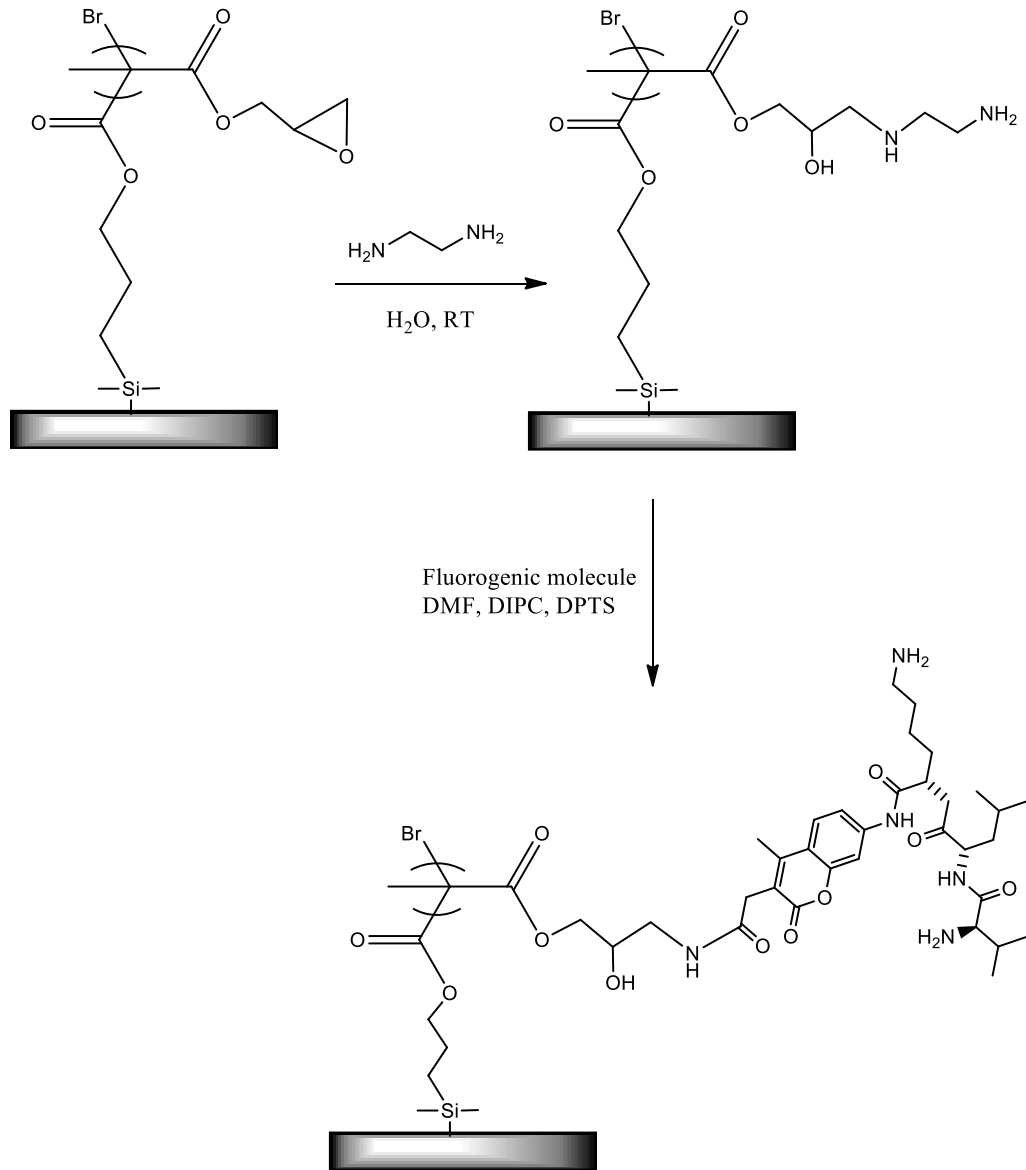


Figure 2. Functionalization of PGMA brushes with diethylamine and VLKF.

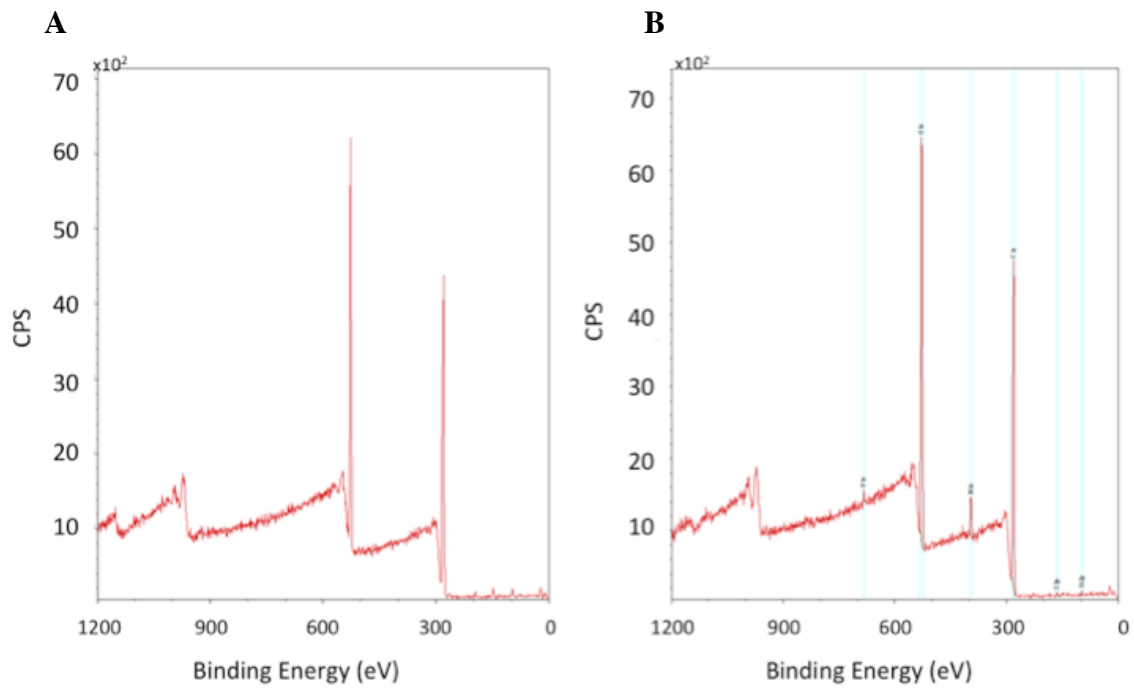


Figure 3. XPS of PGMA brushes without diethylamine (A) and functionalized with diethylamine (B). Presence of amine is indicated by peak at 395 eV.

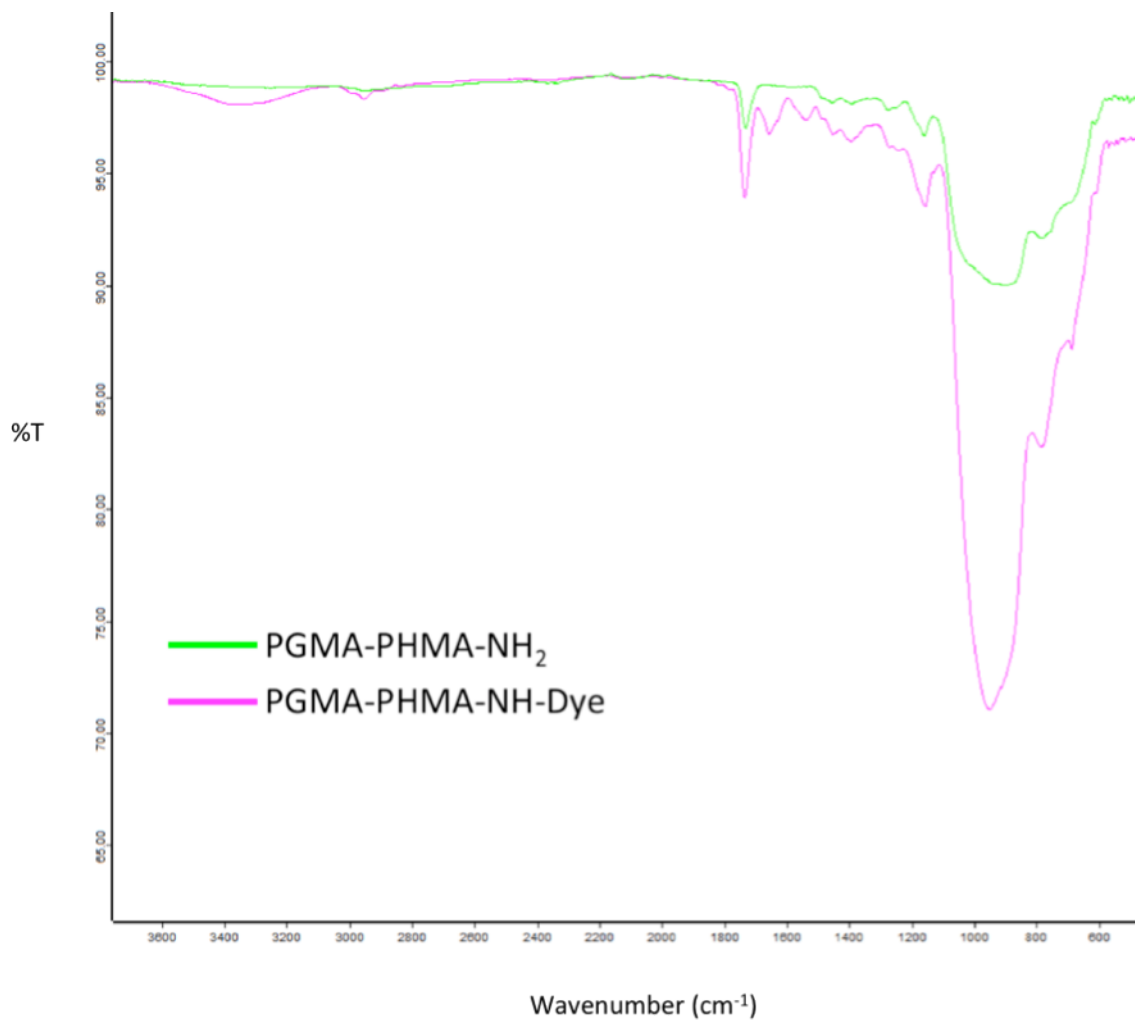


Figure 4. Shows IR spectra of PGMA-PHEMA brush systems. The green curve represents a PGMA-PHEMA-NH₂ brush, the pink curves is PGMA-PHEMA-NH-Dye. The new peak around 1538 cm^{-1} is from aromatic vibrations and the new peak at 1650 cm^{-1} can be attributed to the formation of an amide bond between the amine functionalized brushes and the activated carboxylic acid of the coumarin dye.

functionalized with the dye. The presence of new peaks in the PGMA-PHEMA-NH-Coumarin spectra (pink) compared to the control, PGMA-PHEMA-NH₂ (green), confirms the brushes have been chemically altered. The emergence of peak 1540 cm⁻¹ is characteristic of in plane vibrations of aromatic rings and the band at 1650 cm⁻¹ can be attributed to the amide bond formed between the dye and the brush (R-CO-NHR). Fluorescence imaging was also performed to verify the presence of the coumarin on the brushes. In order to accurately assess the fluorescent extent of the dye, it needed to be deprotected. After initial attachment of the coumarin, the protecting Fmoc group on the terminal amine was removed by piperidine in DMF. Figure 5 shows fluorescent micrographs of the polymer brush system functionalized with the coumarin dye (A) and without (B). Upon excitation at 365 nm, the coumarin dye in solution shows strong blue emission with a peak at around 420 nm. A DAPI filter set was used which has a good excitation range (340 – 380 nm), but the emission range is just on the shoulder of our molecule's emission peak (435 – 485 nm). Despite the filter cut off point, we were able to observe blue fluorescence of the coumarin dye attached to the polymer brushes, with a few small specks of high fluorescence which are attributed to dust contamination. No fluorescence was observed for PGMA-PHEMA-NH₂ (B) indicating that no dye was immobilized on the brushes.

In addition to fluorescent substrate attachment, the brushes can also be investigated in terms of cell adhesion and proliferation. Chiang *et al.* studied the cellular interaction of RBL cells on PAA brushes.¹⁵ Their findings showed cell adhesion when the brushes were patterned at feature sizes smaller than the dimensions of the cell. These results are suggested to be attributed to fibronectin being secretion

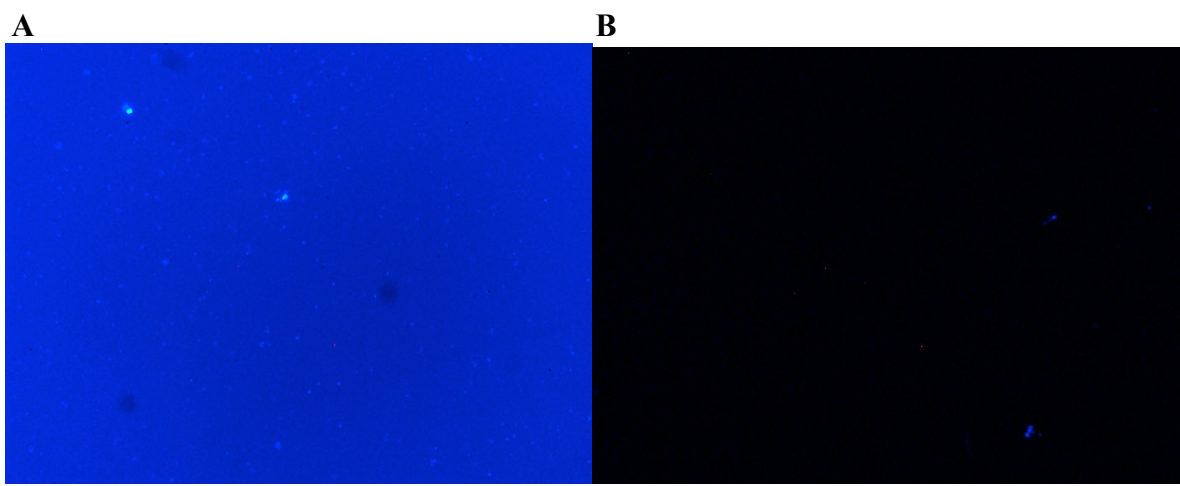


Figure 5. Fluorescent images using a DAPI filter set. Blue fluorescence is observed on the PGMA-PHEMA-NH-Dye brushes (A) due to the fluorescent emission of the coumarin dye. No fluorescence is observed in PGMA-PHEMA-NH brushes (B) because they are not functionalized with the dye.

from the cells onto the brushes and engaging cell-surface integrins. They also found brush thickness was important in cell adhesion, thinner brushes were better able to promote cell adhesion. Our initial experiments confirmed that human endothelial cells can be grown on non-derivatized polymer brushes. PGMA-NH₂ brushes, grown from coverslip and ranging in thickness (10.3, 57.4, and 316 nm), were sterilized and rinsed multiple times in a buffer solution. *Human umbilical vein endothelial cells (HUVECs)* were harvested and plated on brushes. The samples were monitored and phase photos were taken on 2, 4, and 9 days in culture (figure 6). Results show that the cells adhered on all three different sized brushes. Brushes of thickness 10.3 nm and 316 nm showed the best culture of cells, and after 9 days the 10.3 nm brushes reached 80% confluence. Observations at day 4 and 9 of the HUVEC plated on 316 nm brushes showed organization into a monolayer as well as formation into a single strand. Such patterns are often observed with endothelial cells used to study angiogenesis because of their ability to form capillary-like structures in response to certain stimuli. Overall most of the brush samples conformed to the typical endothelial cell cobblestone pattern. Additionally in order to check the integrity of the cytoskeleton, the HUVEC cells were stained with phalloidin (figure 7). Unhealthy cells autofluoresce in green; therefore as the cytoskeleton (phalloidin) becomes disorganized and breaks down, the cells appear less red and more green. The F-actin cytoskeleton (phalloidin) is intact for all brushes. Cells are often plated using fibronectin as a cell culture substratum. Fibronectin is an extracellular matrix glycoprotein that facilitates the attachment and cytoplasmic spreading of all types of anchorage-dependent cells.

Studies have shown it plays a major role in enhancing cell adhesion, growth,

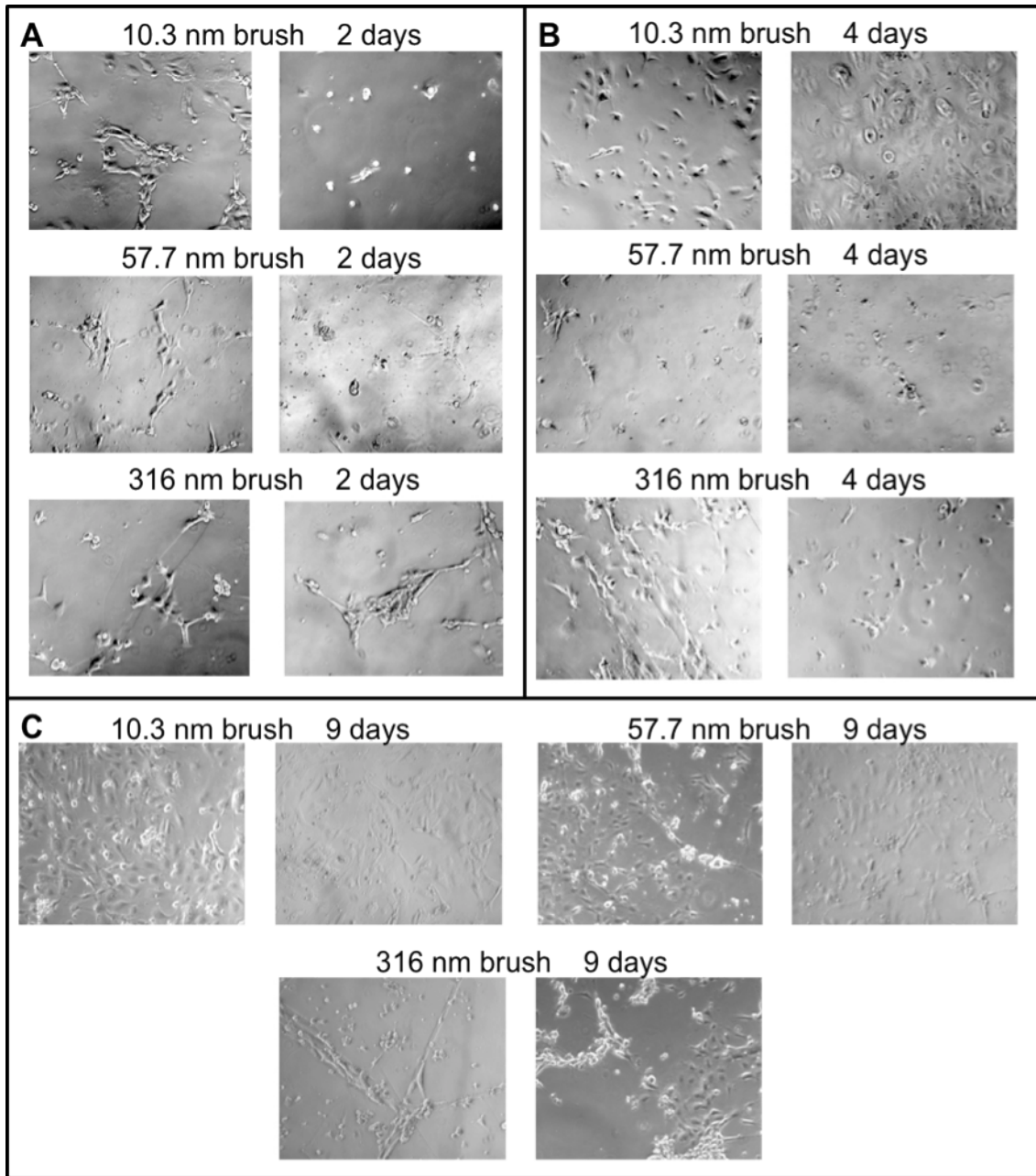


Figure 6. HUVEC cells were plated on PGMA-NH₂ brushes at 30,000 cells/500 μ l/well.

Multiple phase images were taken at day 2 (A), day 4 (B), and day 9 (C) of culture.

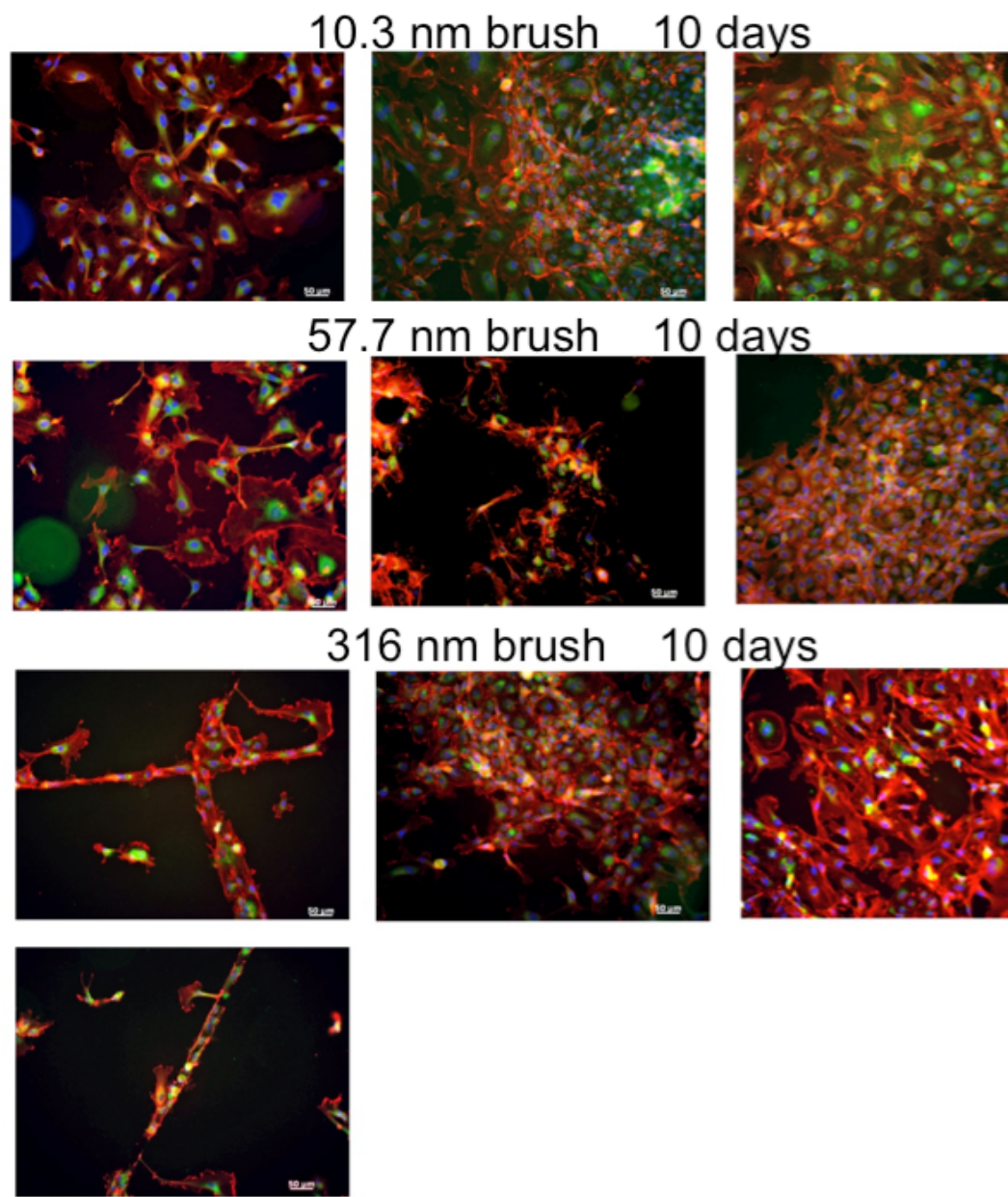


Figure 7. Samples shown are 10 days in culture. HUVEC cells were stained with Phalloidin, Autofluorescence, and DAPI.

differentiation, and affects the routes of cell migration both *in vivo* and *in culture*.^{16,17} Therefore brush samples were coated with a thin layer of fibronectin to test if the HUVEC cells would better adhere. Just as before, the brushes were first sterilized with ethanol and rinsed with buffer solution before being coated with 7 mg/ml of fibronectin in the same buffer at 37 °C. HUVEC cells were harvested with 0.05% Trypsin/0.53 EDTA for 2 minutes and then plated on the samples. As expected, more HUVEC cells adhered to the brushes that were coated with the fibronectin in the initial seeding. Figure 8 (A and B) shows phase images collected on days 2 and 4 in culture similar to the previous set of data, samples of 10.3 nm and 316 nm thick brushes had better cell growth. However after only 2 days of seeding, the HUVEC cells covered the sample surface compared to the brushes without fibronectin which took up to 9 days, demonstrating again the ability of fibronectin to promote and foster the adherence and growth of cells. Additionally, these samples demonstrated greater organization of the F-actin cytoskeleton (phalloidin) (figure 8, C) with no observation of autofluorescence.

Finally, the motility of cells on these brushes was explored. To visualize the HUVEC cell migration, fluorescent dye DiIC₁₂ was used. First, brush samples plated at 15,000 cells/PGMA-NH₂ were directly stained with the dye. However, the dye attached to the brushes and prevented the cells from moving. To avoid this, cells were first treated with DiIC₁₂ in tissue culture dishes and then split and plated on the brushes coated with the fibronectin. Cells moved successfully on this surface, as monitored by a live confocal microscope, proving these functional brushes are

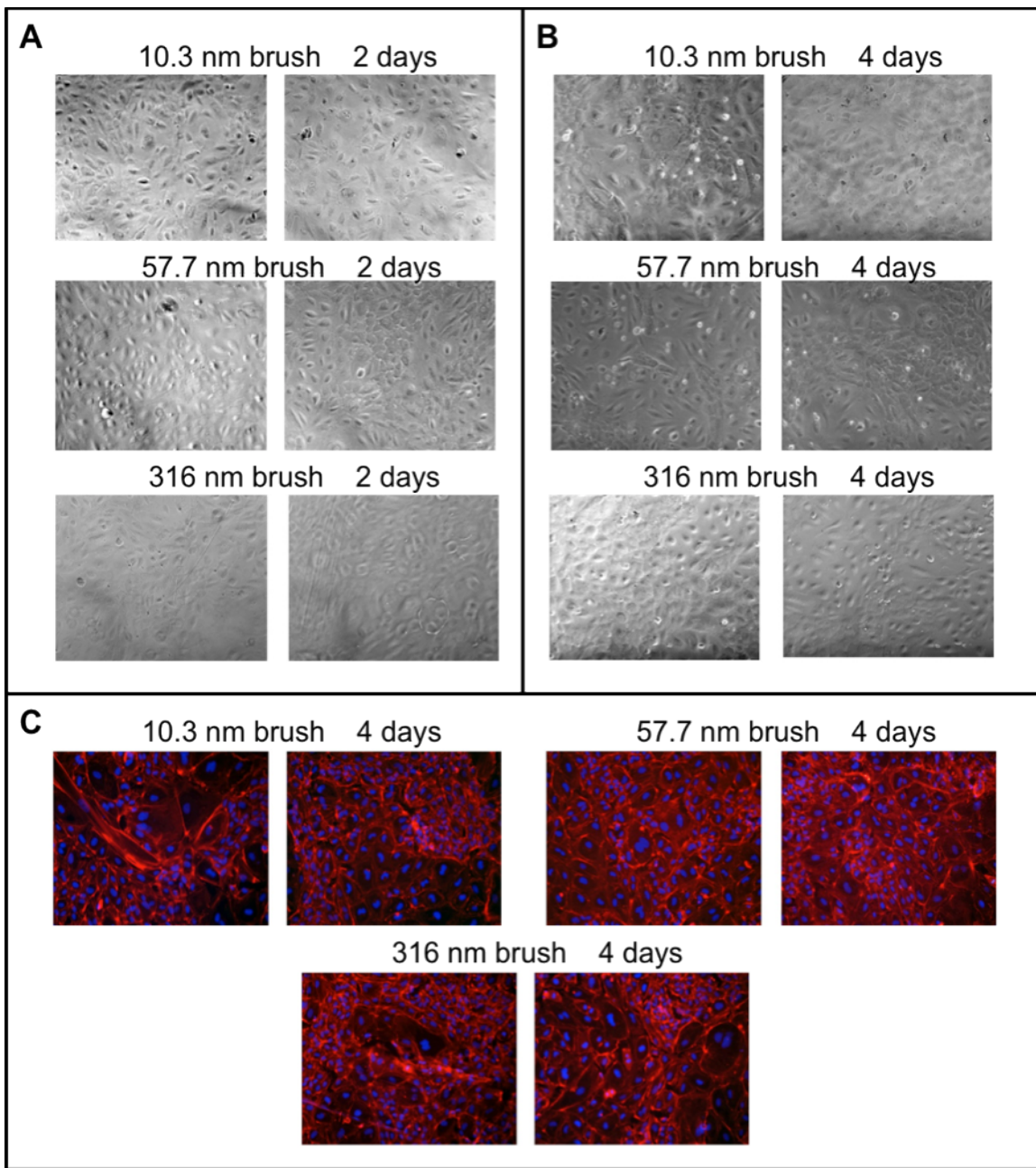


Figure 8. Cells were plated 30,000 cell/500 μ l/well on fibronectin (7 μ g/ml) coated brushes. Multiple phase images were taken at 2 days (A) and 4 days (B) in culture. HUVEC cells were stained with **Phalloidin**, and **DAPI** after 4 days in culture.

practical scaffolding material for in vitro cell tracking.

Conclusion

Polymer brushes have been used as scaffold materials for interfacing with biological media on the cellular level based on their responsive nature, ease of ligand attachment, and nonspecific adsorption properties. Therefore it is conceivable that these polymers can be of significant aid in the study and investigation of cellular behavior and activity. We have demonstrated the ability to functionalize a polymer brush system with a fluorescent substrate capable of interacting with HUVEC cells. The two types of polymer brushes we utilized were both able to reach loading capacities at levels which could be characterized fluorescently. Additionally, cellular growth and proliferation was monitored over extended time periods and found viable on both thin and thick brushes (10.3 nm and 316 nm). After 9 days the endothelial cells generated typical cobblestone patterns on the thin brushes, but formed “brick wall” patterns on the thicker samples. The addition of a thin coat of fibronectin on top of the brushes increased cellular growth and adhesion, resulting in a more ordered F-actin cytoskeleton. HUVEC cell motility was also observed on the functionalized brushes provided that the cells were pretreated with fluorescent dye before plating on the samples.

To date, we have demonstrated the synthesis of a plasmin-specific peptide (D-val-leu-lys)-containing fluorogenic plasmin substrate, confirmed its attachment (as well as the coumarin dye molecule) to the polymer brushes, and verified cellular compatibility with amine functionalized brushes. The next step is to show enzymatic cleavage of

the peptide permitting the fluorescence of the coumarin dye; however, the current system does not show a significant increase in fluorescence either on the brushes or in solution. Thus we are investigating redesigning the dye and aid the enzymatic reaction. The current cleavage point contains a very stable amide group, perhaps too stable such that the enzyme is unable to cleave the peptide bond. To overcome this, we plan on adding a CF₃ moiety on the coumarin dye to pull electron density away from the amide bond and make it more susceptible to enzyme attack. With a few synthetic tweaks, the fluorescence of the peptide substrate in solution and attached to the brushes should be magnitudes of order greater after enzymatic incubation or cellular exposure.

By combining the functionalization techniques of specially designed fluorescent tags on polymer brushes with brushes that promote cellular confluence, a system that will allow quantitative temporal and spatial analysis of specific protease activities on the surface of living, motile cells can be generated.

Acknowledgements

This work is supported by the Cornell Grant for Intercampus Collaborative Research and has made use of the Nanobiotechnology Center shared research facilities at Cornell University. All cell cultures and cell imaging were carried out by Dr. Katherine Hajjar's group, Department of Cell and Developmental Biology, Weill Cornell Medical College. Also, special thanks to Dave Calabrese for his synthesis of the fluorogenic substrates.

REFERENCES

- (1) Wang, Y.; Nakayama, M.; Pitulescu, M. E.; Schmidt, T. S.; Bochenek, M. L.; Sakaibara, A.; Adams, S.; Davy, A.; Deutsch, U.; Lüthi, U.; Barberis, a.; Benjamin, L.; Mäkinen, T.; Nobes, C. D.; Adams, R. H. *Nat. Cell. Biol.* **2010**, 465, 483.
- (2) Carmeliet, P. *Nature*, **2005**, 438, 932.
- (3) Flood, E. C.; Hajjar, K. A. *Vasc. Pharmacol.* **2011**, 54, 59.
- (4) Milner, S. T. *Science* **1991**, 251, 905.
- (5) Zhao, B.; Brittain, W. J. *Prog. Polym. Sci.* **2000**, 25, 677.
- (6) Carignano, M. A.; Szleifer, I. *Macromolecules* **1995**, 28, 3197.
- (7) Rastogi, A.; Nad, S.; Tanaka, M.; Da Mota, N.; Tague, M.; Baird, B. A.; Abruna, H. D.; Ober, C. K. *Biomacromolecules* **2009**, 10, 2750.
- (8) Li, L. Q.; Hu, W. P.; Chi, L. F.; Fuchs, H. *J. Phys. Chem. B* **2010**, 114, 5315.
- (9) Guo, W.; Xia, H. W.; Cao, L. X.; Xia, F.; Wang, S. T.; Zhang, G. Z.; Song, Y. L.; Wang, Y. G.; Jiang, L.; Zhu, D. B. *Adv. Funct. Mater.* **2010**, 20, 3561.
- (10) Welch, M.; Rastogi, A.; Ober, C. *Soft Matter* **2011**, 7, 297.
- (11) Antonio, T.; Cabral, M. F.; Cesarino, I.; Machado, S. A. S.; Pedrosa, V. A. *Electrochem. Commun.* **2013**, 29, 41.
- (12) Stuart, M. A. C.; Huck, W. T. S.; Genzer, J.; Muller, M.; Ober, C.; Stamm, M.; Sukhorukov, G. B.; Szleifer, I.; Tsukruk, V. V.; Urban, M.; Winnik, F.; Zauscher, S.; Luzinov, I.; Minko, S. *Nat. Mater.* **2010**, 9, 101.
- (13) Moore, J. S.; Stupp, S. I. *Macromolecules* **1990**, 23, 65.

- (14) Shah, R. R.; Merreceyes, D.; Husemann, M.; Rees, I.; Abbott, N. L.; Hawker, C. J.; Hedrick, J. L. *Macromolecules* **2000**, *33*, 597.
- (15) Chiang, E. N.; Dong, R.; Ober, C. K.; Baird, B. A. *Langmuir* **2011**, *27*, 7016.
- (16) Pankov, R.; Yamada, K. M. *J. Cell Sci.* **2002**, *115*, 3861.
- (17) Akiyama, S. K.; Yamada, S. S.; Chen, W. T.; Yamada, K. M. *J. Cell Biol.* **1989**, *109*, 863.